THE ROLE OF NPM-ALK SIGNALING IN TUMOR CELL METABOLISM

by

Scott Robert Paul McDonnell

A dissertation submitted in partial fulfillment
of the requirements for the degree of
Doctor of Philosophy
(Molecular and Cellular Pathology)
in the University of Michigan
2013

Doctoral Committee:

Professor Megan S. Lim, Chair
Professor Kathleen Cho
Research Associate Professor Nicholas Donato
Associate Professor Peter C. Lucas
Assistant Professor Ivan Maillard
Assistant Professor Zaneta Nikolovska-Coleska

to children with cancer

ACKNOWLEDGEMENTS

Graduate school has been an amazing time in my life, and many people throughout my tenure at Michigan have played vital roles in my thesis work. Whether through mentorship, collaborative research or emotional support, everyone in my life has contributed to this body of work presented here. My success is yours and I can't thank you enough.

My mentors Dr. Megan Lim and Dr. Kojo Elenitoba-Johnson have been immensely critical to this work. I thank you both for your guidance, advice and support during my graduate career. I have been very lucky to be mentored by two incredibly intelligent individuals who constantly put my needs as a graduate student above their own, as this is a quality not easy to come by. I would also like to acknowledge my thesis committee members (Dr. Lucas, Dr. Cho, Dr. Donato, Dr. Maillard and Dr. Nikolovska-Coleska) for their support and guidance throughout my graduate career. I also truly appreciate the support from Dr. Nick Lukacs and the Pathology graduate program, including Laura Hessler and Laura Labut.

I would also like to thank the members (past and present) of the Lim and Elenitoba-Johnson labs. Carlos Murga-Zamalloa, Steven Hwang, Delphine Rolland, Fuzon Chung, Anagh Sahasrabuddhe, Kaiyu Ma, Joon Ahn, Thiru Velusamy, Mark Kiel, Johnvesley Basappa, Xiaofei Chen, Zilin Nie, Elena Ivan, Veronica Mendoza, Carla McNeil, Adam Kronk, and Jean-Marc Fontaine. Each and every one of you has helped me in my research, whether through technical advice, hands-on help, or casual conversation around coffee and I greatly appreciate it.

This work has succeeded only because of the important collaborations we fostered. Thank you to Venky Basrur, Kevin Conlon and Damian Fermin for help with the proteomic work. Thank you to Charles Burant, Chunhai Ruan, and Sasha Raskind for help with the metabolomic studies. Finally, thank you to Craig Thomas

for providing us the PKM2 activating compounds as well as your intellectual collaboration.

My work in the lab couldn't have progressed as well as it did without the love and support from the people in my life outside of the lab. I would like to thank all of my extended family in Michigan that welcomed us and made Michigan a home. I have met some amazing, life-long friends in Ann Arbor. Kreg, David, Seyth, Molly, Bernadette, Liz, Ian, Simon, River, Laura; thank you for everything and remember that there will always be a place for you in San Diego to come visit. To my parents, thank you for all of your love and support. You have opened so many doors for me and this thesis is very much a product of that. To my brother, Andrew, you have always set the example of which I strive to reach every day. To my grandparents, you have been a constant inspiration in my life and provided me with diverse life experiences that have influenced who I have become. And to my parents-in-law, thank you for your love and support and for allowing me to drag your daughter across country to expand my education.

Finally, and most importantly, thank you Davina. You are the one who has provided me love and support day-in and day-out for the last five years. I couldn't image coming out to Michigan and enduring though graduate school without you. I love you.

This dissertation is the culmination of influences from everyone mentioned here. I hope I made you all proud.

PREFACE

Anaplastic large cell lymphoma represents about 10-15% of pediatric lymphomas and has an aggressive clinical course with frequent relapse. The majority of these tumors are characterized by translocations involving the *ALK* gene. The most common is the chromosomal translocation t(2;5)(p23;q35), which is the driving oncogenic mutation in these tumors. The consequence of the translocation is the in the expression of a constitutively active tyrosine kinase, the NPM-ALK fusion protein. While significant progress has been made in deciphering the signaling mechanisms induced by NPM-ALK, a comprehensive understanding of how NPM-ALK induces cell proliferation and survival is lacking. This level of understanding is essential for the development of novel therapeutics to treat patients with ALCL and other ALK driven neoplasms. The aim of this study is to utilize unbiased screening approaches to identify novel mediators of NPM-ALK signaling, with the goal of uncovering potential therapeutic targets.

TABLE OF CONTENTS

LIST OF FIGURES

LIST OF TABLES

LIST OF ABBREVIATIONS

3-phosphoglycerate (3-PG), 3-phosphoglycerate dehydrogenase (PHGDH), 3-phosphoinositide dependent protein kinase-1 (PDK1), 5-aminoimidazole-4-carboxamide ribonucleotide formyltransferase/IMP cyclohydrolase (ATIC), 6-phosphofructo-2-kinase (PFK-2), 6-phosphogluconate dehydrogenase (6PGD), ALK lymphoma oligomerization partner on chromosome 17 (ALO17), anaplastic large cell lymphoma (ALCL), Anaplastic lymphoma kinase (ALK), ATP-citrate lyase (ACLY), casein kinase 2α (CK2α), central nervous system (CNS), clathrin heavy chain-like 1 (CLTCL), colorectal carcinoma (CRC), complement component 1, q subcomponent binding protein (C1QBP), cysteinyl-tRNA synthase (CARS), Database for Annotation, Visualization and Integrated Discovery (DAVID), diffuse large B-cell lymphoma (DLBCL), Disheveled (Dvl), echinoderm microtubule-associated protein-like 4 (EML4), empty vector (EV), Enolase (ENO1), epidermal growth factor (EGF), extracellular domain (ECD), fibroblast growth factor receptor (FGFR1), fructose 6-phosphate (F6P), fructose-1,6-bisphosphate (FBP), gas chromatography (GC), Gene Ontology (GO), glucose 6-phosphate (G6P), glutaminase (GLS), glycogen synthase (GYS), Hematoxylin and eosin (H&E), hepatocyte growth factor receptor (HGFR), hexokinase 1 (HK1), Immunohistochemistry (IHC), inflammatory myofibroblastic tumors (IMT), insulin receptor kinase (IRK), interquartile range (IQR), isopropyl β-

D-1-thiogalactopyranoside (IPTG), Jelly Belly (Jeb), kinesin family member 5B (KIF5B-ALK), kinesin light chain 1 (KLC1-ALK), Kyoto Encyclopedia of Genes and Genomes (KEGG), lactate dehydrogenase (LDH), leukocyte tyrosine kinase (LTK), low-density lipoprotein class A (LDLa), meprin, A5 protein and receptor protein tyrosine phosphatase mu (MAM), metabolite set enrichment analysis (MSEA), metal oxide affinity chromatography (MOAC), midkine (MK), mitogen-activated protein kinase (MAPK), Moesin (MSN), mycosis fungoides (MF), natural killer/T-cell lymphomas (NK/T-NHL), neurofibromatosis type 1 (NF1), non-Hodgkin lymphoma (NHL), non-muscle myosin heavy chain (MYH9), nucleophosmin (NPM), nudix-type motif 5 (NUDT5), phosphatidylinositol 3'-kinase (PI3K), phosphatidylinositol-3,4,5-triphosphate (PIP3), phosphoenolpyruvate (PEP), phosphoglucomutase 1 (PGM1), phosphoglycerate mutase (PGAM1), phosphotyrosine (pY), pleiotrophin (PTN), protein tyrosine kinase (PTK), protein tyrosine phosphatase, nonreceptor Type 3 (PTPN3-ALK), pyruvate dehydrogenase kinase 1 (PDK1), Pyruvate kinase M2 (PKM2), RAN binding protein 2 (RANBP2), receptor protein tyrosine phosphatase (RPTP), receptor tyrosine kinase (RTK), renal cell carcinoma (RCC), ribose 5-phosphate (R5P), SEC31 homologue A (SEC31L1), sequestosome 1(SQSTM1), Sézary syndrome (SS), signal transducer and activator of transcription 3 (STAT3), tandem affinity purification tag (TAP-tag), thioredoxin reductase 1 (TXNRD1), TRK-fused gene (TFG), tropomycin 3 and 4 (TPM3/TPM4), ultrahigh performance liquid chromatography-tandem mass spectrometry (UHLC-MS/MS), Vinculin (VCL), xylose 5-phosphate (X5P)

ABSTRACT

NPM-ALK is a fusion tyrosine kinase that drives oncogenesis in a subset of anaplastic large cell lymphoma. Based on the role of NPM-ALK in cancer initiation and progression, we pursued a mass spectrometry-based phosphoproteomic approach aimed at the unbiased identification of novel mediators of NPM-ALK signaling. The analysis of cell lines under differing NPM-ALK activation conditions revealed a significant number of proteins that regulate cellular metabolism to be affected by NPM-ALK signaling. We therefore, pursued an untargeted metabolomic screen aimed at the identification of specific metabolites and metabolic pathways that are regulated by NPM-ALK. This analysis revealed significant alterations in pathways implicated in the Warburg effect and biomass production, including glycolysis, the pentose phosphate pathway, pyrimidine metabolism, etc. Metabolic flux analysis revealed an NPM-ALK-driven up-regulation of these pathways and down-regulation of energy production. We hypothesized that PKM2 and GSK3β, both identified in the phosphoproteomic study, mediate the metabolic changes. Biochemical studies revealed that NPM-ALK directly phosphorylated PKM2, decreasing its enzymatic activity and driving a metabolic shift away from energy production and toward biomass production. Chemical activation of PKM2 or expression of a mutant PKM2 resulted in a reversal of this metabolic shift and decreased tumorigenesis. The phosphoproteomic analysis identified another

candidate mediator of NPM-ALK signaling, GSK3β. Through the PI3K/AKT pathway, NPM-ALK regulated pS^{9}-GSK3β, inhibited its activity and provided proteasomal protection for Mcl-1, CDC25A and GYS. This pathway increased proliferation and survival, while increasing glycogen production as a form of metabolic regulation. Studies described in this dissertation globally characterize the ALK driven phosphoproteome and metabolome while providing mechanistic discoveries of two novel NPM-ALK driven pathways. This work provides significant advances to our understanding of oncogenesis and will lead to advances in targeted therapies for ALK driven neoplasms.

CHAPTER 1

INTRODUCTION

Anaplastic Lymphoma Kinase

Structure

Anaplastic lymphoma kinase (ALK) is a receptor tyrosine kinase (RTK) in the insulin receptor subfamily[1,2]. The full length protein contains 1620 amino acids and most closely resembles the leukocyte tyrosine kinase (LTK). The two proteins share 57% amino acid identity and 71% similarity over their overlapping sequences with initial characterization of ALK revealing a putative transmembrane domain and an extracellular domain. The initial translation of this 177 kDa polypeptide undergoes N-glycosylation and results in a 200 kDa mature protein that is expressed on the cell surface that is capable of being tyrosine phosphorylated[1]. The extracellular domain (ECD) of ALK contains (from N-terminus to C-terminus) a signaling sequence, a MAM (meprin, A5 protein and receptor protein tyrosine phosphatase mu) domain containing putative pleiotrophin binding sites, an LDLa (low-density lipoprotein class A) motif, another MAM domain as well as a glycine-rich domain adjacent to the transmembrane domain (Figure 1.1)[3,4]. ALK contains a protein tyrosine kinase (PTK) domain with identifiable ATP binding sites and putative binding sites for IRS1, SHC, PI3K and PLCγ spread throughout the intercellular domain (ICD)[4]. The presence of the LDLa domain within the ECD supports the role of ALK as a receptor

for ligand signaling as these domains are common among cell surface receptors and have been shown to be critical in ligand binding[5-7].

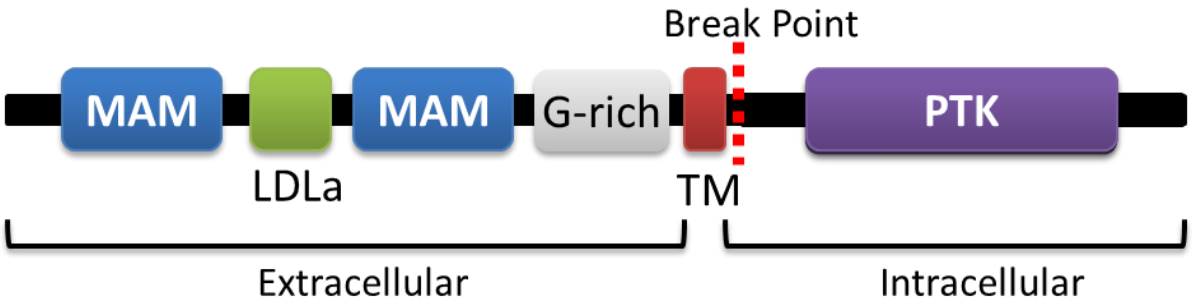

Figure 1.1: Anaplastic Lymphoma Kinase domain structure. ALK is a Receptor tyrosine kinase. The extracellular domain contains two MAM (meprin, A5 protein and receptor protein tyrosine phosphatase mu) domains with putative pleiotrophin binding sites, an LDLa (low-density lipoprotein class A) motif, and a glycine-rich domain adjacent to the transmembrane domain. The intracellular domain contains the protein tyrosine kinase domain which is responsible for the propagation of downstream signaling events. The conserved translocation breakpoint is indicated immediately following the transmembrane domain.

The ALK kinase domain consists of amino acids 1116-1392 and shows significant differences in sequence alignments as compared to other members of the RTK family of proteins[8]. The activation loop (A-loop) of ALK contains the same 3 tyrosine motif (YXXXYY) as seen in other RTK proteins of the same subfamily such as insulin receptor kinase (IRK). This A-loop is responsible for autophosphorylation and activation of the kinase, however the 3 amino acids separating first and second tyrosine residues differ significantly from other members of this family. Specifically, IRK contains a Y**ETD**YY motif while ALK contains Y**RAS**YY. This internal triplet has been shown to confer recognition and specificity for autophosphorylation as a peptide containing the IRK A-loop cannot be phosphorylated by ALK unless the

triplet is mutated to match that of ALK[8]. Mutational analysis of the 3 tyrosine residues on the ALK A-loop revealed that the first residue is necessary for autophosphorylation and subsequent functional activity[9]. Phosphorylation of these A-loop tyrosine residues is necessary for the phosphorylation of 8 additional tyrosine residues located throughout the ICD, the activation of downstream signaling mechanisms and the oncogenic potential of the kinase[10]. Crystal structure analysis of the ALK catalytic domain has validated the mutational studies of the A-loop function as well as provided structural insight to the observed substrate specificity of ALK[11].

ALK Ligands

The natural ligand activating ALK signaling has been a relatively contested issue within the literature. Studies in the Drosophila homologue of mammalian ALK (dALK) have identified Jelly Belly (Jeb) as capable of binding to and activating the RTK. Jeb is a secreted LDL receptor repeat protein that is necessary for normal development of the visceral mesoderm[12]. The resulting binding of Jeb to dALK has been shown to control normal muscle development in Drosophila and mediate the physiological role of Jeb[13,14]. However, no known homologue to Jeb exists in vertebrates and the Drosophila Jeb is incapable of activating mouse ALK[15]. In mammalian cells, pleiotrophin (PTN) and midkine (MK) proteins have been shown to bind to the ECD of ALK and activate its downstream signaling pathways[3,16-18]. PTN and MK are both heparin binding growth factors that share about 50% amino acid identity [19]. The role of PTN and MK as ligands to ALK is still under debate as several groups have presented conflicting data about the ability for these proteins to

activate ALK signaling. These groups were unable to achieve phosphorylation or activation of ALK with PTN or MK[20-24].

Several groups have published data providing additional evidence regarding ALK and its ligand function. Prior to the characterization of PTN and MK as potential ligands, Iwahara et al. reported the presence of an epidermal growth factor (EGF)-like domain in the ECD of ALK[2]. They suggest that this may serve as an internal ligand and facilitate receptor dimerization or cell-cell interactions. However, empirical evidence for these hypotheses has yet to be presented. Perez-Pinera et al. provided a potential explanation for the discrepancy of PTN and MK as an ALK ligand[25]. Here, the role of PTN in ALK activation was shown to be indirect. PTN can bind and activate the receptor protein tyrosine phosphatase (RPTP) β/ζ and its downstream signaling pathway. This results in inhibition of the phosphatase that inactivates ALK, leading toward more activation of the receptor. Another report suggests that ALK serves as a dependence receptor[26,27]. ALK receptor induces apoptosis when expressed in Jurkat cells in the absence of ligation. While, PTN failed to cause ALK activation, the group showed that a monoclonal antibody capable of activating ALK induced an anti-apoptotic phenotype in these cells. These data suggest that cells expressing the ALK receptor are addicted to ALK ligand activity or activation, yet the physiological mechanism for ligation is yet to be understood.

ALK Expression

Normal expression of wildtype ALK is extremely restricted and is limited to the central nervous system including the thalamus, mid-brain, olfactory bulb and ganglia[2,28]. ALK expression is seen most predominantly in the neurons with additional expression in glial cells and endothelial cells of the central nervous system (CNS). Additionally, ALK expression is strong in these tissues as early as E15 of mouse development but quickly decreases following birth. At 3 weeks of age, ALK expression reaches a minimum level but is still detectable through adulthood. These data suggest that wildtype ALK plays an important role in the development and function of the central nervous system.

Drosophila ALK

Several groups have focused their efforts on understanding the role of ALK in Drosophila in order to decipher its physiological role. Drosophila ALK was first characterized by Loren et al. where they identified dALK as a novel receptor tyrosine kinase[4]. They reported expression of the protein in developing CNS as well as additional expression in the developing visceral mesoderm. The mesoderm expression of ALK was coincident with phospho-ERK expression. To further this notion, the same group later showed that loss of function mutations in dALK resulted in defects in gut development suggesting a role for ALK in the visceral mesoderm during embryogenesis[29]. More recently, a series of reports have emerged suggesting additional roles for ALK in developmental and behavioral control. Cheng et al. reported that ALK is necessary for protecting neuroblast growth during nutrient

restriction by signaling through PI3K[30]. These data illustrate that previously unknown mechanisms to protect vital organs during development in the event of starvation. However, this also has implications in human tumor biology as many cancers exhibit starvation resistant phenotypes[31]. An additional study showed that ALK negatively regulates both body size and associative learning in Drosophila through the activation of *dNf1* (ortholog of the Neurofibromatosis type 1 (NF1) disease gene) signaling pathways and inhibition of ALK was shown to rescue the *dNf1* mutant phenotype[32]. Recently, Lasek et al. reported that ALK is associated with altered behavior responses to alcohol and showed that mutant flies lacking functional dAlk had resistance to the sedative effects of alcohol consumption[33]. While these data were originally discovered in the Drosophila model system, Lasek et al. confirmed these results in mice and humans suggesting a role for ALK kinase in response to ethanol. Taken together, these studies support a role for ALK in a variety of neurological, developmental and behavioral phenotypes.

Mouse ALK

While *ALK* knockout mice appear to be normal, fertile and viable, several behavioral and psychological defects were identified[33-35]. Bilsland et al. were the first to report phenotypic findings from *ALK* knockout mice showing the homozygous knockout of the ALK kinase domain resulted in increased basal hippocampal progenitor cell proliferation and increased dopamine metabolism in the frontal cortex[34]. While these mice had no developmental or anatomical problems, behaviorally, they displayed signs of decreased depression and increased performance in hippocampal-dependent tasks. Recently, additional phenotypes

were reported in ALK deficient mice that supports the role for ALK in neurogenesis and brain function[35]. Here, mutant ALK was associated with reduced neurogenesis but increased spatial memory function. Specifically, ALK mutant mice exhibited fewer doublecortin-positive cells (an indirect measure of neurogenesis)[36]. Consistent with their Drosophila studies, Lasek et al. reported that ALK knockout mice have altered behavior responses to ethanol including increased ethanol consumption and longer sedation times[33]. These studies support the role for ALK in neural development and behavioral phenotypes.

ALK as an Oncogene

While the physiological role of ALK seems to be nuanced by subtle changes in brain development and function, the pathologic role of ALK is anything but ambiguous. The *ALK* gene is frequently involved in chromosomal translocations (Table 1.1), mutations and amplifications that are often seen in a variety of neoplasms from diverse cellular origins.

Table 1.1: Recurrent ALK Translocations in Cancer

Chromosomal Abnormality	Fusion Protein	Partner Protein	Disease
t(2;5)(p23;q35)	Nucleophosmin	NPM-ALK	ALCL, DLBCL
t(1;2)(q25;p23)	Tropomyosin 3	TPM3-ALK	ALCL, IMT
t(2;19)(p23;p13)	Tropomyosin 4	TPM4-ALK	ALCL, IMT, ESCC
t(2;3)(p23;21)	TRK-fused gene	TFG-ALK	ALCL, NSCLC
inv(2)(p23;q35)	ATIC	ATIC-ALK	ALCL, IMT
t(2;17)(p;23;q23)	Clathrin heavy chain like 1	CLTC1-ALK	ALCL, IMT, DLBCL
t(2;X)(p23;q(11-12)	Moesin	MSN-ALK	ALCL
t(2;17)(p23;q25)	ALO17	ALO17-ALK	ALCL
t(2;2)(p23;q13) inv(2)(p23;p15;q31)	RAN binding protein 2	RANBP2-ALK	IMT
t(2;22)(p23;q11.2)	Non-muscle myosin heavy chain	MYH9-ALK	ALCL
t(2;11;2)(p23;p15;q31)	Cysteinyl-tRNA synthase	CARS-ALK	IMT
t(2;4)(p23;q21)	SEC31 homologue A	SEC31L1-ALK	IMT, DLBCL
inv(2)(p21;p23)	Echinoderm microtubule-associated protein-like 4	EML4-ALK	NSCLC, Breast, CRC
t(2;10)(p23;p11)	kinesin family member 5B	KIF5B-ALK	NSCLC
t(2;14)(p23;q32)	kinesin light chain 1	KLC1-ALK	NSCLC
t(2;9);p23;q31)	Protein tyrosine phosphatase, nonreceptor type 3	PTPN3-ALK	NSCLC
t(2;5)(p23;q35.3)	Sequestosome 1	SQSTM1-ALK	DLBCL
t(2;10)(p23;q22)	Vinculin	VCL-ALK	RCC

Anaplastic Large Cell Lymphoma

The role for ALK in tumorigenesis has been most thoroughly studied in the context of anaplastic large cell lymphoma (ALCL). ALCL is a form of non-Hodgkin lymphoma (NHL) initially described by Stein et al. in 1985[37]. Here, ALCL was identified as similar to Hodgkin lymphoma based on the expression of CD30, but morphologically different based on the presence of “bizarre” large cells and other markers. Now, these “bizarre” cells are considered to be the hallmark cells of ALCL.

A comprehensive analysis of the morphologic features of these cells was first eloquently described by Benharroch et al.

> *"…all cases shared one common feature, notably the presence of a population of large cells with a highly characteristic morphology. The nucleus lay eccentrically within these cells and was horseshoe or kidney shaped. In most cases, some crown-like nuclei could also be seen. Nucleoli were less prominent than in Reed-Sternberg cells and often an eosinophilic region was seen near the nucleus, probably representing a prominent Golgi apparatus."*[38]

ALCL is most often observed in children or young adults, representing 10-30% of all pediatric non-Hodgkin lymphoma[39,40]. The expression of ALK is a characteristic feature in 60-80% of ALCL cases, and this distinction in ALK expression status is significant as the ALK-negative cases of ALCL have been shown to have a reduced 5-year survival rate compared to ALK-positive ALCL[41,42]. The expression of ALK is a consequence of recurrent chromosomal translocations involving the *ALK* gene locus. The translocation present in about 80% of ALK+ALCL cases determined to be t(2;5)(p23;q35)[43-46]. The characterization of this chromosomal translocation led to the first description of ALK and gave it its namesake[47].

t(2;5) in ALCL

The chromosomal translocation t(2;5)(p23;q35) is the quintessential genetic abnormality resulting in expression of oncogenic ALK. The result of which is the fusion of the tyrosine kinase domain of ALK with a portion of nucleophosmin (NPM).

NPM is a ubiquitously expressed nucleolar protein that has a variety of cellular functions including nuclear shuttling, ribosomal biogenesis and genomic stability[48]. Importantly, NPM contains an oligomerization domain at its N-terminus that remains intact following the t(2;5) translocation. The consequences of this translocation are profound, as it results in the loss of the *ALK* regulatory and promoter regions that normally silence ALK expression in lymphocytes and other adult tissues. Instead, the resulting fusion gene (NPM-ALK) is placed under the regulatory control of the NPM promoter which is highly active in most cell types including lymphocytes. Additionally, the resulting fusion protein, NPM-ALK, has been shown to be capable of autophosphorylation and constitutive activation[49]. While NPM-ALK expression has transformative effects on NIH3T3 cells, deletion of the NPM portion of the fusion protein abolishes this capability[50]. The reason for which is the presence of the oligomerization domain of NPM that aides the dimerization of the ALK kinase domain, mimicking ligand binding in the native protein. Finally, the t(2;5) translocation results in aberrant localization of ALK because the breakpoint occurs just after the transmembrane domain causing the fusion protein to no longer be localized in the membrane. Instead, NPM-ALK can be found in the cytoplasm and nucleus[49]. Although the nuclear localization signal in NPM is lost as a result of t(2;5), NPM-ALK can been seen in the nucleus. Presumably, this is a result of the formation of heterodimers with NPM-ALK and full length NPM. However, Brischof et al. noted that the NPM-ALK dimerization is the key transforming feature of this oncogene and not the nuclear localization[49].

Variant ALK translocations in ALCL

While the presence of t(2;5) is the most common *ALK* mutation in ALCL, several other translocations involving *ALK* have been observed. These additional fusion partners include Tropomycin 3 and 4 (TPM3/TPM4)[51-53] TRK-fused gene (TFG)[54,55], clathrin heavy chain-like 1 (CLTCL)[56], 5-aminoimidazole-4-carboxamide ribonucleotide formyltransferase/IMP cyclohydrolase (ATIC)[57-59], Non-muscle myosin heavy chain (MYH9)[60], Moesin (MSN)[61,62], and ALK lymphoma oligomerization partner on chromosome 17 (ALO17)[63]. The common feature that the majority of these ALK fusion proteins have in common is their ability to form dimers and thus induce constitutive activation of the ALK kinase domain. Specifically, the TPM and TFG fusion partners are capable of dimerization through α-coiled-coiled structures which could give rise to ALK activation[51,55]. Interestingly, unlike NPM, TPM3 and TFG are cytoplasmic proteins therefore the TPM3-ALK and TFG-ALK fusion proteins are also localized to the cytoplasm. ATIC-ALK is thought to be activated through a similar means of dimerization initiated by the ATIC region of the fusion protein[58]. A clear case for dimerization in CTCL-ALK is a little less straightforward. However, since CTCL-ALK has been shown to localize in vesicles within ALCL cells, it is likely that the fusion protein is binding to clathrin-coated vesicles, thus providing the close proximity necessary for activation of ALK[56]. While MSN does not appear to have oligomerization properties, it does localize to the cell membrane (as does the MSN-ALK fusion protein). This co-localization could provide the close proximity similar to CTCL-ALK and subsequent ALK activation[61]. While MYH9 does contain an oligomerization domain, it is lost as a result of the chromosomal translocation.

Functional analysis of the MYH9-ALK fusion protein showed lack of tyrosine kinase activity *in vitro* but appears to be activated *in vivo,* suggesting the possibility that MYH9-ALK is acting in conjunction with other proteins to achieve activation[60].

Inflammatory Myofibroblastic Tumors

Inflammatory myofibroblastic tumors (IMT) are members of a broad spectrum of neoplastic and non-neoplastic entities termed "inflammatory pseudotumors"[64]. These tumors were originally considered a benign postinflammatory condition rather than a neoplastic process. The tumors are most commonly found in children and young adults, though all ages are affected. Although the location of the tumors varies greatly, they are most frequently identified as pulmonary, intra-abdominal or retroperitoneal in location. There is a low risk for recurrence and distant metastasis of IMTs. Histologically, the tumors are characterized by spindle cell proliferation in a collagenous stroma with prominent infiltration of plasma cells and lymphocytes. Importantly, ALK positive staining can be seen in about 50% of cases (ALK+ staining is seen mostly in younger patients)[65,66]. It was the identification of 2p23 chromosomal rearrangements and ALK gene expression that helped to reclassify these tumors as neoplastic in origin[67].

The first ALK fusion proteins to be discovered in IMTs were the TPM3-ALK and TPM4-ALK oncogenes[68]. These proteins were found to be constitutively active and drove the oncogenic phenotype of IMT. Since this discovery, a variety of other ALK fusion partners have been identified in IMT, several of which are shared with ALCL, including ATIC-ALK and CLTC1-ALK[69,70]. However, some of the observed

ALK rearrangements in IMTs have yet to be identified in ALCL. These include CARS-ALK, RANBP2-ALK, PPFIBP1-ALK, and SEC31L1-ALK[63,71-74].

Non-Small Cell Lung Cancer

ALK translocations and fusion protein expression have also been identified in non-small cell lung cancer (NSCLC). About 6% of NSCLC patients have shown expression of the ALK protein with an increased frequency in non-smokers[75,76]. The expression of ALK in NSCLC was originally found to be a consequence of the chromosomal aberration inv(2)(p21;p23) and the fusion of *ALK* to echinoderm microtubule-associated protein-like 4 (*EML4*) gene. Since its original discovery, several EML-ALK gene fusion variations have been identified. At least eleven of these share the same portion of ALK, but varying lengths of the EML4 portion[75,77-79]. The common feature between all EML4-ALK variations is the coiled-coil domain at the N-terminal region of EML4 that has been shown to be necessary and sufficient for the oncogenic capacity of EML4-ALK. Interestingly, these mutations seem to be mutually exclusive from EGFR and KRAS mutations supporting the role of EML4-ALK as a driving oncogene and ALK+ NSCLC as a distinct clinical entity[80]. Additionally, several other ALK mutations have been identified in NSCLC at a lower frequency than EML4-ALK. These include TGF-ALK, KLC1-ALK (kinesin light chain 1), KIF5B-ALK (kinesin family member 5B) and PTPN3-ALK (protein tyrosine phosphatase, nonreceptor Type 3) suggesting a broader significance for ALK in these tumors[81-84].

Diffuse Large B-Cell Lymphoma

ALK translocations have also been identified in rare cases of diffuse large B-cell lymphoma (DLBCL). This was originally identified in 1997 and represented the first case of ALK oncogenic expression outside of ALCL[85]. The most common cause of ALK expression is the t(2;17)(p23;q23) translocation resulting in the expression of CLTC1-ALK[86-88]. Since then, other fusion proteins including NPM-ALK, SQSTM1-ALK (sequestosome 1) and SEC31A-ALK have been identified[89-91]. ALK+DLBCL represent a distinct subtype of DLBCL with the presence of immunoblastic or plasmablastic cells with prominent nucleoli. These tumors stain positive for CD138, CD45, CD4 and EMA while lacking staining for CD3, CD30, and CD56[92]. Interestingly, mouse models of ALK overexpression develop tumors that resemble ALK+DLBCL[93].

Neuroblastoma

The expression of ALK was also identified in neuroblastoma however, the expression is not a result of chromosomal translocations[94]. Instead, overexpression of ALK as a result of copy number variations was identified along with activating point mutations[95]. It is important to note the extent to which ALK contributes to the oncogenesis of these tumors is still under debate. Compared to cell lines expressing NPM-ALK, full length ALK expressing cells show little to no phosphorylation of the receptor, leading to the hypothesis that its expression is physiologic as opposed to pathologic[20]. ALK overexpression in neuroblastoma often accompanies amplifications in *MYCN* and studies suggest cooperation between these oncogenes[96-98]. In addition to ALK amplification, several activating point mutations have been identified that contribute to the oncogenesis of

neuroblastoma[99-101]. Dozens of point mutations have since been characterized and tend to cluster in or near the kinase domain of ALK. Residues R1275 and F1174 seem to be hot spots for mutations and correlate with elevated *MYCN* amplification and poor prognosis[102]. Furthermore, 2 truncated forms of ALK have recently been identified (ALKdelta4-11 and ALK^{del2-3}) in neuroblastoma that are constitutively activated and possess transformative properties[103,104].

Other ALK Expressing Tumors

Translocations in the *ALK* gene locus have been identified in rare cases of several other cancer types. Colorectal carcinoma (CRC) has been shown to carry EML-ALK mutations in 2.4% of cases and recently, a case of C2orf44-ALK was also reported in CRC[105,106]. Using a phosphoproteomic approach to identify oncogenic kinases in ovarian cancer, Ren et al. identified the oncogenic ALK expression in about 2% to 4% of ovarian cancers[107]. The expression of ALK was identified in two contexts; a result of ALK copy number gains in one patient and the FN1-ALK fusion protein in another. A study in renal cell carcinoma (RCC) identified 2 (out of 6) patients to contain ALK translocations with the expression of the novel VCL-ALK fusion protein[108]. Finally, ALK expression was reported in a subset of breast cancers, however, it is not clear whether the ALK expression is a result of full length ALK or translocations[109].

ALK Signaling

Mutations in ALK have been shown to drive the initiation and progression of the tumors discussed above. Much effort has therefore been placed on

understanding the signaling events that propagate from ALK to elicit this oncogenic effect. While the complex and overlapping signaling networks are still under investigation, three major pathways have emerged as the key mechanisms mediating ALK induced oncogenesis.

STAT3 Pathway

ALK has been shown to phosphorylate and activate the signal transducer and activator of transcription 3 (STAT3) through several important studies (Figure 1.2)[110-113]. STAT protein family members are activated by growth factor receptors, cytokine receptors and interferon receptors[114]. The consequence of the phosphorylation and activation of STATs is the dimerization and nuclear translocation of the proteins where they act as transcription factors.

STAT3 signaling has been shown to be critical for ALCL proliferation and survival. STAT3 knockdown and pharmacological inhibition leads to impaired tumorigenesis in ALCL mouse models and is required for the transformation of mouse embryonic fibroblasts[113]. Expression of a dominant negative STAT3 also leads to apoptosis and G1 cell cycle arrest[112]. Furthermore, phosphorylated STAT3 has been identified in primary human ALCL tumors along with its nuclear translocation[110]. More importantly, expression of phosphorylated STAT3 corresponds with NPM-ALK expression across other lymphoma subtypes.

While ALK also binds and activates JAK3, the role of JAK3 as a mediator in STAT3 activation is unclear. JAK3 was reported to not be required for STAT3 activation, yet additional studies report that the inhibition of JAK3 results in

decreased STAT3 phosphorylation and subsequent apoptosis[110,115,116]. Furthermore, activation of JAK3 has been seen in human tumors and associates with ALK expression[117]. Additional investigation is necessary to illuminate the role of JAK3 in the NPM-ALK/STAT3 signaling pathway.

The activation of STAT3 plays an essential role in ALK mediated tumorigenesis as seen by *in vitro* and *in vivo* models. Signaling through STAT3 induces the transcription of numerous genes responsible for increased survival, increased proliferation and immune suppression. Specifically, STAT3 induces expression of numerous survival promoting genes including *Bcl-2*, *Bcl-X_L*, *Bcl2A1*, *Survivin*, *Mcl-1*, *C/EBPβ*[110,118-120]. BCL-2 and BCL-XL are anti-apoptotic proteins and their increased expression enhances the survival of NPM-ALK expressing cells[121]. STAT3 also induces the expression of survivin (a member of the inhibitor of apoptosis (IAP) family). Patients with increased survivin levels predicts poor clinical outcome suggesting an important role for STAT3/survivin in ALCL aggressiveness[122]. STAT3 signaling also promotes the expression of numerous pro-proliferation genes including *Cyclins, CD278, c-Myc, Sox2 and C/EBPβ*[120,123-126]. *CD278 (ICOS)* has been shown to be directly regulated by STAT3 signaling[125]. In fact, STAT3 directly increases *CD278* expression in addition to down regulating miR-219 which selectively inhibits *CD278* expression. NPM-ALK signaling through STAT3 also results in expression of the embryonic stem cell transcription factor Sox2[126]. While expression of Sox2 was seen in most ALCL cells, transcriptional activity of Sox2 is only present in a small subset. This Sox2 expression is important

for ALK+ ALCL tumorigenesis and suggests a major role for a subset of ALCL cells maintaining a stem cell-like transcriptional program.

NPM-ALK induced STAT3 activation supports an immunosuppressive phenotype that enables tumorigenesis, which is accomplished through the excretion of IL-10 and TGF-β as well as the expression of FoxP3 and CD274 (B7-H1)[127,128]. This expression pattern results in a T regulatory (Treg) cell phenotype initiated through STAT3 signaling. The IL-10 excretion limits proliferation of peripheral blood mononuclear cells while enhancing the viability of the tumor cells. CD274 is a ligand for PD-1 and inhibits T-cell activation[129].

STAT3 signal has been shown to be substantiated in ALCL through crosstalk with other pathways. The accumulation and transcriptional activation of β-catenin has been observed in ALK+ALCL cell lines and tumors[130]. STAT3 expression and activation is dependent on this β-catenin activity, as this activity points toward the activation and cooperation with the WNT signaling pathway. Other members of this pathway, including casein kinase 2α (CK2α) and Disheveled (Dvl-2/3) have been shown to regulate ALCL growth[131,132]. Interestingly, CKα was shown to regulate the serine phosphorylation of NPM-ALK which, in turn, is required for autoactivation of NPM-ALK[133]. This convoluted feed-forward signaling loop suggests that ALK signaling and WNT signaling work together to not only increase proliferation and survival, but to further enhance their own signaling cascades.

NPM-ALK has also been shown to activate STAT5B[134]. JAK2 is constitutively active in ALCL cells due to the expression of NPM-ALK[135]. The activation of JAK2

leads to the activation of STAT5B and the subsequent transcriptional activation of downstream effectors such as β-casein. The JAK2/STAT5B signaling pathway has been shown to be necessary for ALCL proliferation and survival through JAK2 inhibition (AG490) and expression of dominant-negative STAT5B mutant. Conversely, STAT5A has been shown to be a tumor suppressor in ALCL cells[136]. This study reported the role of NPM-ALK in inducing DNA methylation of the *STAT5A* promoter through STAT3 activation. This results in the epigenetic silencing of STAT5A expression. Forced expression of STAT5A results in suppression of NPM-ALK expression and a corresponding reduction in ALCL proliferation.

NPM-ALK mediated STAT3 signaling is also substantiated through coordinated expression (or lack thereof) of protein phosphatases. ALCL tumors have been shown to lack expression of SHP1 tyrosine phosphatase expression through the methylation of its promoter[137,138]. Introduction of exogenous SHP1 into ALCL-derived cell lines results in decreased JAK3 and STAT3 phosphorylation and induced the proteasomal degradation of JAK3 and STAT3[120,139]. The result of which is the down-regulation of cyclin D3, Mcl-1 and Bcl-2 and a subsequent reduction in proliferation. This represents a second example of epigenetic regulation to enhance STAT3 signaling and oncogenesis. Conversely, expression of serine/threonine phosphatase PP2A has been shown to increase STAT3 activation through the removal of inhibitory serine phosphorylations[111].

STAT3 activation in ALCL is also enhanced through cytokine receptors. NPM-ALK induces the expression of IL-22R1 which is aberrantly expressed in these tumors[140]. This expression leads to increased STAT3 activation and oncogenesis.

Similarly, IL-21R is also expressed in ALCL tumors and cell lines, although by NPM-ALK independent mechanisms[141]. STAT3 signaling and ALCL proliferation is substantiated by this IL-21R activation, and IL-9 also contributes to JAK3/STAT3 activation in ALK+ ALCL[142]. Neutralizing IL-9 antibody treatment leads to cell cycle arrest in ALCL cells through p21 and Pim-1 dependent pathways. Finally, IL-2Rγ acts as a tumor suppressor and is epigenetically silenced in NPM-ALK expressing cells[143]. STAT3 activation via NPM-ALK results in DNA methylation at the IL-2Rγ promoter. Reconstitution of IL-2Rγ results in loss of NPM-ALK expression, suggesting these two proteins act in contrast to limit the expression of the other.

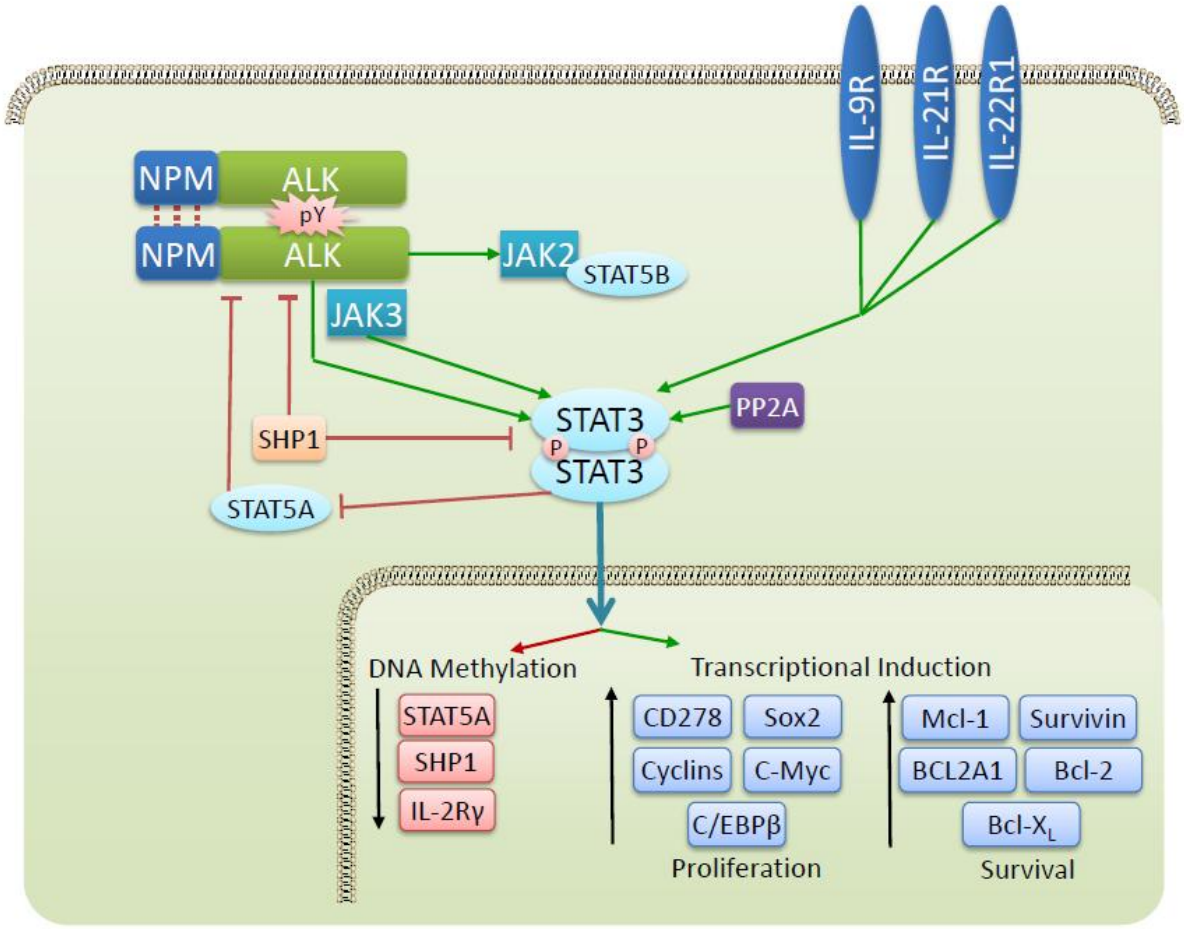

Figure 1.2: NPM-ALK induced STAT3 signaling. NPM-ALK activates STAT3 through direct phosphorylation and via JAK3 activation. Negative regulators of NPM-ALK signaling are epigenetically silenced through DNA methylation by STAT3 activity (STAT5A, SHP1, IL-2Rγ). STAT3 activation is further propagated by cytokine signals in ALCL (IL-9R, IL21R and IL22R1) and through the activity of PP2A which removes inhibitory serine phosphorylations from STAT3. Active STAT3 translocates to the nucleus to drive the transcription of genes that promote proliferation and survival. JAK2/STAT5B activation by NPM-ALK also contributes to oncogenesis.

PI3K/AKT Pathway

A second major signaling pathway directed by NPM-ALK kinase activity is the phosphatidylinositol 3'-kinase (PI3K)/AKT pathway and is typically activated by receptor tyrosine kinases (RTK) through the phosphorylation of PI3K (Figure 1.3)[144]. The active of PI3K then generates phosphatidylinositol-3,4,5-triphosphate (PIP3) at the membrane surface. PIP3 recruits AKT (PKB) to the membrane where it is phosphorylated by 3-phosphoinositide dependent protein kinase-1 (PDK1) at the T308 residue and then becomes active. AKT serves as a "master" kinase in this pathway and is responsible for an array of downstream effects.

NPM-ALK has been shown to constitutively activate the PI3K/AKT pathway. Slupianek et al. reported that PI3K associates with NPM-ALK and activated AKT was found in both ALCL-derived cell lines and primary tumors[145]. Furthermore, the activity of this pathway is necessary for the oncogenic phenotype driven by NPM-ALK, as seen by inhibition of this pathway with wortmannin and LY294002 as well as expression of dominant negative PI3K or AKT mutants[146]. The resulting activation of the PI3K /AKT pathway by NPM-ALK increases proliferation and survival of ALCL. PTEN is a phosphatase responsible for the negative regulation of this pathway by removing the phosphate on position 3 of PIP3 thereby stopping the signaling cascade[147]. However, ALCL tumors have been shown to lack PTEN expression leading to uncontrolled PI3K/AKT signaling[148].

Active AKT phosphorylates S9-GSK3β to inhibit its enzymatic activity[149]. GSK3β is a serine/threonine kinase that marks proteins for proteasomal degradation

and plays a critical role in numerous signaling pathways[150]. The inhibition of GSK3β by NPM-ALK deregulates the normal turnover of proteins affecting the cell cycle (CDC25A, JunB) and apoptosis (Mcl-1)[149,151]. Inhibition of NPM-ALK results in the activation of GSK3β and the subsequent proteasomal degradation of CDC25A and Mcl-1. The reduced proliferative and oncogenic capacity resulting from ALK inhibition can be partially rescued by GSK3β knockdown or chemical inhibition, which suggests that GSK3β inhibition is an important mediator of the NPM-ALK oncogenic phenotype.

In addition to protecting the proteins that drive proliferation, NPM-ALK signaling through AKT targets proteins for degradation that inhibit proliferation. NPM-ALK directs the AKT dependent phosphorylation of $p27^{Kip1}$, which is a cyclin-CDK inhibitor that induces cell cycle arrest[152,153,154]. NPM-ALK expressing cells avoid this cell cycle arrest through the constant proteasomal degradation of $p27^{Kip1}$. Down regulation of $p27^{kip1}$ is also achieved through the AKT induced phosphorylation of the FOXO3a transcription factor[155]. The phosphorylation of FOXO3A results in its cytoplasmic retention and the resulting down regulation of its transcriptional targets $p27^{Kip1}$ and Bim-1.

The activation of the PI3K/AKT pathway also contributes to the activation of the Sonic Hedgehog signaling pathway in ALCL. AKT activation results in SHH expression and, through the inhibition of GSK3β, the accumulation of GLI1[153,156]. SHH and GLI1 were shown to be highly expressed in ALCL-derived cell lines and tumors. The expression and activation of SHH and GLI1 also positively regulate the activity of the PI3K/AKT pathway leading to a feed-forward loop and the dependence

on AKT signaling[153]. AKT activation also plays a role in the activation of mTOR resulting in the activation of S6rp, p70S6K and 4E-BP1[157,158].

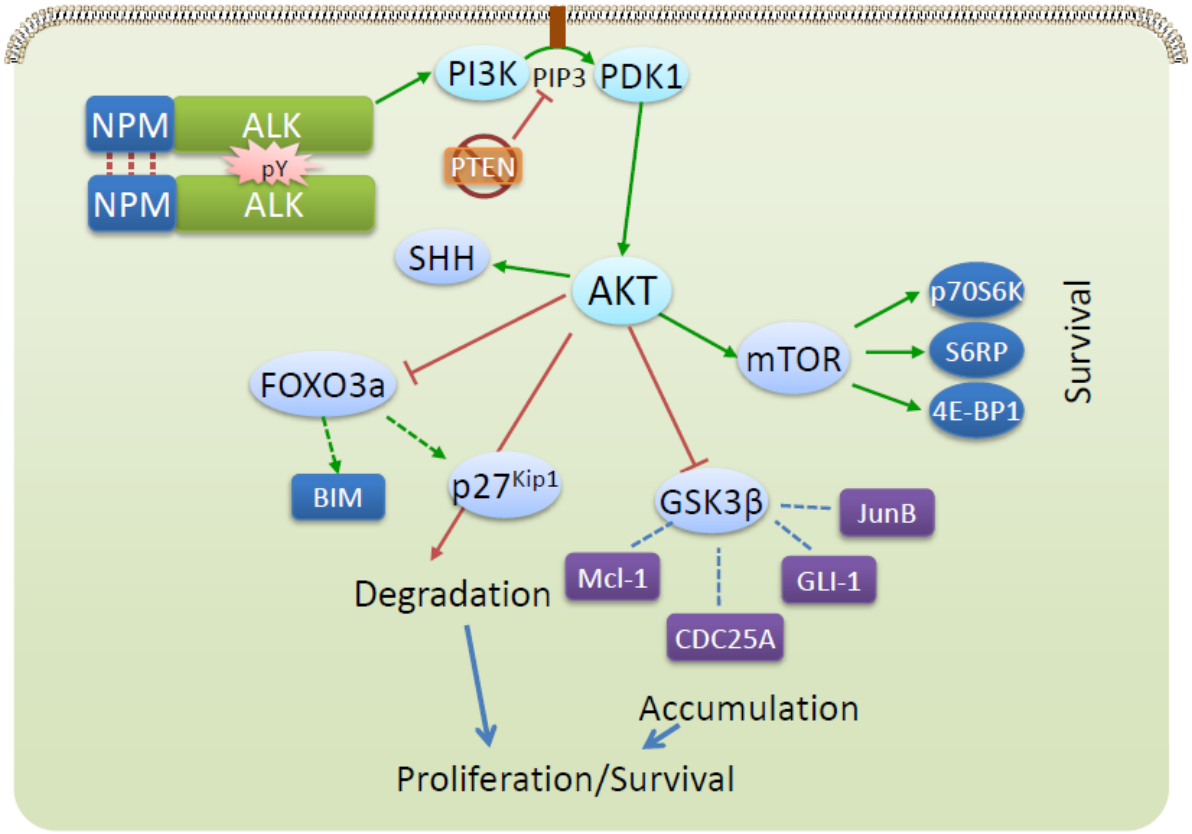

Figure 1.3: NPM-ALK induced PI3K/AKT signaling. NPM-ALK activates PI3K to phosphorylate phosphatidylinositol at the membrane surface. This recruits PDK1 to phosphorylate the serine/threonine kinase AKT. PTEN is the phosphatase responsible for the negative regulation of this pathway and is frequently lost in ALCL. AKT activates the mTOR pathway and inactivates GSK3β via serine-9 phosphorylation. Since GSK3β targets Mcl-1, CDC25A, GLI-1 and JunB for degradation, these pro-proliferation and survival protein accumulate. AKT also, targets $p27^{Kip1}$ for degradation and inhibits the FOXO3a transcription of BIM and $p27^{Kip1}$. AKT signaling potentiates Sonic hedgehog signaling through the expression of SHH and the accumulation of GLI-1.

MAPK Pathway

A third commonly studied signaling pathway driven by NPM-ALK is the mitogen-activated protein kinase (MAPK) pathway (Figure 1.4). Activation of c-Raf, MEK1/2, and extracellular signal regulated kinase 1/2 (ERK1/2) was identified in ALCL-derived cell lines and tumor samples[159]. NPM-ALK was found to activate MEK1/2 and ERK1/2 independent of c-Raf activity. Importantly, the activation of this pathway was necessary for the transformation capabilities of NPM-ALK. The activation of MEK1/2 is regulated through several signaling events. Shp2 and Grb2 were shown to interact with NPM-ALK and are necessary for the activation of MEK1/2[160,161]. Additionally, NPM-ALK induces Ras activation through binding to Shc, PLC-γ and IRS-1 which, in turn, is necessary for ERK activation and downstream activity, including AP-1 transcriptional activity[162]. The increased expression of JunB via ERK signaling is likely responsible for the increased AP-1 expression[163]. The MAPK protein Cot has also been implicated in the activation of ERK1/2 in the context of NPM-ALK[164].

Through activation of the Ras-ERK pathway, NPM-ALK is able to exert an array of downstream effects on cell proliferation and survival. Specifically, the ERK activation of mTOR results in phosphorylation of S6rp and 4E-BP1[157,165]. The mTOR activation in this context is nutrient dependent and thus involves the inhibition of TSC1/2 and the activation of Rheb. The activation of mTOR results in regulation of expression of cell cycle mediators including cyclin A, p27 and p21 while inhibiting the tumor suppressor Rb[165]. ERK activation also increases expression of Bcl-X_L and CDK4 to further increase survival and cell cycle progression respectively[159].

NPM-ALK also activates the JNK pathway[166]. Active JNK and cJun is present in ALCL-derived cell lines and tumors and physically interacts with NPM-ALK through immunoprecipitation experiments. JNK, in turn, activates cJun which controls the transcriptional activity of AP-1[166] and expression of cyclin D3 and cyclin A. Activation of cJun also down-regulates p21 allowing for increased cell cycle progression.

A characteristic biomarker for ALCL is CD30 expression on the tumor cell surface[40]. CD30 has been shown to be expressed through the NPM-ALK mediated ERK signaling[167]. ERK activated JunB is responsible for the transcriptional up-regulation of CD30[168]. CD30 cooperates with NPM-ALK to increase survival through an NF-κB mediated pathway[169].

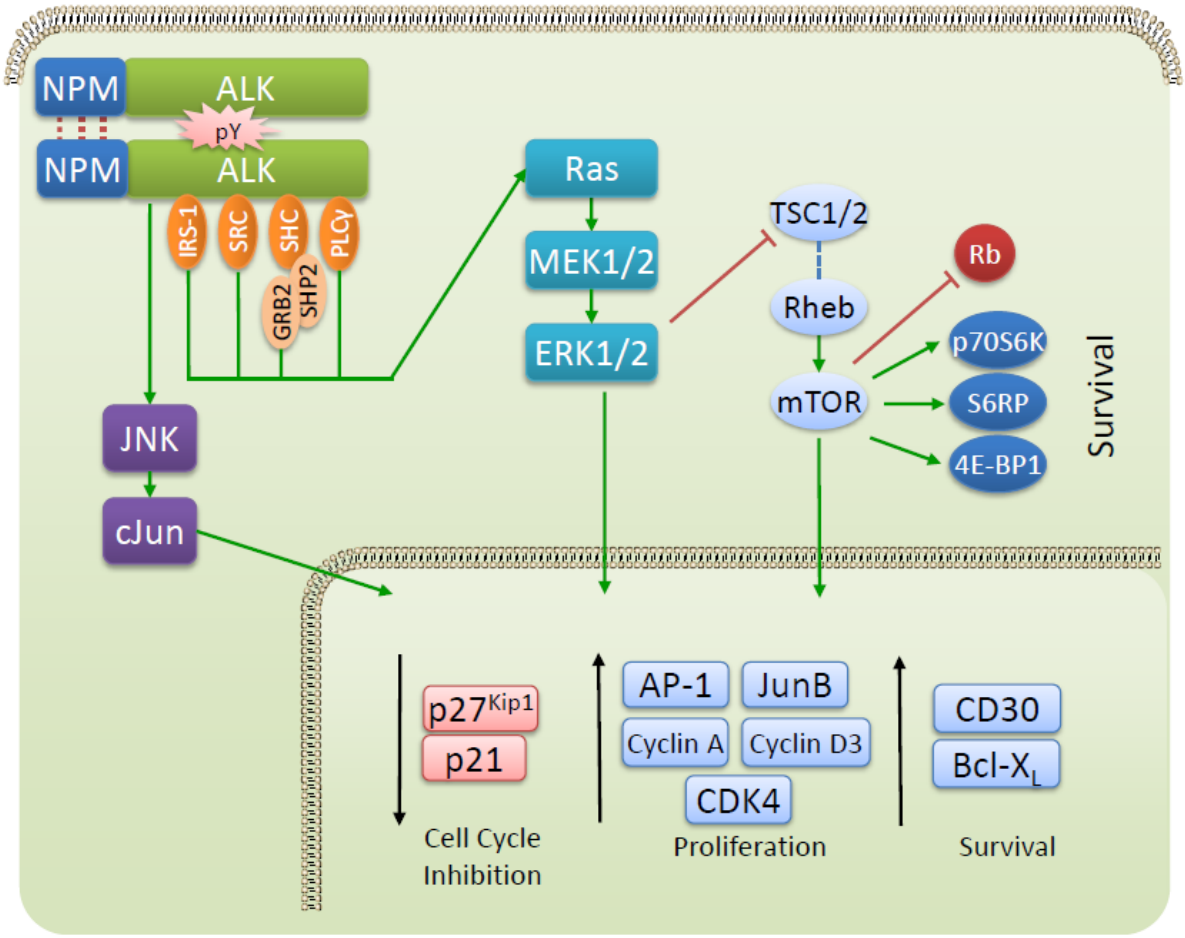

Figure 1.4: NPM-ALK induced MAPK signaling. NPM-ALK activates the Ras-MEK1/2-ERK1/2 signaling pathway through several NPM-ALK interacting proteins. IRS-1, SRC, SHC, and PLCγ have all been implicated in the activation of this pathway. ERK1/2 activity inhibits the TSC1/2 complex which frees Rheb to activate mTOR. This results in activation of p70S6K, S6RP, and 4E-BP1 and inhibition of the Rb tumor suppressor. NPM-ALK also activates the MAPK protein JNK which activates the cJun transcription factor. The activation of these pathways activates the transcription of pro-survival and proliferation genes while inhibiting the expression of cell cycle checkpoint genes.

Genomic and proteomic characterization of ALK

Large scale genomics and proteomics have been immensely important tools for the characterization of ALK mediated oncogenesis. Gene expression profiling has offered an unparalleled view of NPM-ALK driven expression patterns and insights into the classification of peripheral T-cell lymphomas. Results from patient samples and cell lines reveal major differences between ALK+ and ALK- ALCL including the overexpression of *BCL6, PTPN12,* and *CEBPB* while underscoring the importance of the STAT3 signaling pathway[170,171]. Importantly, gene expression profiling has provided insights into the classification of ALK+ALCL from other T-cell NHLs[171,172].

In addition to gene expression analysis, proteomic studies have offered further insight into the signaling mechanism driven by NPM-ALK. These screening approaches are capable of generating novel hypotheses for the identification of ALK signaling mediators. Interactome studies, either through co-immunoprecipitation or tandem affinity purification, were capable of identifying previously known and novel ALK interacting proteins[173]. Specifically, Crockett et al. identified many known ALK interacting proteins including PI3K, JAK3, STAT3, GRB2, IRS1 and PLCγ[174]. Additionally, they identified many unknown ALK interacting proteins including those involved in the MAPK signaling pathway that were later validated to be important in ALK regulated oncogenesis (MEK1, JNK, MAPK1, etc). Determination of the protein expression changes induced by NPM-ALK was carried out by Lim et al. through isotope-coded affinity tag (ICAT) followed by LC-MS/MS[175]. This study identified the

NPM-ALK regulation of protein expression involved in cell proliferation, ribosome synthesis, survival, angiogenesis and cytoarchitectural organization.

The use of proteomics for the identification of novel mediators of ALK signaling can be extended to proteins that may not physically interact with ALK through the use of techniques pioneered by Rush et al[176]. Phosphotyrosine-specific antibodies are used to purify the phosphoproteome prior to mass spectrometry analysis. Adaptations of this technique have proven successful in the identification of novel mediators of ALK signaling[149,160,177,178]. Interestingly, this technique was employed in NSCLC and resulted in the discovery of the EML4-ALK translocation in these tumors[82]. Since NPM-ALK is a driving and constitutively active kinase in ALCL, these phosphoproteomic strategies are sensitive to the changes in protein phosphorylation under differing ALK expression and activation conditions. While these screening studies provide powerful opportunities for discovery, it is the downstream biological validation that is important for understanding ALK directed tumorigenesis.

Pharmacological Inhibition of ALK

With the identification of NPM-ALK as a driving oncogene in ALCL, ALK kinase inhibitors have become an area of high therapeutic interest. Targeting ALK activity with small molecule inhibitors was first reported by Wan et al through the use of fused pyrrolocarbazoles[179]. Treatment of these compounds of ALK+ ALCL derived cell lines resulted in decreased NPM-ALK phosphorylation and inactivation of downstream signaling mechanisms including STAT3, AKT and ERK1/2. These

biochemical effects accompanied a decrease in cell proliferation and an increase in apoptosis. These studies provided rationale for the pharmacological inhibition of ALK as a promising therapeutic target in cancers expressing deregulated ALK.

The current leading compound for the inhibition of ALK is Crizotinib (PF-02341066)[180]. Crizotinib was originally designed as a c-Met (aka hepatocyte growth factor receptor (HGFR)) inhibitor and an improvement on the chemical structure known as PHA-665752. The co-crystal structure of c-Met with PHA-665752 allowed for the generation of compounds with improved chemical interactions and pharmaceutical properties. The lead compound, Crizotinib (2-amino-5aryl-3-benzyloxypyridine series) has a molecular weight of 450.34 and an improved distribution coefficient (log D = 1.96) compared to PHA-665752[180]. Crizotinib inhibits ALK with a cellular IC_{50} of 8.0 nM against c-Met. The selectivity of Crizotinib was investigated against a panel of more than 120 human kinases. Through this study, ALK was identified as a potent target of Crizotinib, with an IC_{50} of 20 nM[180]. The next kinase to be targeted is RON with a 10-fold less potency that c-Met. Thirteen kinases are inhibited by Crizotinib within a 100-fold range of c-Met.

Crizotinib shows strong pre-clinical efficacy in ALK and c-Met driven tumors[181-183]. Crizotinib treatment results in cell cycle arrest, reduced proliferation and reduced tumor xenograft growth in ALCL derived cell lines[181]. Specifically, SCID-Beige mice harboring Karpas299 xenograft tumors saw a complete regression in tumor volume after 15 days of 100mg/kg, QD oral dose of Crizotinib. Dosing was stopped at day 17 and tumors re-grew. Interestingly, when dosing resumed on day 62, complete regression of tumors was again observed after 14 days of treatment[181].

Crizotinib has shown clinical success and is currently FDA approved for the treatment of NSCLC harboring ALK translocations[184]. This clinical study on 82 patients with ALK+ NSCLC showed a 57% response rate from Crizotinib while 33% of the patients retained stable disease[184]. While clinical trials for Crizotinib in ALCL are still underway, initial findings in 2 patients with relapsed disease showed complete regression of lesions and report at least 5 months of sustained response[185]. Preliminary results from clinical studies with Crizotinib in IMT showed one patient with complete radiographic remission following 1.5 years of Crizotinib treatment, while a second patient showed no response to therapy[186].

While initial treatment with Crizotinib shows broad success, the tumors have been shown to acquire resistance to this therapy. Initial response to therapy lasts between 4 to 34 months with an average of 10.5 months[187]. Mechanisms for Crizotinib resistance are varied. The point mutation L1196M EML4-ALK was shown to be resistant to Crizotinib treatment in cell lines[188]. However, this mutation remained sensitive to other structurally distinct ALK inhibitors (NVP-TAE684 and AP26113). Other mutations such as F1174L, G1202R, S1206Y and 1151Tins as well as EML4-ALK gene amplification were found to confer Crizotinib resistance in cell lines and patient samples[187,189]. In addition to changes to the *ALK* gene, ALK+ NSCLC patients were shown to acquire Crizotinib resistance through the activation of other kinases such as KIT and EGFR.

The clinical trials with ALK inhibitors, such as Crizotinib, have made progress in the treatment of ALK deregulated cancers. However, challenges remain with the high chance of resistance to this form of therapy. Further work to identify second

round ALK inhibitors or combined therapies will likely improve the success of sustained remission of these diseases.

CANCER METABOLISM

Cancer cells exhibit very different metabolic requirements than normal cells. While normal cells focus their metabolic needs toward energy (ATP) production, cancer cells on the other hand, require the synthesis of biomass (nucleotides, amino acids, lipids) as a fundamental necessity for cell division[190]. The important distinction between cancer cell and normal cell metabolism was first identified by Otto Warburg and is generally termed the "Warburg effect" or aerobic glycolysis[191,192]. Warburg observed that cancer cells tend to "ferment" glucose into lactate even under the presence of abundant oxygen and based on these observations, Warburg suggested that cancer arises from a defect in oxidative phosphorylation (Figure 1.5).

The conceptual explanation for a cancer cell's requirement to divert its metabolism away from oxidative phosphorylation lies in the limiting requirements for proliferating cells. It is well known that oxidative phosphorylation is very efficient in producing energy, turning out 18 times more ATP than glycolysis. However, ATP may not be the limiting factor in rapidly proliferating cells[190,193]. Instead, a dividing cell must replicate its entire contents in order to successfully divide into two daughter cells. It is this biomass (amino acids, lipids and nucleic acids) that becomes the limiting factor for cell division. Consequently, tumor cells reduce their reliance on the

TCA cycle and oxidative phosphorylation. When a molecule of glucose passes all the way through glycolysis and the TCA cycle, it is completely catabolized into CO_2 and H_2O in an effort to extract maximal energy from every molecule of glucose. However, the end products of this catabolism are essentially useless to a dividing cell. Instead, the shutting down of the TCA cycle allows for build-up of glycolytic intermediates which then can be diverted from cellular respiration and energy production to serve as the starting materials for biomass production[190]. The observed increase in lactate production is a necessary byproduct of a metabolism based heavily on glycolysis. NADH is consumed through glycolysis and can be regenerated by the conversion of pyruvate to lactate. It is this drive to maintain the NAD+/NADH redox balance that makes the elevated flux to lactate necessary.

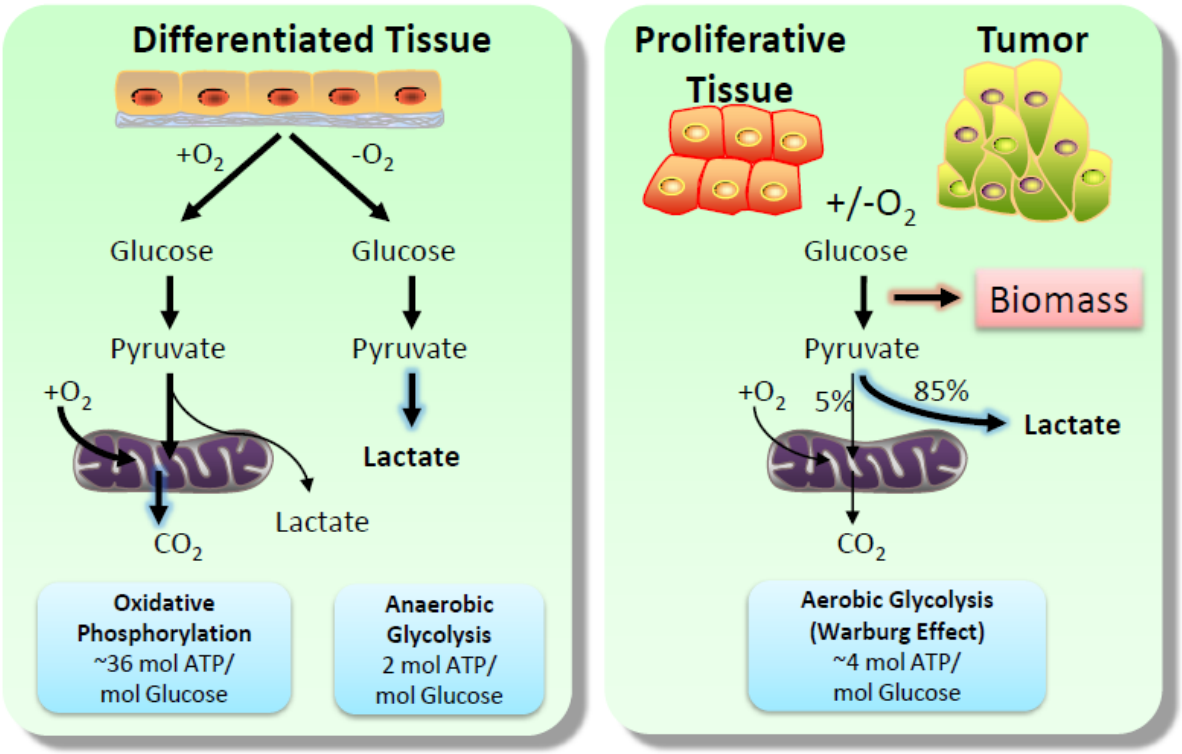

Figure 1.5: Metabolic programing in normal and proliferating tissues. Normal differentiated tissues utilize two distinct metabolic programs based on the availability of oxygen. In the presence of oxygen, glucose is catabolized completely to CO_2 and H_2O through the TCA cycle and oxidative phosphorylation. This allows for the maximal amount of energy to be extracted from each molecule of glucose. In the absence of oxygen, glycolysis alone is used for glucose breakdown and lactate is generate to maintain redox balance. In proliferating tissue including tumors aerobic glycolysis is utilized regardless of oxygen availability. About 85% of glucose is converted to lactate, 5% is shuttled into the TCA cycle and the remaining is used to produce biomass necessary for proliferation.

Much of the biomass needed for cell proliferation originates from intermediates of glycolysis (Figure 1.6). Nucleotide synthesis is dependent on the production of ribose-5-phosphate through the pentose phosphate pathway originating from the upper half of glycolysis. Lipid synthesis originates from several metabolites in glycolysis including glyceraldehyde-3-phosphate and 3-phosphoglycerate as well as acetyl-CoA. The amino acids serine glycine and

cysteine are generated from 3-phosphoglycerate in glycolysis, while alanine can be generated from pyruvate. It is this dependence on glycolytic intermediates that drives cancer cells to increase the glycolytic flux while decreasing oxidative phosphorylation.

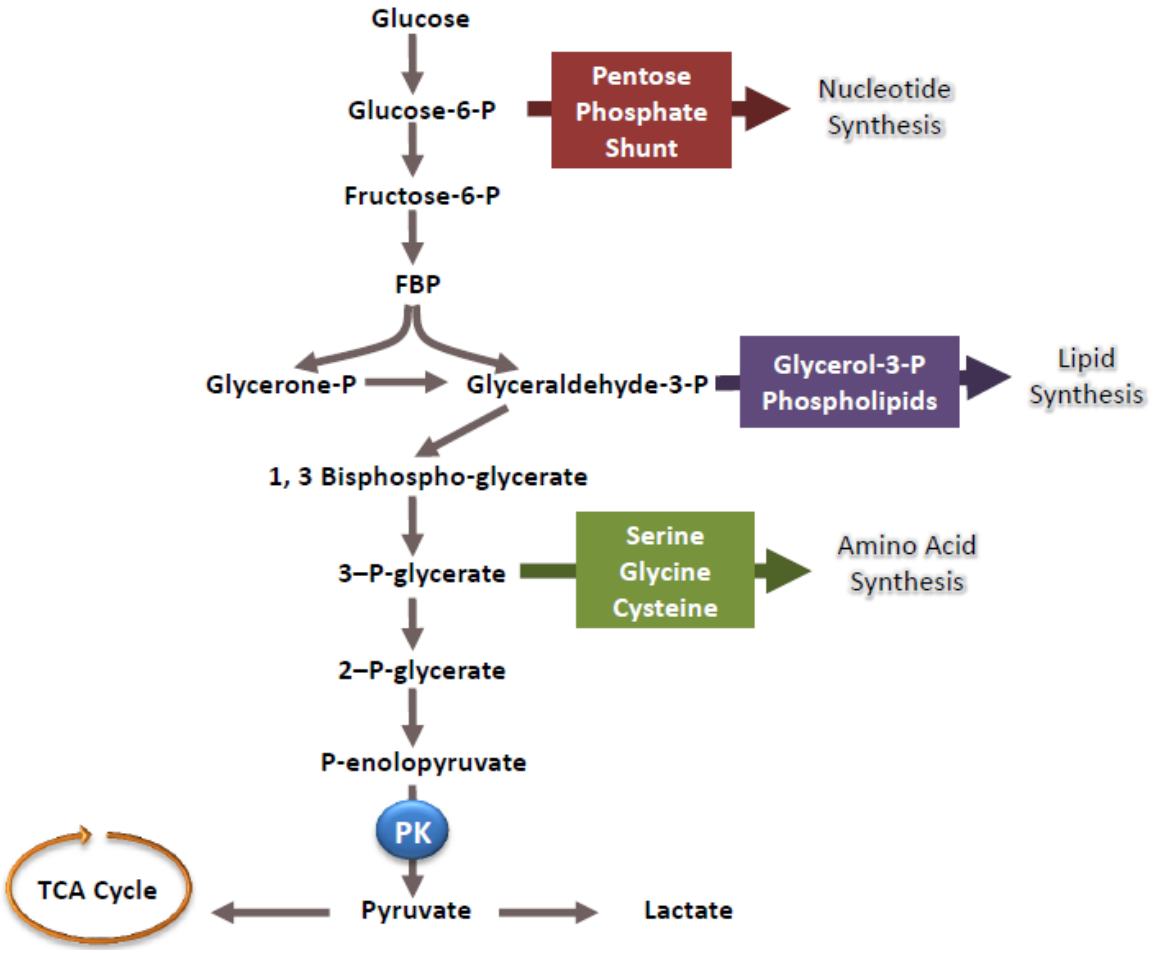

Figure 1.6: Glycolysis provides precursors for biomass production. Many biosynthetic pathways originate from glycolytic intermediates. The pentose phosphate pathway which produces the ribose backbone for nucleotide synthesis originates from glucose-6-phosphate. Much of lipid synthesis originates from glyceraldehyde-3-phosphate. Serine, glycine, and cysteine metabolism originates from 3-phospho-glycerate and also provides precursors for other amino acid synthesis. Through the negative regulation of pyruvate kinase at the end of glycolysis, these glycolytic intermediates can accumulate and become available for biomass production.

Regulation of Cancer Metabolism by Signaling

Cancer cells achieve this metabolic rewiring through a variety of mechanisms including activation of growth factor signaling, deletion of tumor suppressor activity and initiation of oncogenic transcriptions programs.

PI3K/AKT/mTORC1

The PI3K/AKT pathway is activated downstream of many growth factor receptors and is deregulated in many human cancers[194]. The activation of AKT leads to increased glucose uptake and glycolytic rate[195]. AKT increases expression of Glut1 glucose transporter and the translocation of Glut4 to the cell surface, allowing for more glucose uptake into the cell[196,197]. Hexokinase 1 (HK1) and 6-phosphofructo-2-kinase (PFK-2) are also activated by AKT which traps glucose inside the cell and commits it to glycolysis, respectively[197,198]. AKT also exerts metabolic control through TCA cycle driven effects. ATP-citrate lyase (ACLY) is phosphorylated and activated by AKT, promoting the removal of citrate from the TCA cycle and directing it toward lipid synthesis[199-201].

An important downstream mediator of AKT signaling is the mTOR complex 1 (mTORC1). Activation of mTORC1 has been shown to regulate cell mass/size through the regulation of protein synthesis[202]. The activation of mTORC1 by AKT is orchestrated through the phosphorylation and inhibition of TSC1/TSC2 complex and allows for the activation of mTORC1 by Rheb. Additionally, mTORC1 is activated in response to cellular energy depletion, in which low ATP/AMP ratios activate AMPK to phosphorylate TSC2 and Raptor[203,204]. mTORC1 activation regulates a broad

network of metabolic genes that contributes to the cancer metabolic phenotype[205]. Specifically, mTORC1 activation induces HIF-1α expression in order to drive expression of glycolytic genes and consequent increased glycolytic flux. This is coupled with the decrease in oxidative phosphorylation through the expression of pyruvate dehydrogenase kinase 1 (PDK1) to inhibit PDH activity[206]. Furthermore, mTORC1 targets SREBP expression to drive lipid synthesis and the pentose phosphate pathway[205].

c-Myc

The c-Myc transcription factor also plays a major role in the reprogramming of cancer metabolism. c-Myc is deregulated in many cancers and offers a mechanism through which metabolic reprograming occurs through gene regulation[207]. Many glycolytic enzymes are targets of c-Myc transcriptional activity, including GLUT1, phosphoglucose isomerase, phosphofructokinase, glyceraldehyde-3-phosphate dehydrogenase, phosphoglycerate kinase, enolase and lactate dehydrogenase[208,209]. The increased expression of glycolytic enzymes increases glucose uptake, glycolytic rate and lactate production, all of which are important contributors to the Warburg effect. Interestingly, the increased glucose uptake by cancer cells has long been used for the imaging of human cancers using ^{18}F-fluorodeoxy-glucose positron emission tomography (^{18}FDG-PET)[210]. A recent study suggests that in many patients, the high level of ^{18}FDG uptake is likely due to deregulation of c-Myc in the tumor cells[211].

Apart from its role in up-regulating glycolysis, c-Myc exerts control over mitochondrial biogenesis and respiration. Overexpression of c-Myc causes an increase in mitochondrial mass and oxygen consumption[212]. While this may seem counterproductive to the aim of the Warburg effect, the increased mitochondrial activity is a result of c-Myc driven glutamine metabolism. c-Myc increases glutamine uptake through the induction of glutamine transporters ASCT2 and SLC7A5[213]. Also, glutamine catabolism is increased through the expression of mitochondrial glutaminase (GLS). c-Myc represses expression of miR-23a/b which down regulates GLS levels. This increased glutaminolysis provides carbon and nitrogen molecules to biomass production, as well as feeding into the TCA cycle as α-ketoglutarate for increased energy production. The role of c-Myc driven glutamine metabolism offers a counterview of the Warburg effect, in which glycolysis is uncoupled from the TCA cycle and cancer cells become addicted to both glucose and glutamine.

Regulation of glycolysis

Cancer cells adapt ways to tightly regulate glycolysis in order to drive biomass production. Pyruvate kinase M2 (PKM2) can be phosphorylated by growth factor receptors to reduce its activity[214]. This will be discussed further in the next section. However, the reduced PKM2 activity corresponds to an alternate glycolytic pathway that takes place in many cancer cells. Pyruvate is generated in the absence of PKM2 activity through the donation of the phosphate on phosphoenolpyruvate (PEP) to phosphoglycerate mutase (PGAM1)[215]. This phosphorylated PGAM has increased activity and thus leads to a positive feedback

loop which increases pyruvate and lactate generation. Furthermore, PGAM1 activity provides feedback to the biomass producing pathways. 3-phosphoglycerate (3-PG) (substrate of PGAM1) inhibits the pentose phosphate pathway through binding to 6-phosphogluconate dehydrogenase (6PGD), while 2-phosphoglycerate (product of PGAM1) activates 3-phosphoglycerate dehydrogenase (PHGDH) which drives serine biosynthesis[216].

Lactate production through the activity of lactate dehydrogenase (LDH) is also highly regulated in cancer metabolism. While increased LDH expression levels are driven by HIF-1α and c-Myc, posttranslational regulation of LDH is also important in regulating cancer growth[209,217]. Fibroblast growth factor receptor (FGFR1) phosphorylates LDHA at the Y10 and Y83 residues and results its increased enzymatic activity and increased lactate production. Lactate production is necessary to maintain the NADH/NAD+ redox balance[218]. The blocking of LDHA phosphorylation results in a shift toward oxidative phosphorylation in order to obtain a similar redox balance. The increased lactate production in cancer cells, not only helps to balance the redox potential in cells operating under aerobic glycolysis, but it fuels respiration as well. Tumors contain hypoxic as well as oxygenated regions as a result of the poor blood supply feeding them. Therefore, the cells in the tumor that generate abundant lactate provide this metabolite to well oxygenated cells to support oxidative metabolism[219].

Pyruvate Kinase M2

One of the genes that have been implicated in driving the Warburg Effect is Pyruvate Kinase M2 (PKM2). Pyruvate kinase is the enzyme responsible for catalyzing the final step in glycolysis: the conversion of phosphoenolpyruvate to pyruvate while producing ATP. It exists in four isoforms which differ in their tissue distribution and activity (Table 1.2). Pyruvate kinase L (PKL) isoform is expressed in liver, kidney and intestinal tissues while Pyruvate kinase R (PKR) isoform is expressed in erythrocytes[220]. PKM1 isoform is expressed in brain and muscle tissue and has no known regulators of its high level of activity. Finally, PKM2 is the isoform that is expressed in all proliferating cells including embryonic cells, adult stem cells and tumor cells, giving it the classification as the "tumor specific" isoform. While PKL and PKR are encoded by separate genes, PKM1 and PKM2 are splice variants of the same gene (PKM) (Figure 1.7). Skipping exon 9 and including exon 10 results in the production of a regulatable form of pyruvate kinase (PKM2). It was recently shown that PKM2 helps to drive tumor growth and that this is reversed with forced expression of PKM1[221].

Table 1.2: Isoforms of pyruvate kinase

	PKM1	PKM2	PKL	PKR
Tissue Distribution	Brain, Muscle	Proliferating cells, stem cells, tumor cells	Liver, Kidney, Intestine	Erythrocytes
Encoding Gene	PKM	PKM	PKL	PKR
# Amino Acids	531	531	543	574
Kinetic Characteristics	Tetrameric with high PEP affinity	Tetrameric with high PEP affinity Dimeric with low PEP affinity	Tetrameric with low PEP affinity	Tetrameric with low PEP affinity
Regulation	None	FBP Phosphorylation Oncoprotein and peptide binding	FBP Inhibited by ATP Inhibited by cAMP-dependent phosphorylation Regulated by diet	FBP Inhibited by ATP Inhibited by cAMP-dependent phosphorylation Regulated by diet

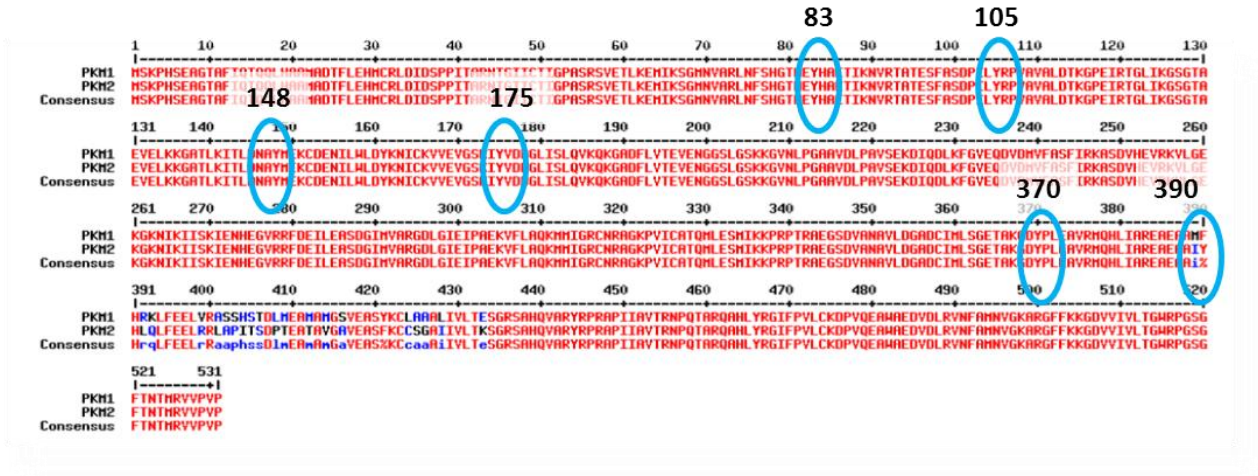

Figure 1.7: Sequence alignment of PKM1 and PKM2. Sequence alignment of PKM1 and PKM2 shows region of differential exon splicing between residues 389 and 433. Circles identify tyrosine residues that have been shown to be phosphorylated by proteomic studies.

PKM2 in its most active state exists as a homo-tetramer. The binding of its allosteric regulator fructose-1,6-bisphosphate (FBP) locks PKM2 into its tetramer form increasing its activity[222]. When this tetramer is disrupted, the resulting dimer form of PKM2 is significantly less active. It is this ability for PKM2 to be regulated (unlike PKM1) that is utilized by tumor cells to adjust their metabolism to favor growth and proliferation. By reducing the activity of PKM2, the metabolites flowing through glycolysis become backed-up and start to accumulate in the cell. This allows for the diversion of these metabolites into alternative metabolic pathways designed for the production of biomass (Figure 1.8).

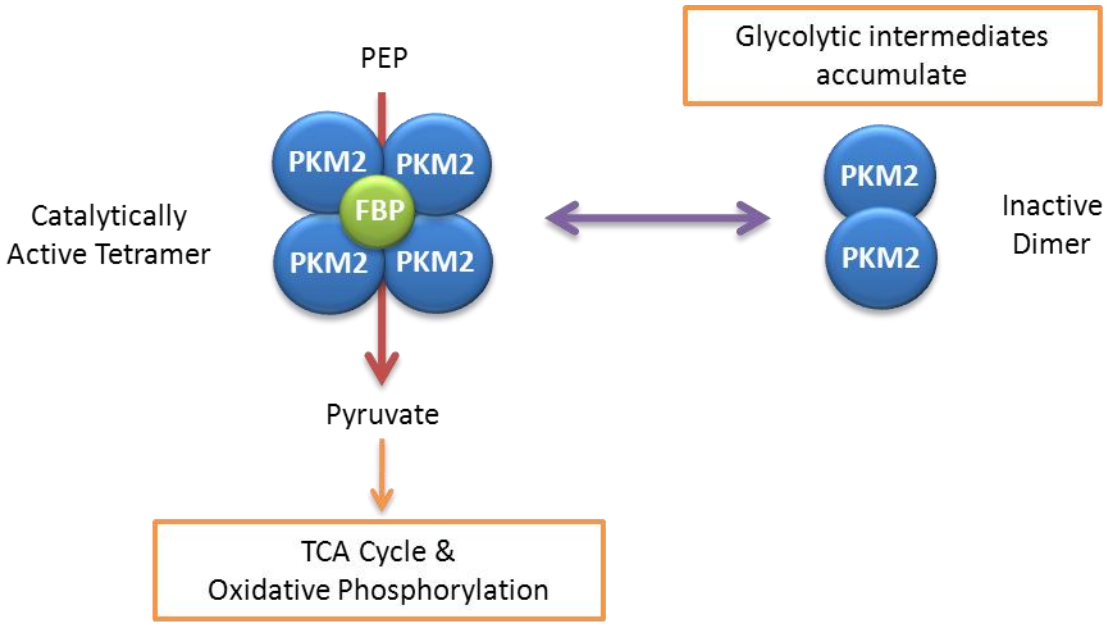

Figure 1.8: Regulation of PKM2 activity. In its most active state, PKM2 exists in a tetramer conformation, stabilized by FBP. The rapid conversion of PEP to pyruvate supports oxidative metabolism in which pyruvate is catabolized in the TCA cycle. The tetramer can be disrupted via phosphorylation of PKM2 or through binding to phosphorylated peptides. The resulting dimer conformation is less active and allows for the accumulation of glycolytic intermediates, which can be used for biomass production.

Cancer cells have been shown to regulate PKM2 in several ways. The first was observed when PKM2 was found to be a phosphotyrosine binding protein[223]. Here, PKM2 was found to bind to peptides containing phosphotyrosine residues. The consequence of this was the disruption of FBP binding and inhibition of PKM2 enzymatic activity. This leads to the diversion of metabolites to anabolic processes that support cell growth. Since many tumors have abundantly active tyrosine kinase signaling, the phosphotyrosine binding properties of PKM2 provide the nexus between oncogenic kinase signaling and tumor metabolism.

A second observation on how PKM2 is regulated by cancer cells came in the more direct link between kinase signaling and PKM2 activity. A phosphoproteomic screening of ZNF198-FGFR1 expressing cells identified several PKM2 tyrosine residues as potential phosphosites regulated by this constitutively active oncogene (Figure 1.7)[224]. It was discovered that Y105 of PKM2 can be directly phosphorylated by FGFR1 as well as several other oncogenic tyrosine kinases. This Y105 phosphorylation was also shown to disrupt FBP binding and thus inhibit PKM2 enzymatic activity, resulting in a proliferative advantage.

PKM2 has become a promising target for the therapeutic intervention of cancer metabolism. PKM2 activating compounds have shown feasible in pre-clinical studies to regulate tumor growth[225,226]. Although these reagents are not particularly cytotoxic, they do reduce proliferation and limit tumorigenesis, providing rationale for PKM2 activation in a clinical setting[225]. Interestingly, several groups are also developing PKM2 inhibitors and cancer therapeutics[227-229]. The rationale follows that PKM2 is selectively expressed in tumor cells and is necessary for oncogenesis.

Shikonin is one active compound that has inhibitory effects on PKM2. Interestingly, Shikonin selectively inhibits PKM2 while PKM1 is unaffected, allowing for efficient tumor targeting[228]. PKM2 inhibitors can decrease the rapid glycolytic rate that is characteristic of tumor cells and induce cell death[229]. The fact that PKM2 activators and inhibitors are promising anti-cancer agents, makes the oncogenic regulation of this enzyme highly important. This suggests that either completely active or completely inactive PKM2 is detrimental to oncogenesis and finding the "sweet spot" in enzymatic activity is necessary for metabolic reprogramming and biomass generation. Alternatively, new roles for PKM2 in transcriptional regulation and protein phosphorylation have recently been uncovered[230-234]. To date, the PKM2 activators and inhibitors have only been tested against the ability of PKM2 to convert PEP to pyruvate and it is unclear how they affect PKM2's other cellular roles.

SUMMARY AND RATIONALE

Mutations involving the *ALK* gene are involved in the pathogenesis of many cancer types. A comprehensive understanding of the signaling mechanisms driven by ALK to induce oncogenesis is necessary for the development of effective therapeutic agents that target these cancers. Furthermore, while other tyrosine kinases have been shown to induce metabolic changes, the role for ALK in metabolic regulation is unknown. The following studies aim to identify novel mediators of ALK signaling with an emphasis on proteins involved in cellular metabolism.

CHAPTER 2

Integrated Phosphoproteomic and Metabolomic Analysis Reveals NPM-ALK Driven Metabolic Reprogramming

ABSTRACT

The mechanisms underlying the pathogenesis of NPM-ALK expressing anaplastic large cell lymphoma (ALCL) are not completely understood. To identify novel mediators of NPM-ALK signaling we pursued an unbiased phosphoproteomic screen. Many metabolic proteins and pathways were shown to be altered by NPM-ALK activity. Therefore, an untargeted metabolomics screen was utilized to characterize the metabolic changes driven by NPM-ALK activity. Dramatic metabolic changes were observed in glycolysis and many of the biomass producing pathways. Integrating the phosphoproteomic and metabolomic data highlighted the changes in glycolysis, TCA cycle and nucleotide metabolism. Metabolic flux analysis characterized the carbon flux through these key pathways and illustrated a NPM-ALK driven metabolic shift from energy production toward biomass production. These data establish the first link between NPM-ALK and metabolic regulation while providing a global and integrated view of these metabolic regulations.

INTRODUCTION

Anaplastic large cell lymphoma (ALCL) is a subtype of peripheral T-cell lymphoma representing 3% of adult non-Hodgkin lymphomas and 10-15% of all childhood lymphomas[40]. They are aggressive tumors characterized by large cells with abundant cytoplasm and multiple pleomorphic nuclei. The World Health Organization (WHO) classification of lymphoid malignancies recognizes two forms of systemic ALCL based on the presence of chromosomal translocations in the anaplastic lymphoma kinase (*ALK*) gene[47]. The t(2;5)(p23;q35) translocation involves *ALK* gene at 2p23 locus and the Nucleophosmin (*NPM*) gene at 5q35 and is present in more than 80% of pediatric ALCLs. The resulting expression of the constitutively active tyrosine kinase (NPM-ALK) drives oncogenesis in these tumors[49]. *ALK* encodes a receptor tyrosine kinase of the insulin receptor superfamily which is involved in neural development[35]. Mutations of the full length *ALK* receptor have been identified in a subset of sporadic and inherited neuroblastomas[101]. The oncogenic potential of NPM-ALK has been demonstrated by its ability to activate numerous canonical growth factor signaling pathways including PI3K/AKT, JAK/STAT, PLCγ[112,145,149,174,175,235].

Cellular reprogramming of energy metabolism is an emerging hallmark of cancer [236]. Metabolic reprogramming via the “Warburg effect” is characterized by alternate glycolysis and increased lactate production even in the presence of abundant oxygen [192]. While resting cells need to continuously produce energy, proliferating neoplastic cells shift their metabolism toward biomass (nucleic acids, amino acids, lipids) production in order to accumulate material required for further

replication[193].

Recent technical developments in large-scale mass spectrometry-based phosphoproteomic analysis have demonstrated the powerful potential for rapid discovery of multiple kinase substrates that are deregulated in cancer [237,238]. The analysis of phosphoproteins at a global level has been a technical challenge due to a number of factors including their low abundance, lability of the phosphorylation and substoichiometric phosphorylation-site occupancy of phosphoproteins[239]. Thus, robust methods to isolate maximal number of phosphopeptides with high reproducibility and specificity are required to carry out phosphoproteome analysis. Metal oxide affinity chromatography (MOAC) followed by immunoprecipitation using phosphotyrosine-specific antibodies (pY-IP) to enrich for phosphotyrosine (pY) peptides followed by standard LC-MS/MS analysis for large scale identification of phosphopeptides and phosphorylation sites have been successfully used to identify signaling proteins in cancer[178]. Similarly, metabolomic profiling using GC/LC-MS represents a powerful method for unbiased global measurement of small molecules that impact various aspects of cancer metabolism[240]. Integration of these two powerful large scale approaches has not been explored to elucidate the pathogenesis of NPM-ALK positive ALCL.

To identify novel proteins/pathways that mediate NPM-ALK signaling, we employed a phosphoproteomic study which revealed that numerous proteins within cellular metabolic pathways were regulated by NPM-ALK. Thus, we explored the hypothesis that NPM-ALK regulates cellular metabolism to promote tumorigenesis. We subsequently carried out a mass spectrometry-based metabolomic study in

order to characterize the NPM-ALK-driven metabolic signature. Integrated analysis of the phosphoproteomic and metabolomic studies led to the discovery and characterization of a metabolic switch induced by NPM-ALK. These studies provide a link between NPM-ALK signaling and metabolic regulation on a global scale. We also point to specific modes of metabolic regulation that drive biomass production which is necessary for tumor cell proliferation.

MATERIALS AND METHODS

Cell Culture: All ALCL-derived cell lines (SU-DHL-1, DEL, Karpas299, SUPM2) were maintained in RPMI 1640 supplemented with 10% FBS in 5% CO_2 humidified incubators.

Compounds: ALK inhibitor CEP-26939 (CEP) was acquired from Cephalon [241]. PKM2 activators NCGC00186528 (TEPP-46) and NCGC00186527 (NCGC-527) were provided by the NIH Chemical Genomics Center. Both compounds are from the thieno-[3,2-b]pyrrole[3,2-d]pyridazinone chemical class [225].

Phosphoproteomics: Sixty million cells were treated for 6 hours with CEP or DMSO. Cells were lysed with 9M urea/20mM HEPES pH8.0/0.1%SDS and a cocktail of phosphatase inhibitors (sodium orthovanadate, sodium pyrophosphate and β-glycerophosphate). For each sample, 6mg of protein were reduced with 4.5mM DTT for 30min at 60°C, alkylated with 10mM iodoacetamide for 30min at room temperature in the dark and then digested with trypsin overnight at 37°C. Samples were desalted on a C18 cartridge (Sep-Pak plus C18 cartridge, Waters), then dried before any further processing. Each sample was prepared in triplicate. Metal oxide

affinity chromatography (MOAC) was performed using titanium dioxide (TiO_2) microparticles from GL Sciences Inc (Titansphere® Phos-TiO, GL Sciences Inc., Torrance, CA) in a microparticles-to-protein ratio of 6/1 (w/w). Hydrophilic phosphopeptides were eluted with 5% ammonium hydroxide solution and hydrophobic phosphopeptides were eluted with 5% pyrrolidine solution. After elution, peptides were dried. The equivalent of 5mg of protein was further enriched for phosphorylated tyrosine peptides by overnight immunoprecipitation using a cocktail of anti-phosphotyrosine antibodies (4G10, Millipore /PT-66, Sigma/p-Tyr-100, Cell Signaling Technology). After elution, phosphotyrosine peptides were dried.

Samples from MOAC were reconstituted in 25µl loading buffer (0.1% TFA/2% acetonitrile) while samples from MOAC followed by pY-IP were reconstituted in 35 µl loading buffer. LTQ Orbitrap XL(ThermoFisher) in-line with Paradigm MS2 (Michrom bioresources) was employed for acquiring high-resolution MS and MS/MS data. Ten µl of the peptides was loaded onto a sample trap (Captrap, Bruker-Michrom) that was in-line with a nano-capillary column (Picofrit, 75µm i.d.x 15µm tip, New Objective) packed in-house with 10 cm of MAGIC AQ C18 reverse phase material (Michrom Bioresource). Two different gradient programs, one each for MOAC and phosphotyrosine immunoprecipitation samples, were used for peptide elution. For MOAC samples, a gradient of 5-40% buffer B (95% acetonitrile/1% acetic acid) in 135 min and 5 min wash with 100% buffer B followed by 30 min of re-equilibration with buffer A (2% acetonitrile/1% acetic acid) was used. For phosphotyrosine immunoprecipitation samples, which were much less complex mixture of peptides, 5-40% gradient with buffer B was achieved in 75 min followed by 5 min wash with

buffer B and 30 min re-equilibration. Flow rate was ~0.3µl/min. Peptides were directly introduced into the mass spectrometer using a nano-spray source. Orbitrap was set to collect 1 MS scan between 400-2000 m/z (resolution of 30,000 @ 400 m/z) in orbitrap followed by data dependent CID spectra on top 9 ions in LTQ (normalized collision energy ~35%). Technical duplicate data for each of the MOAC and triplicate data for phosphotyrosine immunoprecipitation samples were acquired.

RAW files were converted to mzXML using msconvert. The mass spectrometry data was then searched with the Swissprot Human taxonomic protein database (2012_04 release) appended with common proteomics contaminants and reverse sequences as decoys. Searches were performed with X!Tandem (version 2010.10.01.1) using the k-score plugin. The search results were then post-processed through the Trans-Proteomic Pipeline (TPP) using PeptideProphet and ProteinProphet. Spectral counts for the Trans-Proteomic Pipeline (TPP) results were obtained for each cell line using the spectral counting software ABACUS.

Metabolomics: Samples were removed from -80°C storage and placed on ice for the duration of the experiment. Triple-distilled H2O (300 µL) was added to each sample tube containing a frozen pellet, and two Process Blanks (PB) were created by placing same volume of H20 into empty tubes. Samples were re-suspended, transferred to the wells of a 1mL deep-well plate containing 2-3 3mm glass beads and homogenized for 5 minutes at room temperature (RT) by a Hard Tissue homogenizer (VWR).

Protein concentration was determined by mixing of a 2µL aliquot of homogenized sample with 198µL of Bradford reagent (Sigma B6916). Assay was performed at RT in a clear, flat bottom, shallow 96-well plate. The plate was vortexed and absorption data collected on BioTek uQuant with KC Junior software (v1.41.8) within 15 minutes after mixing sample and reagent. A 14 point calibration curve was created using bovine albumin (Sigma B4287). All measurements were performed in duplicate on the same plate.

Sample volumes for metabolomic analyses were determined by normalization to a protein content of 8 mg/mL using the formula: 8/x (mg/mL) *100= µL sample volume aliquoted. Pooled human plasma controls (HB, pooled human plasma from in-house reserve of American Red Cross supply stored at -80°C) were processed in parallel with other samples following this step.

For de-proteination the calculated volume of each sample was transferred to a 2mL deep-well plate and diluted with 8 volumes of 100% ethanol containing 13C algal amino acid mixture (Sigma-Aldrich 426199) as a recovery standard. The plate was then vortexed, centrifuged at 4750 RPM, 4°C for 10 min, and supernatant transferred to a new 2 mL deep-well plate. A pre-washed filter plate (Nunc 278010) was attached and the assembly centrifuged at 4750 RPM, 4°C for 10 min to further clarify the samples.

Two identical aliquots of each sample were transferred into glass inserts placed in custom-made 96 well aluminum plates and dried down under the stream of nitrogen

for 1.5 hr. One set of the aliquots was than prepared for GC-MS analysis and another for LC-MS.

LC-MS Method: Dried LC-MS samples were re-suspended in H2O(27µL) containing injection standards (tBoc-L-Alanine, tBoc-L-Asparagine, tBoc-L-Phenylalanine). Two solvent blanks (SB, 100% H2O with t-Boc standards) and 2 water blanks (BB, 100% H2O) were added at the end of the sample prep. All samples were then capped, vortexed at 2000 RPM for 2 minutes, and transferred to the instrument for analysis.

Samples were analyzed on an Agilent 1200 LC / 6530 qTOF LC-MS system using a Waters Acquity HSS T3 reversed-phase column (1.8 µ, 50 mm x 2.1 mm ID). For positive ion detection, mobile phase A was 100% water with 0.1% formic acid and mobile phase B was 100% methanol with 0.1% formic acid. For negative ion detection, formic acid was replaced with 0.1% ammonium bicarbonate. The gradient was as follows: 0-0.5 min 1% B, 0.5-2 min 1-99% B, 2-6 min 99% B, 6-9 min 1% B. The flow rate was 0.35 mL/min and column temperature kept at 40°C. The injection volumes for positive and negative mode were 7 µL and 12 µL respectively. Jetstream ESI source gas temperature was set to 350°C, drying gas flow rate - 10 L/min, nebulizer pressure - 30psig, sheath gas temperature - 350°C and flow rate - 11 L/min. Capillary current was set to 10.0 µA and VCap voltage - to 3500V. Inline mass calibration was performed by delivering reference masses through a dedicated inlet on mass spectrometer. Reference masses were 99.09 and 922.009 m/z (Positive mode) and 62.0009 and 981.9956 M/Z (Negative mode). Data analysis was performed using Find by Formula algorithm of the Agilent MassHunter Qualitative analysis software. Library for the analysis was constructed partially from the

authentic standards and partially by creating “Known Unknowns” from mass spectral features consistently present in a large proportion of the samples. Molecular features were identified by Molecular Feature Extractor (Agilent MassHunter component) and processed using in-house software.

GC-MS Method: The duplicate plate destined for GC analysis was transferred to a dry box (nitrogen atmosphere) and 60µL of derivitization reagent (BSTFA in anhydrous pyridine containing butylated hydroxytoluene as a derivatization standard) was added to each dried sample. Process blanks, solvent blanks (SB, 100% derivative reagent) and blank blanks were processed identically. Samples were sealed using crimp-caps, and the plate was removed from the dry box, vortexed (2000 rpm, 2 min), and incubated (60°C, 30 min) on a heat block. The GC plate was allowed to cool to RT, then transferred to the GC autosampler. GC analyses were done on an Agilent 7890A-5975C inert XL MSD GCMS instrument. Samples were injected (1 uL, split 10:1, 250C) onto a HP-5MS 5% phenyl-methyl Silox (30 m x 250 uM x 0.25 uM) column and eluted (1 mL/min H2, 60C(0.5 min hold), 10 C/min to 80C, 50 C/min to 325C, 4.5 min at 325C for 11.9 min total run time), transferred to the MSD unit (280C), ionized (EI, 70V), and scanned from 800-50 m/z after a solvent delay of 3 min (source 230C, quad at 150C). Data was analyzed using Agilent CHEMSTATION software.

Metabolomic Pathway Analysis: MetaboAnalyst 2.0 was used to generate significant pathways in metabolomics dataset. The raw data was inserted into the software and the phenotype label was set to “discrete” (DMSO vs. CEP). Identified compounds were matched based on KEGG ID. Missing values were replaced by a small value.

The data was normalized by creating a pooled average sample from DMSO group. No data transformation or data filtering was applied, while data was scaled by autoscaling (mean-centered and divided by the standard deviation of each variable). Global test was used for pathway enrichment analysis and out-degree centrality was used for pathway topology analysis. The p-value is assigned based on the coverage and change observed in a given metabolic pathway. A pathway impact score was assigned based on the location of the identified metabolites in a given pathway. A significant threshold was assigned at y=1/x for subsequent analysis. As a control, the same analysis was conducted with DMSO vs. DMSO to establish that the P value was not biased toward the coverage of metabolic pathways as the data is restricted to those metabolites that have been validated.

Metabolic Flux: Cells were treated with DMSO or CEP (300nM) for 6 hours in serum free media. Media was then changed to one containing ^{13}C-glucose for or 30 minutes. A mixture of methanol chloroform and water were used to extract metabolites from pelleted cells. Following centrifugation at 10000rpm for 5 min, supernatant containing metabolites were transferred to autosampler vials for LC-MS analysis. Agilent 1200 chromatography (Santa Clara, CA), Luna (Phenomenex, Torrance, CA) NH2 HILIC (hydrophilic interaction chromatography) column was used for chromatographic separation. Agilent 6200 series Time-of-flight mass spectrometer was used for detection and quantification. Data were processed by MassHunter workstation software, version B.04 (Agilent, Santa Clara, CA).

RESULTS

Phosphoproteomic analysis reveals NPM-ALK-mediated phosphorylation of metabolic proteins

We utilized a mass spectrometry-based phosphoproteomic strategy aimed at the identification of novel mediators of NPM-ALK signaling (Figure 2.1). A two-phase enrichment strategy that allows for the identification of serine, threonine and tyrosine phosphorylated peptides was used for LC-MS/MS. All experiments were conducted in biological triplicates with an NPM-ALK+ ALCL cell line (SU-DHL-1).

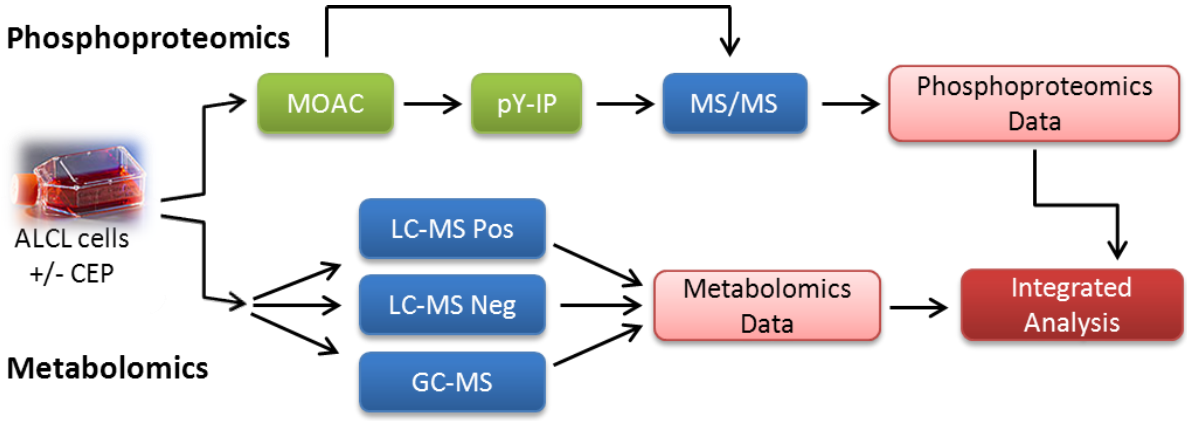

Figure 2.1: Integrated phosphoproteomic and metabolomic experimental design. NPM-ALK+ cell lines were exposed to ALK inhibitor (CEP) or DMSO. Phosphorylated peptides were enriched with metal oxide affinity chromatography (MOAC) followed by immunoprecipitation with pY antibodies and subjected to tandem mass spectrometry analysis. For the metabolomics, the cell lysates were subjected to liquid chromatography mass spectrometry (LC-MS) in both positive and negative mode, as well as gas chromatography mass spectrometry (GC-MS).

Prior to analyzing the phosphoproteome under ALK inhibition conditions, several cell lines were subjected to this analysis without drug treatment (Figure 2.2). The ALK+ cell lines SU-DHL-1 and DEL (Figures 2.2A and B, respectively) portray a

characteristic phosphoproteomic signature for cells expressing a constitutively active kinase. Plotting the number of proteins on the y-axis vs. number of phosphopeptides identified for each protein on the x-axis, reveals ALK as an extreme outlier (23 and 24 unique ALK phosphopeptides identified for SU-DHL-1 and DEL cell respectively). This was expected since ALK is known to be constitutively active and highly expressed in these cell lines. The interquartile range (IQR) was used as a threshold from which we identified known and novel ALK signaling mediators. Some of these were identified in Figure 2.2 (STAT3, SHC1, IRS-1 from SU-DHL-1 and PIK3AP1, SHC1 from DEL). Conversely, OCI-LY10 (a DLBCL cell line with no known driving oncogenic kinase) cells showed a very different phosphoproteomic signature (Figure 2.2C). Only 64 phosphorylated proteins were identified compared to over 200 for the ALK expressing cells. Furthermore, no outlier was identified and the IQR analysis finds very few proteins to be heavily phosphorylated.

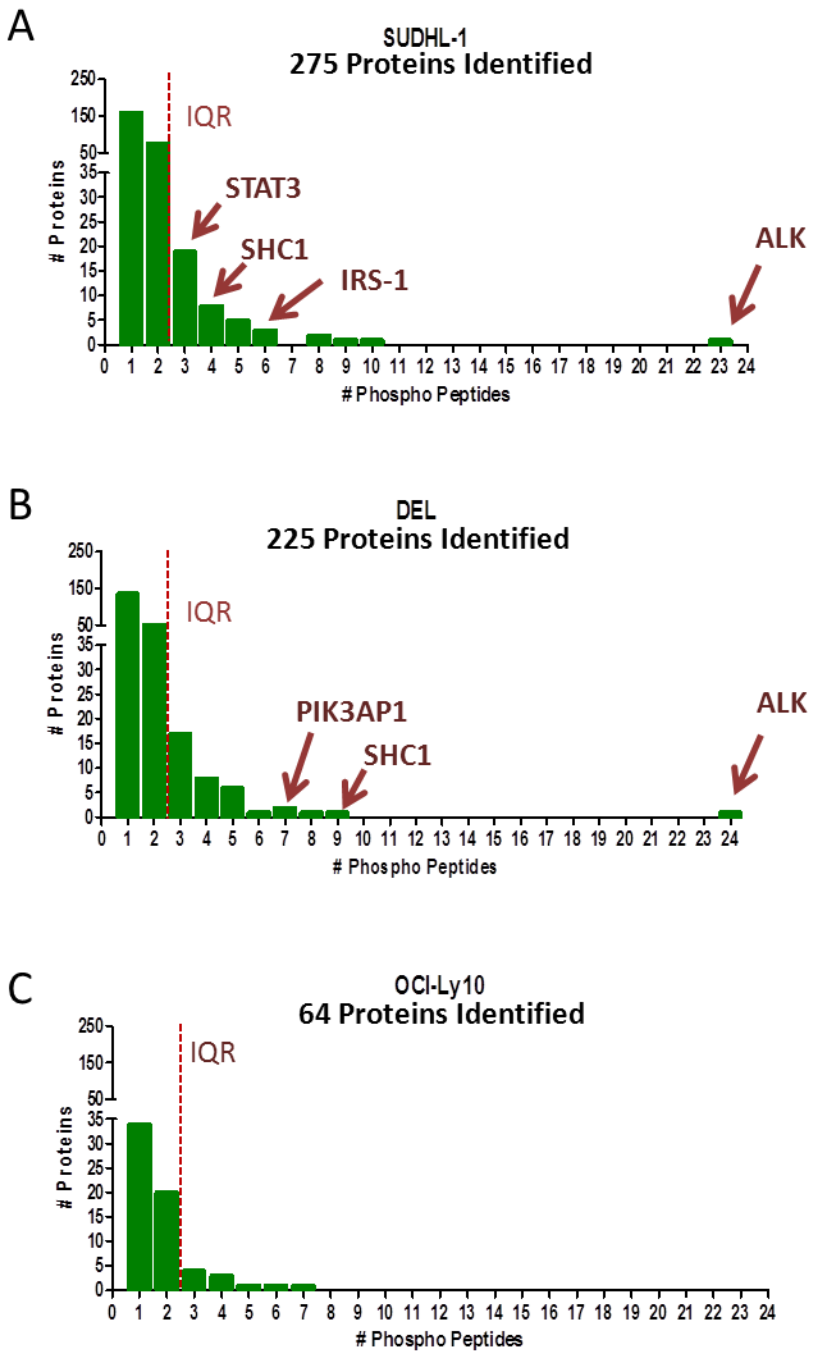

Figure 2.2: Phosphoproteome signature for lymphoma cell lines. The number of phosphopeptides for each protein is plotted against the number of phosphoproteins for ALK+ALCL cell lines SU-DHL-1 (A) and DEL (B) and DLBCL cell line OCI-Ly10 (C). Interquartile range (IQR)is plotted along with ALK and known ALK substrates.

Given the known phosphoproteomic signatures of NPM-ALK expressing cells, we repeated these analyses in the presence of an ALK inhibitor identify proteins that changed in this signature. CEP-26939 (CEP) was used to inhibit ALK kinase activity. This compound has a cellular IC_{50} of 100nM and remarkable selectivity at this concentration (Figure 2.3A)[241]. To determine the optimal conditions for these proteomic studies, various drug concentrations and time courses of ALK inhibition were evaluated. Inhibition of ALK tyrosine kinase activity using CEP (300nM for 6 hours) was associated with complete abrogation of autophosphorylation at Y1604-ALK in NPM-ALK+ALCL cell lines (SU-DHL-1 and SUPM2) without impacting cell viability (Figure 2.3B-C). These conditions were used in subsequent phosphoproteomic experiments. MS-based phosphoproteomic analysis of ALCL-derived cell lines revealed that inhibition of ALK resulted in the down-regulation of 569 proteins and up-regulation of 102 proteins. Z-score analysis was used to group proteins based on the directionality and significance of change after ALK inhibition (representative data from 1 biological replicate (technical triplicate) of SU-DHL-1) (Figure 2.4). As expected, the phosphoprotein that changed with greatest significance in response to ALK inhibition was ALK (z-score=-6.0 with 93 spectral counts identified in DMSO treated cells and 1 spectral count in CEP). This result provided confidence in the efficacy of ALK inhibition in this experiment. We established a significance threshold of $|z| \geq 1$ (proteins that changed with greater than or equal to 1 standard deviation from the DMSO control) for the identification of candidate mediators of ALK signaling. Forty-nine proteins met this statistical criterion, including previously known ALK substrates including STAT3 (z=-2.2) and

SHC-1 (z = -3.6)[49,113]. Pyruvate kinase M2 (PKM2) was identified with a z-score of -1.1. Mechanistic studies of PKM2 will be discussed in Chapter 3.

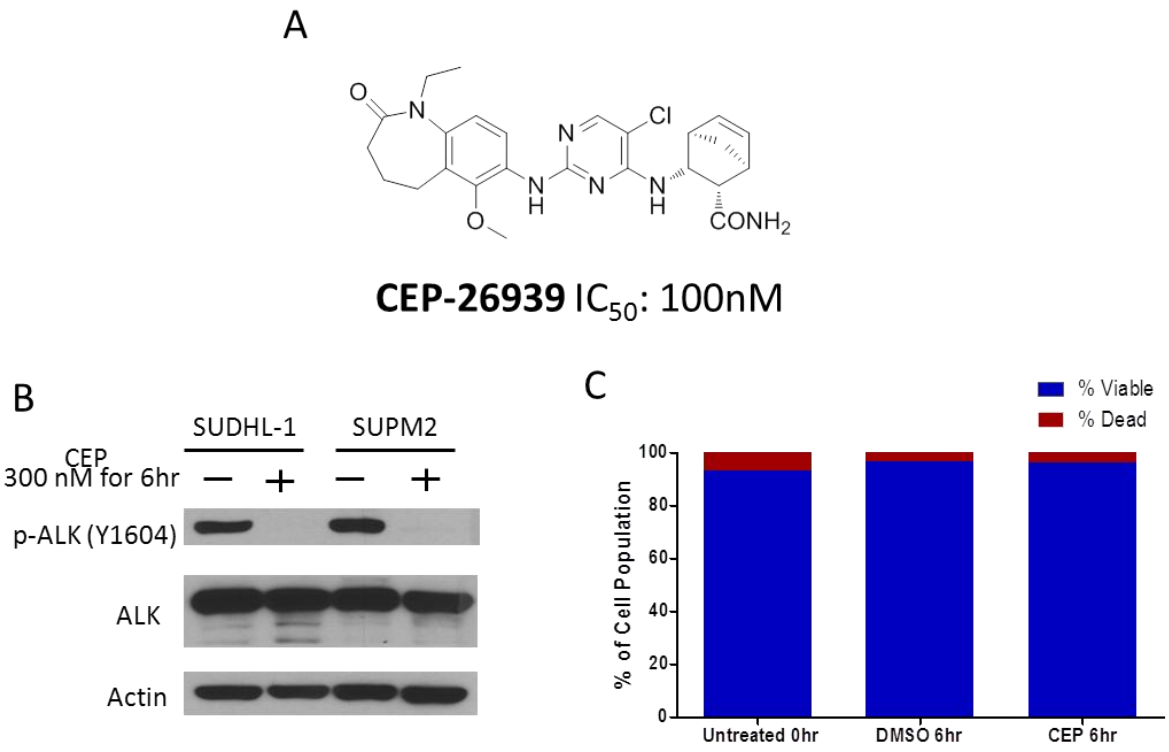

Figure 2.3: Validation of conditions for phosphoproteomic studies. (A) Structure of ALK inhibitor CEP-26939. (B) Immunoblots of SU-DHL-1 and SUPM2 cell lysates treated with 300nM CEP for 6hrs in 1% FBS. (C) The same treatment conditions from (C) were used to determine viability by trypan blue staining.

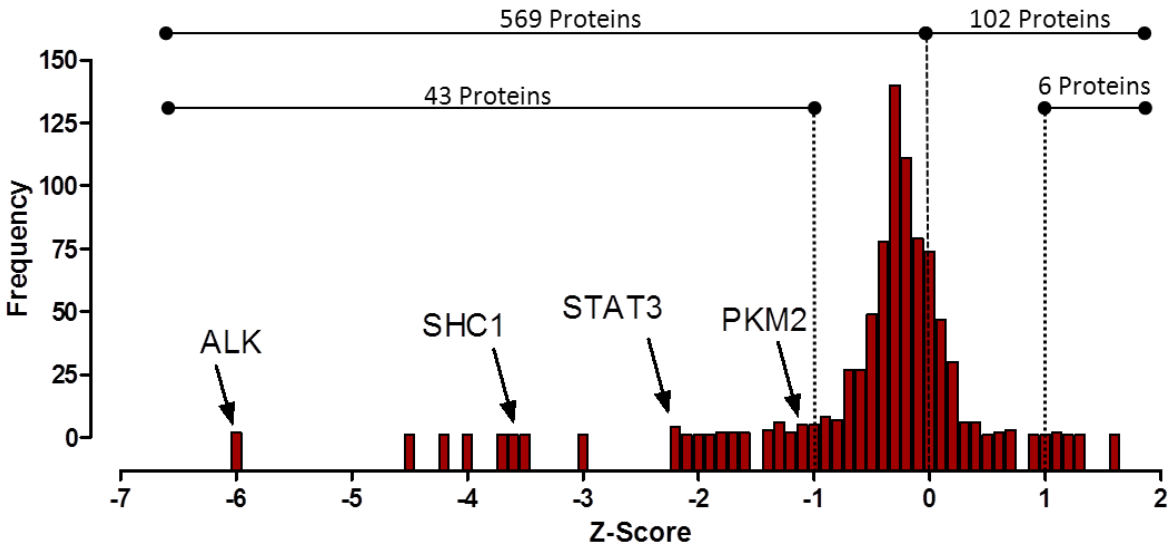

Figure 2.4: Phosphoproteome changes in response to ALK inhibition. Changes in spectral counts following NPM-ALK inhibition are quantified by z-score. The number of proteins (frequency) with a given z-score value are plotted against the z-score. A significance threshold was set at $|z| \geq 1$. Locations of ALK, SHC1, STAT3 and PKM2 are indicated.

In order to functionally categorize the observed changes in the phosphoproteins, we utilized the Database for Annotation, Visualization and Integrated Discovery (DAVID)[242,243] (Figure 2.5A-B). Gene Ontology (GO) biological process term analysis identified numerous processes that are regulated by NPM-ALK activity. The list of significantly represented GO terms include "RNA processing", "gene expression", "transmembrane receptor tyrosine kinase (RTK) signaling pathway", "positive regulation of cell proliferation", and "cell cycle process" among others (Figure 2.5A). Interestingly, the GO term "metabolic process" was also significantly ($p=0.0003$) represented in our data set. Further analysis of the "metabolic process" GO term into its constituents revealed the alterations of metabolic pathways (Figure 2.5D) such as "nucleotide metabolic process", "nitrogen

compound metabolic process", "RNA metabolic process", "macromolecule metabolic process", "biosynthetic process" and "glycolysis".

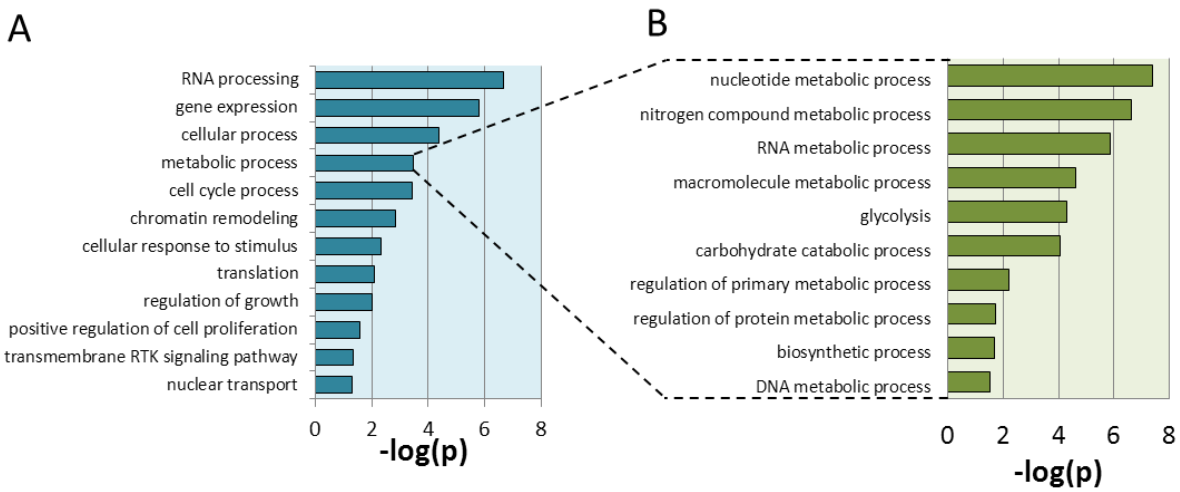

Figure 2.5: Biological process enrichment in phosphoproteomic data. (A) Gene Ontology (GO) term enrichment analysis using DAVID applied to the proteins that changed in spectral counts following ALK inhibition. A subset of the significant terms is displayed. (B) List of GO terms that comprise the "metabolic processes" term.

Table 2.1 lists phosphoproteins clustered based on the KEGG annotated metabolic pathways that were identified by the phosphoproteomic analysis to be regulated by ALK activity. The raw spectral counts identified for each phosphoprotein under both DMSO and CEP treated conditions are tabulated. Data from both metal-oxide affinity chromatography (MOAC) for the serine/threonine phosphoproteome and the MOAC followed by phosphotyrosine immunoprecipition (pY-IP) for the tyrosine phosphoproteome are shown. As demonstrated in Table 2.1, many proteins were identified in both the serine/threonine and tyrosine datasets. The "Merged Difference" column displays the combined data from all three biological replicates as represented by the change in spectral counts following ALK inhibition.

Several key phosphoproteins in glycolysis were identified to be differentially phosphorylated following NPM-ALK inhibition. Specifically, the abundance of phosphorylated peptides derived from PKM2 and Lactate dehydrogenase B (LDHB) were decreased; 28 for PKM2 and 14 for LDHB. Serine phosphorylation of phosphoglucomutase 1 (PGM1) (a regulator of the pentose phosphate pathway) was increased by 16 spectral counts after ALK inhibition. Additionally, large changes were seen in phosphoproteins in nucleotide metabolism including thioredoxin reductase 1 (TXNRD1) (increase of 10 spectral counts), nudix-type motif 5(NUDT5) (decrease of 9 spectral counts) and 5-aminoimidazole-4-carboxamide ribonucleotide formyltransferase/IMP cyclohydrolase (ATIC) (increase of 7 spectral counts). Based on these results, we hypothesized that NPM-ALK regulates cellular metabolism via phosphorylation of proteins involved in key metabolic pathways including glycolysis, pentose phosphate, nucleotide biosynthesis and the TCA cycle.

Table 2.1: Phosphoproteomic results for metabolic proteins.

			Replicate 1		Replicate 2		Replicate 3		Merged		
			DMSO	CEP	DMSO	CEP	DMSO	CEP	DMSO	CEP	Merge Diff
Glycolysis	MOAC										
	P06733	ENO1	6	0	15	7	0	0	21	7	-14
	P00338	LDHA	9	7	6	6	0	0	15	13	-2
	P07195	LDHB	6	7	11	8	0	0	17	15	-2
	P08559	PDHA1	9	10	21	8	6	10	36	28	-8
	Q01813	PFKP	0	1	0	0	0	0	0	1	1
	P00558	PGK1	12	7	3	4	7	12	22	23	1
	P36871	PGM1	2	6	2	13	0	1	4	20	16
	P14618	PKM2	7	4	4	5	0	0	11	9	-2
	Q9NR19	ACSS2	2	6	3	0	0	0	5	6	1
	P60174	TPI1	6	11	6	9	6	5	18	25	7
	pY-IP										
	P06733	ENO1	12	2	60	41	15	14	87	57	-30
	P04075	ALDOA	0	0	0	0	1	0	1	0	-1
	P04406	GAPDH	0	0	2	0	5	8	7	8	1
	P00338	LDHA	18	31	15	11	15	14	48	56	8
	P07195	LDHB	6	2	12	4	19	17	37	23	-14
	P17858	PFKL	0	0	6	0	0	0	6	0	-6
	P00558	PGK1	0	0	3	0	0	1	3	1	-2
	P14618	PKM2	12	3	49	44	30	16	91	63	-28
	P60174	TPI1	0	0	0	0	0	1	0	1	1
Pentose Phosphate Pathway	MOAC										
	P21108	PRPS1L1	0	0	0	0	1	0	1	0	-1
	Q01813	PFKP	0	1	0	0	0	0	0	1	1
	P36871	PGM1	2	6	2	13	0	1	4	20	16
	Q96G03	PGM2	7	1	6	6	0	4	13	11	-2
	pY-IP										
	P04075	ALDOA	0	0	0	0	1	0	1	0	-1
	P17858	PFKL	0	0	6	0	0	0	6	0	-6
	P29401	TKT	0	0	6	2	7	4	13	6	-7
TCA Cycle	MOAC										
	P53396	ACLY	12	4	11	9	4	8	27	21	-6
	P08559	PDHA	9	10	21	8	6	10	36	28	-8
	pY-IP										
	Q9P2R7	SUCLA2	0	0	0	0	4	4	4	4	0
	P53396	ACLY	20	51	108	90	52	46	180	187	7
Nucleotide Metabolism	MOAC										
	Q15054	POLD3	1	0	4	0	1	1	6	1	-5
	Q3B726	TWISTNB	6	2	4	3	2	5	12	10	-2
	Q14181	POLA2	1	0	0	4	0	0	1	4	3
	P24928	POLR2A	3	1	1	0	0	0	4	1	-3
	Q16881	TXNRD1	7	8	2	7	0	4	9	19	10
	P27708	CAD	6	5	22	12	2	5	30	22	-8
	P22234	PAICS	3	1	2	4	0	0	5	5	0
	Q9UKK9	NUDT5	0	3	5	4	1	1	6	8	2
	P21108	PRPS1L1	0	0	0	0	1	0	1	0	-1
	P12268	IMPDH2	4	4	0	0	0	0	4	4	0
	P31939	ATIC	2	5	2	6	0	0	4	11	7
	O15067	PFAS	2	0	0	1	0	0	2	1	-1
	P36871	PGM1	2	6	2	13	0	1	4	20	16
	P14618	PKM2	7	4	4	5	0	0	11	9	-2
	P31350	RRM2	27	28	17	16	9	12	53	56	3
	pY-IP										
	O14802	POLR3A	0	0	2	2	2	0	4	2	-2
	P24928	POLR2A	0	0	8	5	12	4	20	9	-11
	P23921	RRM1	0	0	7	5	4	1	11	6	-5
	P31350	RRM2	2	0	0	0	0	8	2	8	6
	Q16881	TXNRD1	12	7	52	57	18	20	82	84	2
	P11172	UMPS	0	3	6	6	6	6	12	15	3
	P27708	CAD	0	0	0	0	6	6	6	6	0
	Q9H9Y6	POLR1B	0	0	1	0	0	0	1	0	-1
	Q9UKK9	NUDT5	0	0	13	4	12	12	25	16	-9
	P12268	IMPDH2	0	0	0	0	3	2	3	2	-1
	P31939	ATIC	0	4	6	6	7	6	13	16	3
	P14618	PKM2	12	3	49	44	30	16	91	63	-28

Metabolomic analysis reveals NPM-ALK-mediated alterations in biomass producing pathways

Based on robust enrichment of metabolic proteins that were regulated by NPM-ALK (Table 2.1), we carried out metabolomic profiling of ALCL-derived cells in the presence or absence of ALK activity. Metabolites were extracted from lysates of 4 NPM-ALK+ ALCL-derived cells (SU-DHL-1, DEL, SUPM2, SR786) subjected to identical conditions used for the phosphoproteomic studies and analyzed using three independent metabolomics platforms: ultrahigh performance liquid chromatography-tandem mass spectrometry (UHLC-MS/MS) in negative and positive ion modes as well as gas chromatography (GC)-MS. Metabolite levels in cells with and without ALK inhibition were analyzed in biological quadruplicate (See Figure 1A for overall experimental design for metabolomics profiling). As shown in Figure 2.6, we observed large scale and global changes in metabolites (mass spectral features) in response to ALK inhibition. About a quarter (23.6%) of the 4784 mass spectral features from SU-DHL-1 cells changed with an average z-score of greater than 2 or less than -2 (Figure 2.6A). Z-score analyses for the other cell lines tested are shown in Figures 2.6B-D. Of the 4673 mass spectral features identified in SUPM2 cells, 11% of these changed with $|z|>2.0$ (Figure 2.6B). DEL and SR786 cells revealed 17% and 6% of the 4701 and 4638 mass spectral features, respectively to change with $|z|>2.0$ (Figure 2.6C-D).

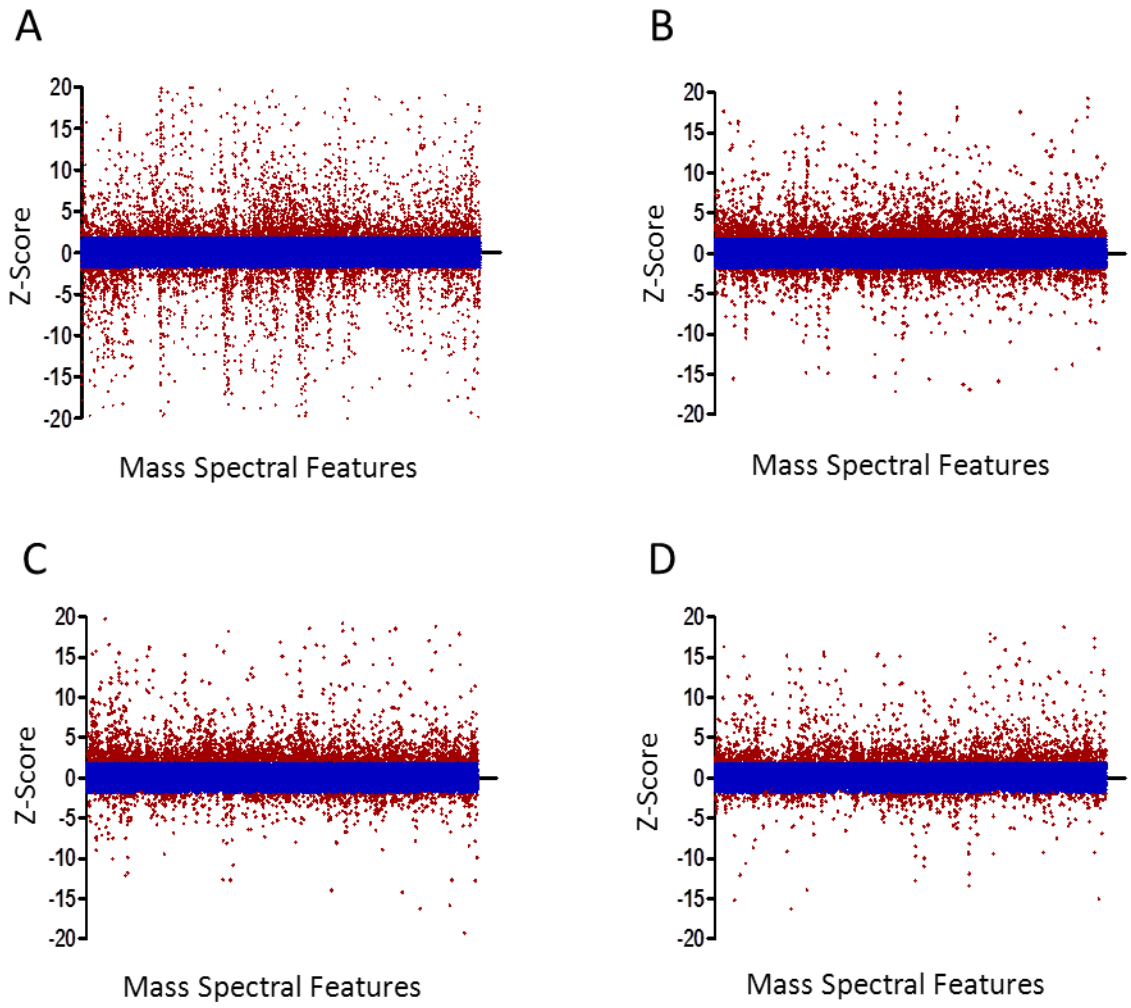

Figure 2.6: Metabolomic analysis reveals widespread metabolic changes driven by NPM-ALK signaling. Z-score analysis of all identified mass spectral features that change in response to NPM-ALK inhibition. Each feature is represented in biological quadruplicate. Blue dots: DMSO. Red dots: CEP treated (A) SU-DHL-1 (B) SUPM2 (C) DEL (D) SR786

The apparent variability in metabolic response to ALK inhibition across cell lines led us to characterize these differences. Random forest analysis[244] was used to cluster the DMSO treated cell lines based on their metabolomic profiles (Figure 2.7A). Importantly, the replicates for each cell lines clustered tightly together suggesting that the observations were reproducible amongst replicates. However,

each cell line clustered independently. This suggests that each cell line exhibits a distinct metabolic phenotype even in the presence of NPM-ALK. These differences may be accounted for by the unknown secondary mutations that exist in these cell lines that could be impacting metabolism. Random forest analysis was also used to determine the metabolic impact of ALK inhibition. SU-DHL-1 (Figure 2.7B), SUPM2 (Figure 2.7C) and DEL (Figure 2.7D) cells showed clustering differences between DMSO and CEP treated cells, as evident by the ability to separate the groups by a straight line. This suggests that ALK inhibition significantly alters the cellular metabolism to the extent that the two conditions represent different metabolic entities. However, SR786 cells (Figure 2.7E) did not show efficient clustering amongst treatment groups, suggesting ALK inhibition has less metabolic consequences in these cells. These data corroborate the z-score analysis shown in Figure 2.6D.

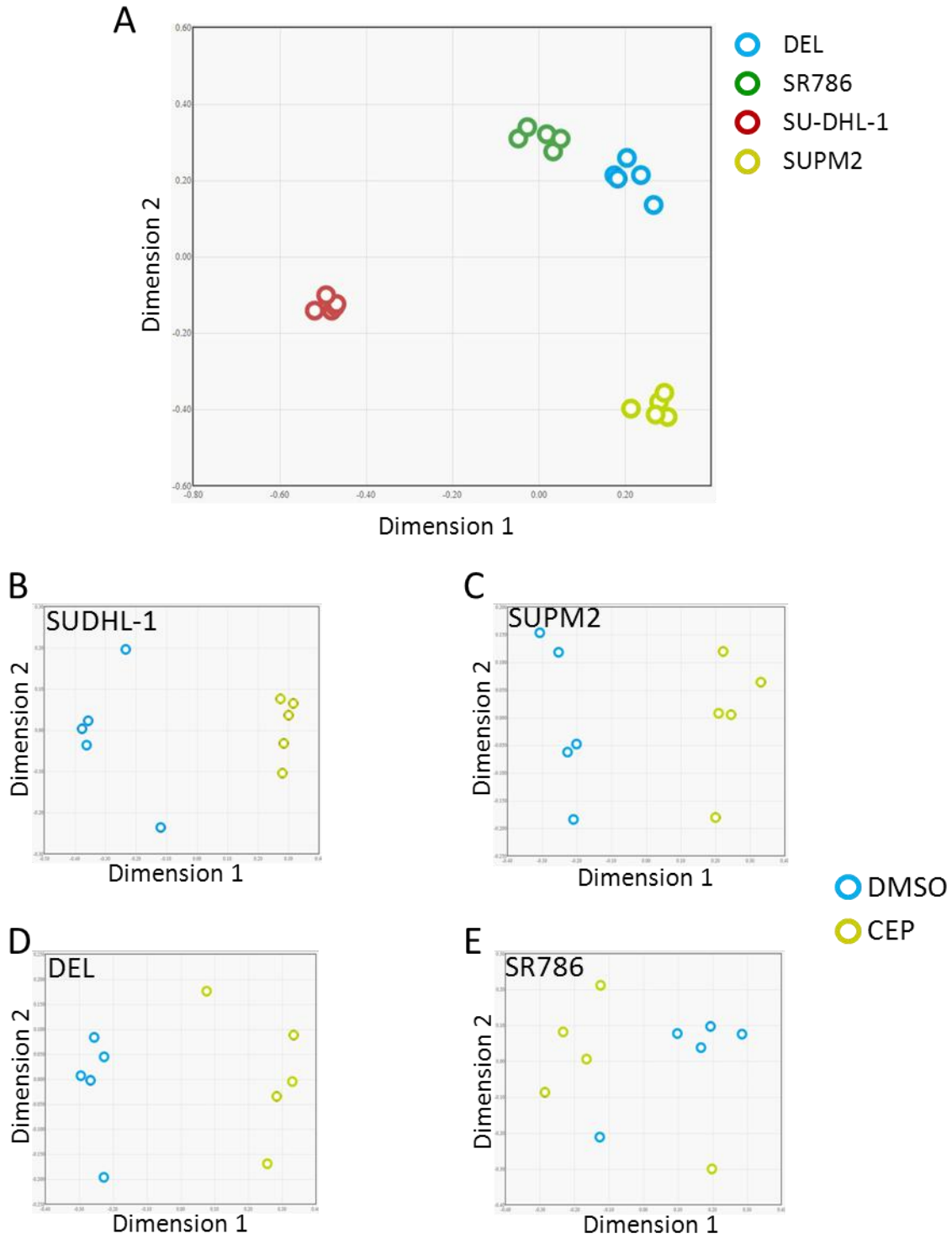

Figure 2.7: Random Forest analysis reveals metabolic differences in ALCL cells and ALK regulated metabolism. (A) Random Forest analysis on metabolomics data from 4 ALCL cell lines. Random Forest analysis on metabolomics data from SU-DHL-1 (B), SUPM2 (C), DEL (D) and SR786 (E) cells treated with DMSO or CEP.

To determine what overlap exists between cell lines, the z-score analysis for each cell line was combined and metabolites that significantly changed ($|z|>1.0$) in at least 2 of the 4 cell lines were tabulated (Table 2.2). Metabolites that increased in response to ALK inhibition were highlighted red while those that decreased were highlighted green. Metabolites that lacked significant change remained uncolored. Several metabolites were consistently upregulated, such as o-phospho-DL-serine, nicotinamide, and 3'-CMP. These metabolites might serve as biomarkers for ALCL, but further investigation is necessary. Furthermore, several metabolites were consistently downregulated including glutaimine, deoxyribose and methionine. Investigation of these metabolites may lead to novel discoveries involving the role of NPM-ALK in metabolic regulation.

Table 2.2: Z-scores for metabolites across four ALCL cell lines. (z>1, red. z<-1, green)

KEGG ID	Name	SUD1	DEL	SUPM2	SR786
C00303	GLUTAMINE	4.10	3.11	1.22	1.11
C01987	2-AMINOPHENOL	3.02	-2.01	2.41	1.09
C00586	2-DEOXY-D-GLUCOSE	9.08	-1.72	3.90	2.21
C01801	DEOXYRIBOSE	1.24	-1.81	3.77	1.50
C01586	HIPPURATE	-1.41	4.45	2.03	1.15
C16440	LYSINE	1.64	2.37	-0.06	1.52
C01733	METHIONINE	0.35	2.06	1.26	1.60
C00534	PYRIDOXAMINE	2.35	1.18	0.12	1.88
C00296	QUINATE	2.06	1.55	1.11	0.43
C00214	THYMIDINE	-3.40	7.19	2.42	1.39
C01004	TRIGONELLINE	-3.33	4.41	3.05	1.91
C00785	UROCANATE	27.11	-0.90	12.93	67484.53
C16436	VALINE	-4.39	3.39	1.24	2.42
C00881	2`-DEOXYCYTIDINE	3.47	0.41	0.42	2.04
C00219	ARACHIDONATE	4.60	-0.46	8.16	0.16
C01420	CYSTINE	1.70	-0.87	2.27	0.60
C00475	CYTIDINE	3.94	-0.60	1.77	0.93
C00425	DEHYDROASCORBATE	1.57	-0.65	8.90	0.84
Z02138	DIOLEOYLPHOSPHATIDYLCHOLINE	2.57	0.97	-0.18	2.33
C06429	DOCOSAHEXAENOIC ACID	1.91	0.56	6.19	0.19
C16439	LEUCINE	-0.03	0.96	1.67	1.88
C00208	MALTOSE	6.48	-3.20	2.24	0.69
CA1511	PENTITOL	4.19	-1.12	4.30	0.80
C01953	PREGNENOLONE	-0.71	2.11	2.40	0.19
C00715	PTERIN	-0.77	-1.31	2.92	1.56
CA1403	SELENOCYSTAMINE	3.28	-0.44	0.57	4.97
C00780	SEROTONIN	-0.22	2.47	2.06	0.85
C00493	SHIKIMATE	11.71	-3.13	9.22	0.50
A00007	SILANOL, TRIMETHYL-, PHOSPHATE (3:1)	-0.57	-0.40	8.41	12.75
C04677	5-AMINOIMIDAZOLE-4-CARBOXAMIDE-1-BETA-D-RIBOFURANOSYL 5`-MONOPHOSPHATE	-2.03	1.86	-4.70	-0.92
C00302	GLUTAMIC ACID	-1.50	-5.27	1.58	0.25
CA1454	N-ACETYL-DL-GLUTAMIC ACID	-9.00	5.19	-2.20	0.16
C02571	O-ACETYL-L-CARNITINE	-6.04	3.61	-3.76	0.62
C00019	S-ADENOSYL METHIONINE	-7.08	3.14	-2.43	0.10
C00670	SN-GLYCERO-3-PHOSPHOCHOLINE	8.05	-1.33	-2.54	-1.68
C00330	2`-DEOXYGUANOSINE	-4.10	0.78	-2.05	-0.30
C05822	3`-CMP	-3.00	-2.88	-1.00	-1.13
C00575	ADENOSINE 3`,5`-CYCLIC MONOPHOSPHATE	-3.37	0.53	-2.68	-0.36
C00020	ADENOSINE 5`-MONOPHOSPHATE	-2.93	0.79	-1.02	-1.81
C00307	CYTIDINE 5`-DIPHOSPHOCHOLINE	-3.78	-0.74	-2.51	-1.55
C00394	GDP-GLUCOSE	-2.46	0.45	-0.70	-7.88
C00051	GLUTATHIONE	-5.63	0.08	-2.75	0.00
C00294	INOSINE	-4.64	0.69	-4.04	0.00
C00153	NICOTINAMIDE	-8.22	0.66	-7.65	-1.03
C00003	NICOTINAMIDE ADENINE DINUCLEOTIDE	-5.16	-0.37	-3.47	-1.07
CA1209	O-PHOSPHO-DL-SERINE	-6.02	0.27	-1.67	-1.15
C00105	URIDINE-5-MONOPHOSPHATE	-2.14	-0.50	0.29	-1.93

Based on the complexity of the data and the differences between cell lines, we chose to focus subsequent studies on SU-DHL-1 since to showed the greatest extent of ALK metabolic regulation (Figure 2.6A). Of the 4784 mass spectral features identified, 502 represented known chemical structures. Unsupervised hierarchical clustering of all mass spectral features revealed a high degree of reproducibility within the replicates and demonstrated a distinct metabolic signature associated with NPM-ALK activity (Figure 2.8A). Supervised clustering using those mass spectral features that showed a change with $p < 0.1$, representing 1284 mass spectral features, revealed a subset of metabolites that decreased (524 mass spectral features) as well as increased (758 mass spectral features) in response to ALK inhibition (Figure 2.8B).

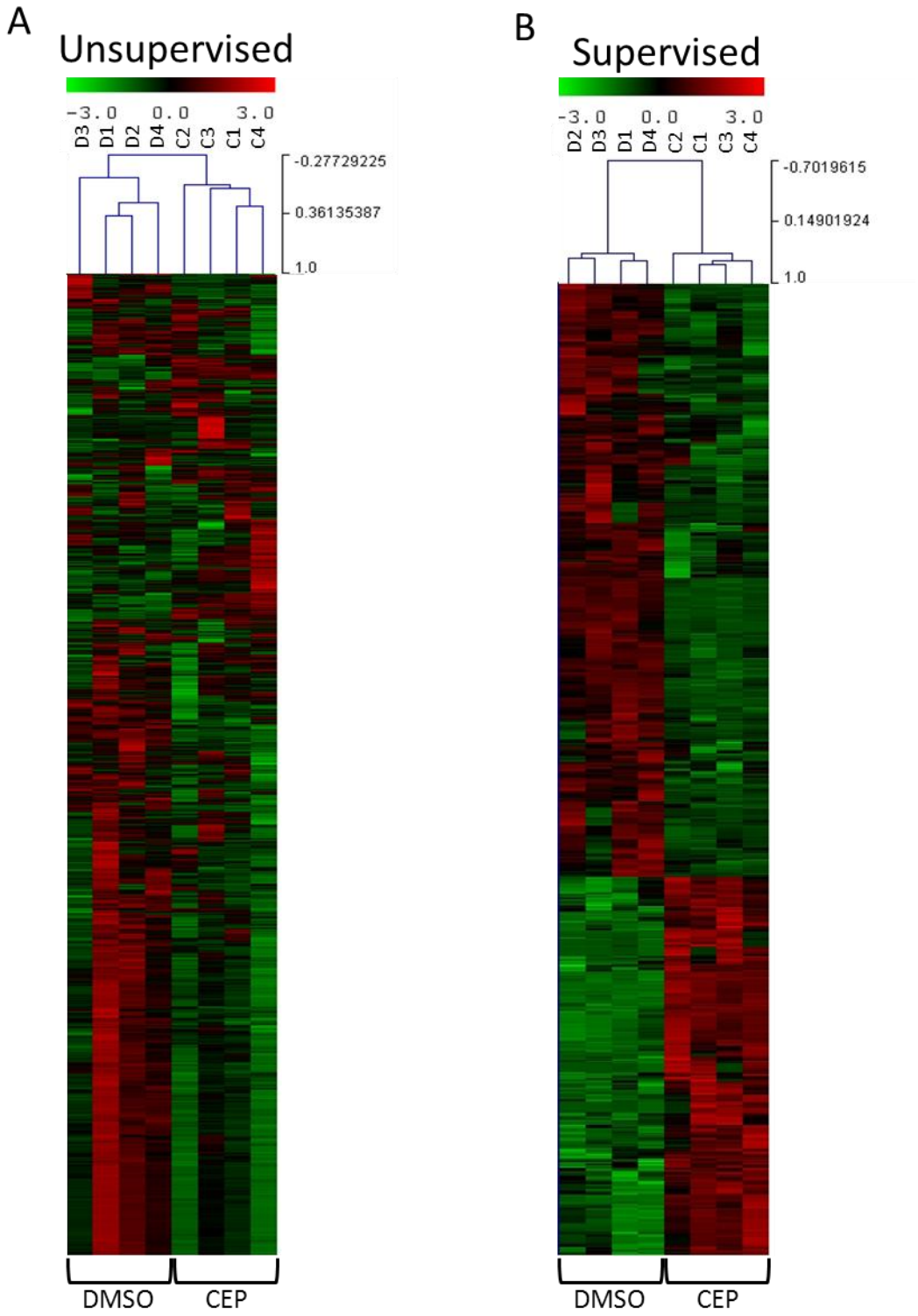

Figure 2.8: Hierarchical clustering of SU-DHL-1 metabolomics data. (A) Unsupervised hierarchical clustering of all identified mass spectral features in DMSO and CEP treated cells (D1-D4 are DMSO samples, C1-C4 are CEP samples). B) Supervised hierarchical clustering of those mass spectral features that changed significantly ($p<0.1$) based on CEP treatment.

To determine the metabolic pathways which were significantly altered by NPM-ALK, we utilized MetaboAnalyst 2.0[245,246] to assess the pathway enrichment within our metabolomic dataset. Pathways were ranked based on two dimensions of significance: a p-value based on metabolite set enrichment analysis (MSEA) and a pathway impact score based on the centrality of the identified metabolites within the directional network. Figure 2.9 shows the results of the MetaboAnalyst analysis with each circle representing a distinct metabolic pathway that is altered by NPM-ALK. The size and color of the circles corresponds to the impact score and the –log(p) values respectively. In order to derive a list of significant pathways from this two-dimensional plot, we assigned a statistical cutoff at $y>1/x$ ($y=-\log(p)$, x=impact score). This cutoff allowed for the exclusion of pathways with either low -log(p) values or low pathway impact scores. Metabolic pathways whose –log(p) value and pathway impact score exceed this threshold were considered to be significantly altered by NPM-ALK signaling. The pathways that met the statistical criteria were ranked by –log(p) value in Figure 2.10. These results showed significant changes in a number of pathways involved in biomass production, including purine metabolism ($p<0.01$) pyrimidine metabolism ($p<0.01$), glycerophospholipid metabolism ($p<0.01$), and glycine, serine and threonine metabolism ($p<0.01$). Importantly, pathways affecting glycolysis ($p<0.01$), the pentose phosphate shunt ($p<0.01$), and the tricarboxylic acid (TCA) cycle ($p<0.01$) which serve as the starting point for many biomass producing pathways involved in the Warburg effect[193] were also significantly altered by NPM-ALK activity.

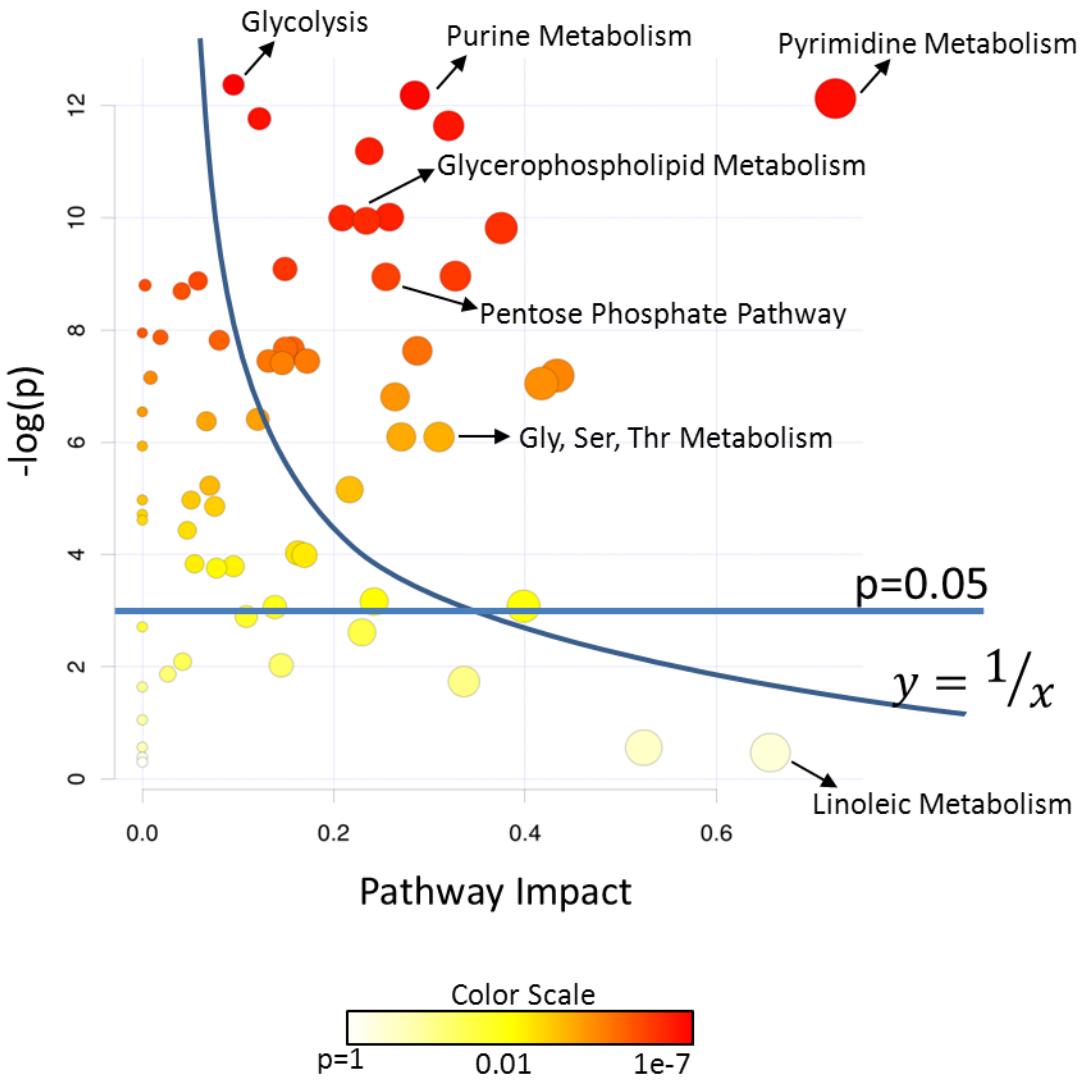

Figure 2.9: Metabolomic pathway analysis using MetaboAnalyst 2.0. Data output from pathway analysis (DMSO vs. CEP). Pathways represented as colored circles. P value is assigned based on the coverage and change observed in a given metabolic pathway. A pathway impact score was assigned based on the location of the identified metabolites in a given pathway. A significant threshold was assigned at y=1/x for subsequent analysis.

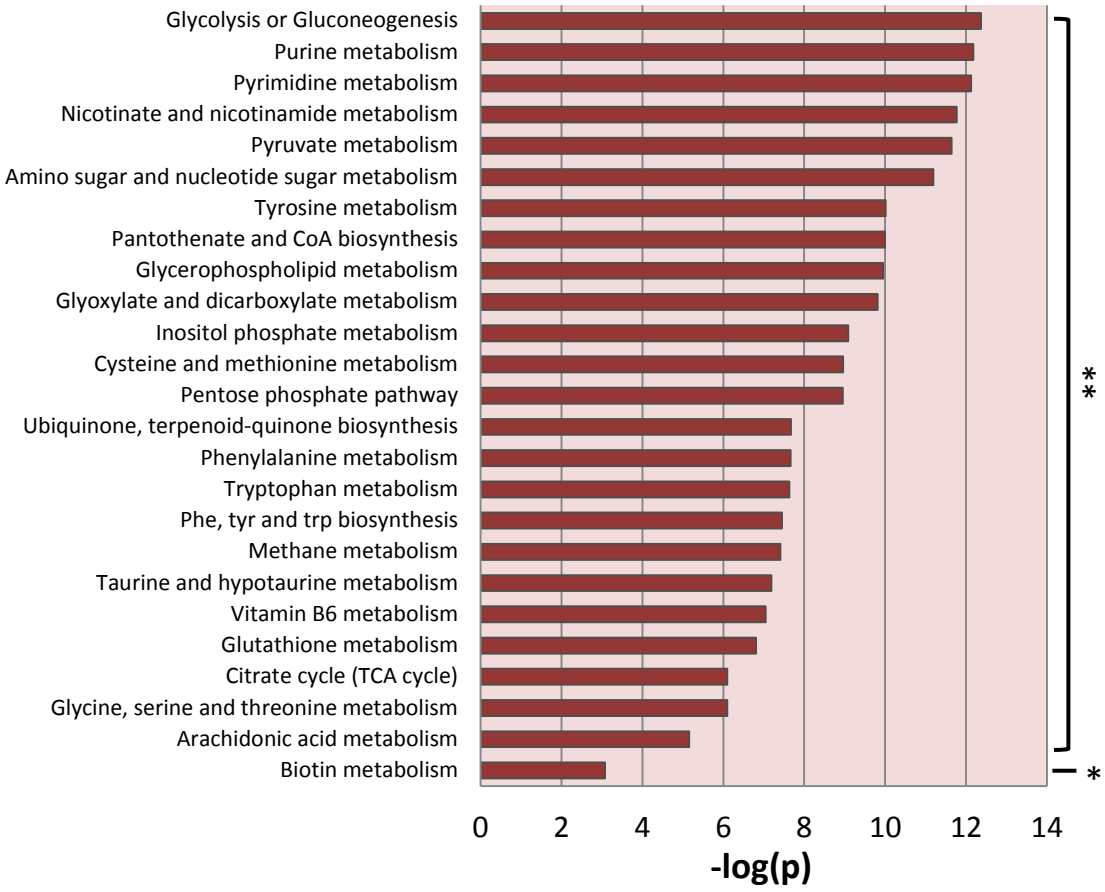

Figure 2.10: Metabolomic pathway analysis reveals changes in key biomass producing pathways. Metabolanaylst 2.0 generated pathways that changed in response to ALK inhibition. Only those pathways that meet the statistical cutoff described in Figure 2.9 are shown. *p<0.05, **p<0.01

Pyrimidine metabolism ranked third in p-value significance and had the highest pathway impact score (Figure 2.9 and 2.10). Figure 2.11A shows the network diagram of pyrimidine metabolism generated by MetaboAnalyst 2.0. The boxes colored in a spectrum from pale yellow to dark red represent metabolites that were identified by the metabolomics profiling, while blue boxes represent metabolites in pyrimidine metabolism that were not identified. The intensity of the

red color corresponds to the level of significance of change in metabolite in response to NPM-ALK inhibition (see color scale). Four of the metabolites that changed are shown in the boxed insets and include cytidine that increased in response to NPM-ALK inhibition and cytosine, orotate and (S)-dihydroorotate which decreased in response to ALK inhibition (Figure 2.11A). Many of the metabolites in this pathway were identified with highly significant change in response to NPM-ALK inhibition suggesting that NPM-ALK plays a critical role in the regulation of nucleotide biosynthesis.

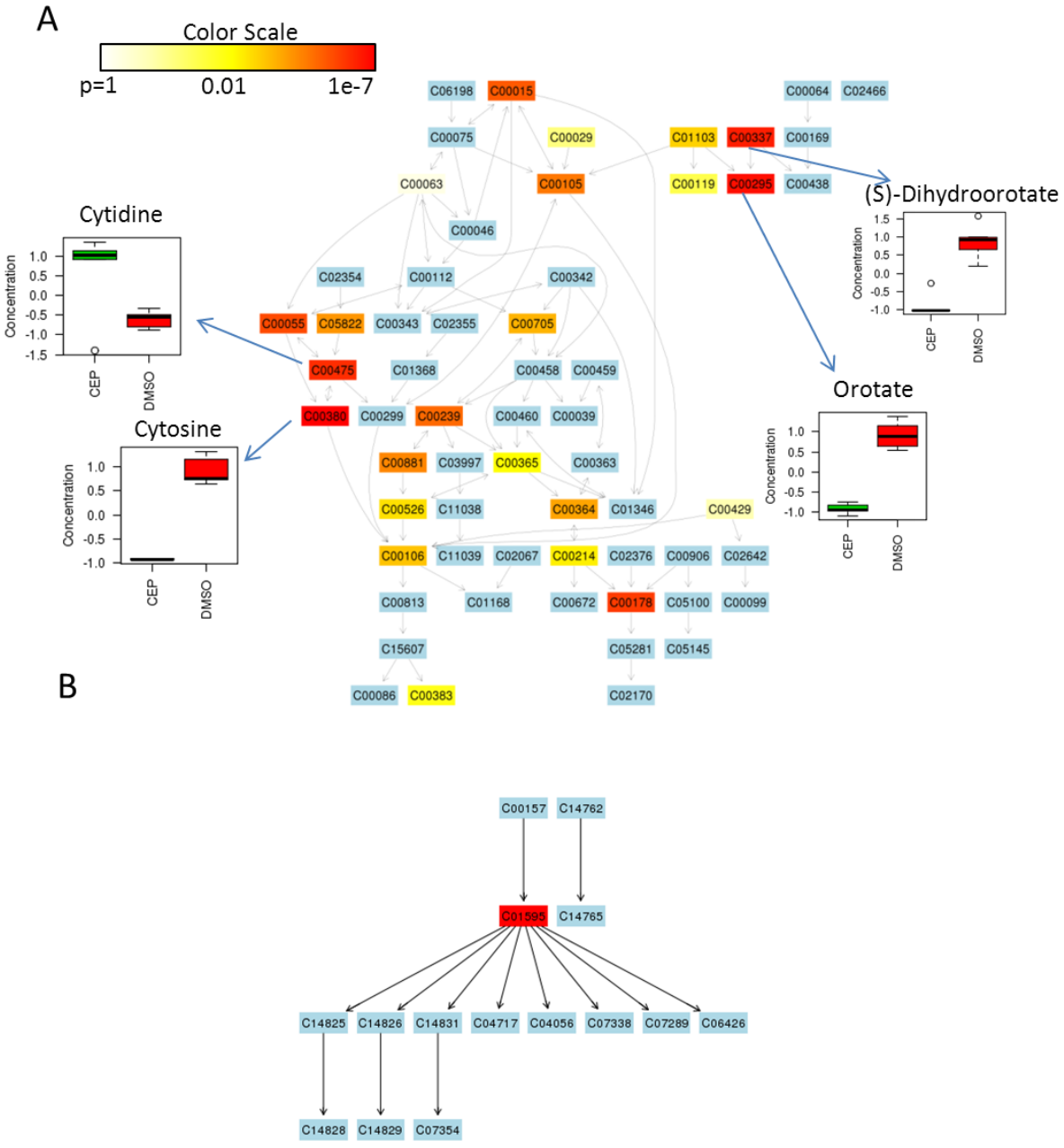

Figure 2.11: Metabolomic pathway analysis shows significant changes in pyrimidine metabolism. (A) Network diagram for components of pyrimidine metabolism that were altered by ALK. The identified metabolites are colored yellow to red according to the significance of change following ALK inhibition (see color scale). Boxed insets represent a subset of metabolites that were changed in response to ALK inhibition (in normalized concentrations). (B) Network diagram for linoleic metabolism.

As an illustrative example of the pathway impact score, the network diagram for linoleic metabolism is shown in Figure 2.11B. Linoleic metabolism generated a high impact score of 0.66 while the –log(p) was very low (0.47) (Figure 2.9). Only one metabolite was identified in linoleic metabolism (red box), however it exists in a critical location within the network (Figure 2.11B). The impact score ranks pathways based on the presence of these critical nodes. Conceptually, if a node with a high level of out-degree centrality (the number of edges derived from a given node) is changed in the analysis, the impact to the entire metabolic pathway would be high. Therefore, linoleic metabolism received a high pathway impact score but a low p-value (based on the lack of pathway coverage identified).

Metabolomics datasets offer a level of complexity and limitation that proteomics data does not. Specifically, while every mass spectral feature identified in a proteomics study can be sequenced and mapped to a protein, not all mass spectral features representing metabolites can be named. This depends on the depth of the library for matching mass spectral features to standards within the library of metabolites. Since the GSEA takes pathway coverage into account, we wanted to validate these results to test whether the pathway analysis we employed was not biased to the number of known metabolites identified To accomplish this we repeated the analysis using control vs. control (DMSO vs. DMSO) (Figure 2.12A). This allowed us to test the outcome with a dataset that shows no significant metabolite changes but represents the same coverage of metabolites per pathway. Since the pathway impact score is based on the location of an identified metabolite within the network, these values were not changed in the control vs. control analysis.

However, since none of the metabolites significantly changed, the p-values were dramatically lowered (see y-axis and color scale) with the most significant pathway having a p-value of 0.25. To further illustrate this point, the average –log(p) values for each analysis are plotted in Figure 2.12B. The average –log(p) for the DMSO vs. CEP analysis was well above the p=0.05 threshold showing that many metabolic pathways are significantly changed. However, the average for the control analysis is well below this threshold with no pathways yielding a significant p value. The results provide confidence in the original analysis (Figure 2.9) showing that NPM-ALK activity regulates biomass production and other key metabolic pathways.

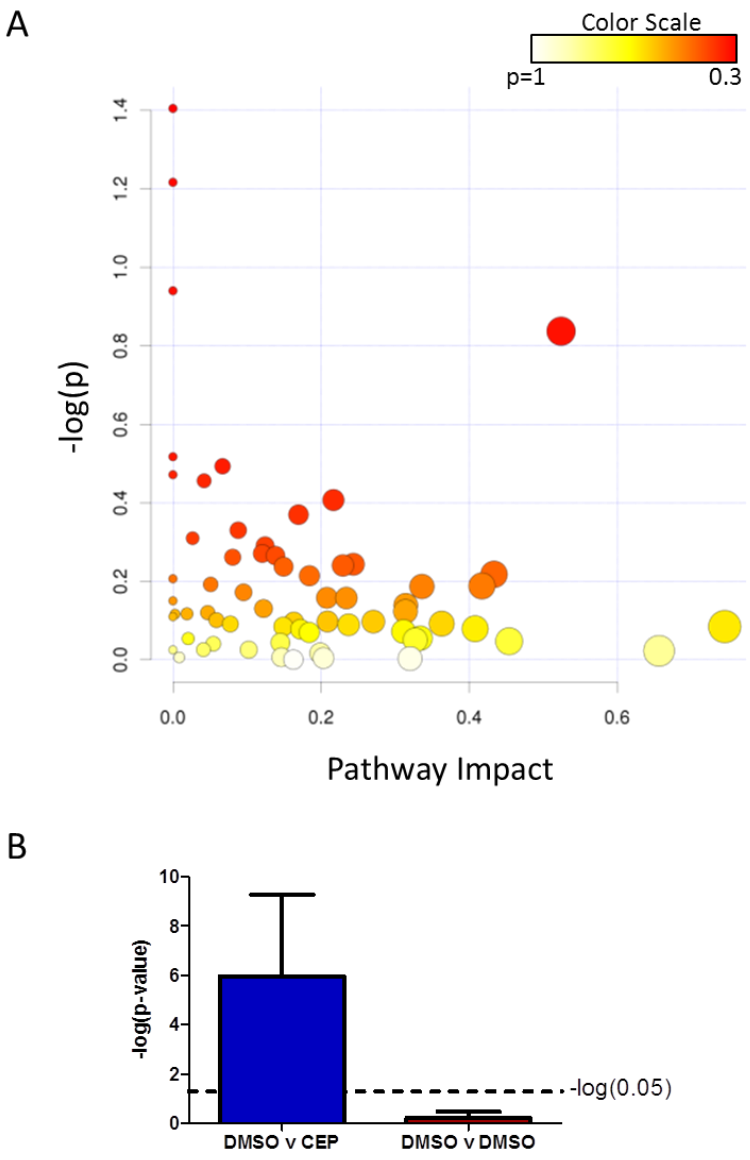

Figure 2.12: MetaboAnalyst 2.0 validation by DMSO vs. DMSO analysis (A) Data output from control pathway analysis (DMSO vs. DMSO). Color scale defines p-value. (B) The average –log(p) values for all pathways in Figure 2.9 and (B) were calculated and graphed. The standard significance cutoff (p=0.05) is highlighted.

Table 2.3 provides a list of the metabolites that were regulated by NPM-ALK using a statistical cutoff of $p<0.1$ based on analysis of four biological replicates of DMSO and CEP treated cells. Quantity of metabolite levels were obtained from normalized area under the curve (AUC) analysis from mass spectrometry. Importantly, we identified changes in metabolites within the significant pathways highlighted by pathway analysis (Figure 2.9). Specifically, many metabolites in pyrimidine and purine metabolism showed an increase following NPM-ALK inhibition (cytidine, deoxycytidine, guanine) whereas others decreased (S-dihydroorotate, cytosine, ADP-ribose). Additional significant changes were seen in the pentose phosphate pathway, glycolysis and fatty acid metabolism as seen by changes in levels of D-ribose 5-phosphate, lactate and CoA, respectively.

Table 2.3: Metabolomic results for NPM-ALK regulated metabolites.

			Normalized Abundance								
			DMSO				CEP				Fold change
Pyrimidine Metabolism	C00055	CMP	16.9	9.2	13.8	21.5	9.9	10.8	9.6	8.3	0.63
	C00105	UMP	14.6	13.3	10.7	16.4	11.8	12.0	11.0	10.2	0.82
	C00106	Uracil	21.4	16.6	9.9	19.6	6.2	7.7	9.9	8.7	0.48
	C00119	5-Phospho-alpha-D-ribose 1-diphosphate	19.4	16.1	17.7	19.3	4.5	7.2	8.0	7.6	0.38
	C00295	Orotate	29.0	23.3	18.5	18.1	4.3	2.7	2.8	1.4	0.13
	C00299	Uridine	13.6	10.6	9.5	10.4	12.3	15.8	14.0	13.7	1.26
	C00337	(S)-Dihydroorotate	31.7	27.1	23.5	17.8	0.0	0.0	0.0	0.0	0.00
	C00364	dTMP	13.8	20.5	16.7	16.5	8.9	7.2	9.0	7.6	0.48
	C00365	dUMP	13.6	13.7	14.3	13.2	9.7	13.1	11.3	11.1	0.82
	C00380	Cytosine	24.3	23.0	22.8	29.4	0.2	0.0	0.0	0.3	0.00
	C00429	5,6-Dihydrouracil	19.8	13.7	18.4	19.5	4.1	7.7	7.5	9.2	0.40
	C00475	Cytidine	6.6	7.6	5.3	9.3	16.5	17.1	18.8	18.8	2.47
	C00881	Deoxycytidine	3.6	4.7	9.2	4.5	23.1	4.8	25.2	24.9	3.54
	C02354	2',3'-Cyclic CMP	47.8	0.0	24.3	27.9	0.0	0.0	0.0	0.0	0.00
	C05822	3'-CMP	12.3	14.0	12.4	15.8	12.1	12.1	11.0	10.4	0.84
Purine Metabolism	C00020	AMP	18.6	22.2	13.5	18.2	3.4	5.5	14.2	4.3	0.38
	C00037	Glycine	11.6	7.6	10.3	14.2	13.3	16.3	14.0	12.7	1.29
	C00117	D-Ribose 5-phosphate	21.2	22.1	18.7	20.0	3.8	5.0	4.7	4.4	0.22
	C00119	5-Phospho-alpha-D-ribose 1-diphosphate	19.4	16.1	17.7	19.3	4.5	7.2	8.0	7.6	0.38
	C00144	GMP	10.2	11.2	9.9	12.9	14.8	13.7	13.8	13.6	1.27
	C00212	Adenosine	16.2	14.4	10.6	15.1	11.0	11.0	11.7	10.1	0.78
	C00242	Guanine	10.4	10.3	8.1	11.1	13.5	15.1	16.6	14.8	1.51
	C00262	Hypoxanthine	12.9	12.7	9.6	11.3	12.3	13.5	14.5	13.1	1.15
	C00294	Inosine	19.2	18.7	12.3	16.6	7.8	7.4	10.0	7.9	0.50
	C00301	ADP-ribose	21.7	15.8	26.7	25.7	1.3	2.9	3.6	2.3	0.11
	C00330	Deoxyguanosine	16.3	15.0	11.1	15.8	10.2	10.2	11.6	9.8	0.72
	C00387	Guanosine	17.4	16.5	12.2	18.1	8.3	8.3	10.7	8.6	0.56
	C00575	3',5'-Cyclic AMP	14.2	14.5	14.6	12.7	11.7	13.5	10.1	8.8	0.79
	C04677	1-(5'-Phosphoribosyl)-5-amino-4-imidazolecarboxamide	8.4	22.4	20.0	16.1	10.4	14.3	5.7	2.8	0.50
G, S, T, Metabolism	C00037	Glycine	11.6	7.6	10.3	14.2	13.3	16.3	14.0	12.7	1.29
	C00263	L-Homoserine	11.6	11.0	10.0	12.9	14.1	14.8	14.7	10.9	1.20
	C00300	Creatine	14.8	15.3	13.5	13.5	10.4	11.5	11.0	10.0	0.75
	C00719	Betaine	14.7	14.9	15.3	14.1	6.4	10.4	10.6	13.5	0.69
Pentose-P Pathway	C00117	D-Ribose 5-phosphate	21.2	22.1	18.7	20.0	3.8	5.0	4.7	4.4	0.22
	C00119	5-Phospho-alpha-D-ribose 1-diphosphate	19.4	16.1	17.7	19.3	4.5	7.2	8.0	7.6	0.38
	C03752	2-Amino-2-deoxy-D-gluconate	0.0	0.0	0.0	0.0	16.6	19.6	48.4	15.4	100.00
Glycolysis	C00111	Glycerone phosphate	19.0	20.6	17.1	16.1	5.7	7.3	6.1	8.0	0.37
	C00186	(S)-Lactate	22.6	16.6	19.6	22.1	3.2	4.8	5.2	5.9	0.24
TCA Cycle/ Oxidative-P	C00042	NAD+	16.2	13.8	17.2	19.9	6.7	8.9	8.9	8.4	0.49
	C00003	Succinate	17.6	19.8	22.3	18.1	6.4	4.7	6.6	4.4	0.28
Glycerophospholipid Metabolism	C00111	Glycerone phosphate	19.0	20.6	17.1	16.1	5.7	7.3	6.1	8.0	0.37
	C00307	CDP-choline	16.6	12.8	13.1	14.7	10.3	12.1	10.5	9.9	0.75
	C00346	Ethanolamine phosphate	8.2	12.9	7.9	12.1	13.9	16.2	16.2	12.6	1.43
	C00670	sn-glycero-3-Phosphocholine	4.8	4.5	4.1	8.4	14.4	26.0	12.7	25.0	3.57
Fatty Acid Metabolism/ Biosynthesis	C00249	Hexadecanoic acid	16.7	16.3	17.2	16.0	7.1	11.2	11.9	3.7	0.51
	C02679	Dodecanoic acid	14.2	14.0	16.8	13.1	8.1	14.6	12.1	7.3	0.72
	C06424	Tetradecanoic acid	17.7	15.4	17.8	14.9	6.9	11.7	11.6	4.0	0.52
	C00010	CoA	31.1	10.0	21.8	27.6	1.6	4.9	1.5	1.6	0.11
	C00489	Glutarate	17.2	21.5	23.1	9.9	9.3	11.0	8.0	0.0	0.39

MetaboAnalyst was also used to compare the metabolic pathway analysis amongst the other ALCL cell lines used in the metabolomics study. Table 2.4 shows the p-values for several of the key biomass producing pathways across 3 NPM-ALK+ ALCL-derived cell lines. The significant pathways are highlighted in red. SU-DHL-1 cells show a high degree in all of the metabolic pathways listed. SUPM2 cells show a similar level of significance across these biomass producing pathways with purine metabolism, pyrimidine metabolism, pentose phosphate pathway and the TCA cycle significantly altered by NPM-ALK activity. However, DEL cells showed far fewer significant pathway alterations following NPM-ALK inhibition, with pyrimidine metabolism being the only one under the $p<0.05$ cutoff. This difference between ALCL cells in response to CEP treatment could be a result of unknown secondary genetic mutations and/or differences in the efficacy of the CEP compound in the different cell lines.

Table 2.4: MetaboAnalyst pathway p-values (p<0.05, red)

	SU-DHL-1	SUPM2	DEL
Glycolysis	4.23E-06	0.099878	0.51017
Purine Metabolism	5.11E-06	0.000257	0.37293
Pyrimidine Metabolism	5.41E-06	0.007274	0.004755
Glycerophospholipid Metabolism	4.78E-05	0.10037	0.074155
Pentose Phosphate Pathway	0.00013	0.020167	0.14345
TCA Cycle	0.002249	0.003947	0.13724
Gly, Ser, Thr Metabolism	0.002251	0.28365	0.2788

Integrated analysis reveals NPM-ALK-regulated metabolic signature

We integrated the phosphoproteomic and metabolomic data sets in order to generate a global and unified view of the NPM-ALK-regulated metabolic signature. We utilized the Kyoto Encyclopedia of Genes and Genomes (KEGG) mapping tools to integrate our phosphoproteomic and metabolomic data sets into the human metabolic reference map (hsa01100)[247,248]. As shown in Figure 2.13, each colored edge represents a metabolic reaction carried out by phosphoproteins (pY, pS and pT) that was regulated by NPM-ALK. Each node represents a metabolite whose concentration was changed after NPM-ALK inhibition (green = down, red = up). There were concurrent changes in both metabolites and proteins in glycolysis, the TCA cycle, and nucleotide biosynthesis pathways suggesting that NPM-ALK modulates metabolite levels in a number of pathways by altering the expression of phosphoproteins.

A more detailed view of the integrated phosphoproteomic and metabolomic data representing components of the glycolytic pathway and pyrimidine metabolism are shown using KEGG's Search&Color Pathway analysis (Figures 2.14 and 2.15). The colored rectangular boxes and circles represent differentially expressed phosphoproteins and metabolites respectively. The color and intensity is reflective of the degree and direction of change following NPM-ALK inhibition, with red representing an increase and green representing a decrease. Figure 2.14 illustrates the glycolytic pathway while Figure 2.15 shows the pyrimidine metabolism pathway which indicates that many components of the glycolytic and pyrimidine metabolism pathways are differentially regulated by NPM-ALK. Notably, the phosphorylation of

many enzymes within glycolysis was decreased (green rectangular boxes) following ALK inhibition. The changes in phosphoproteins and metabolites observed in response to ALK inhibition are shown in Tables 2.1 and 2.3 respectively. Specifically, Enolase (ENO1) and phosphofructokinase, liver (PFKL) showed a merged spectral count (pY) reduction of 30 and 6 spectral counts, respectively following ALK inhibition. Both lactate (Table 2.3) and phosphorylated lactate dehydrogenase (LDH) (Table 2.1) decreased in response to ALK inhibition. Lactate decreased with an average fold change of 0.24 and LDHB decreased with a merged pY spectral count change of -14. These data suggest that NPM-ALK regulates widespread changes in glycolysis, pentose phosphate pathway and pyrimidine metabolism by altering protein phosphorylation.

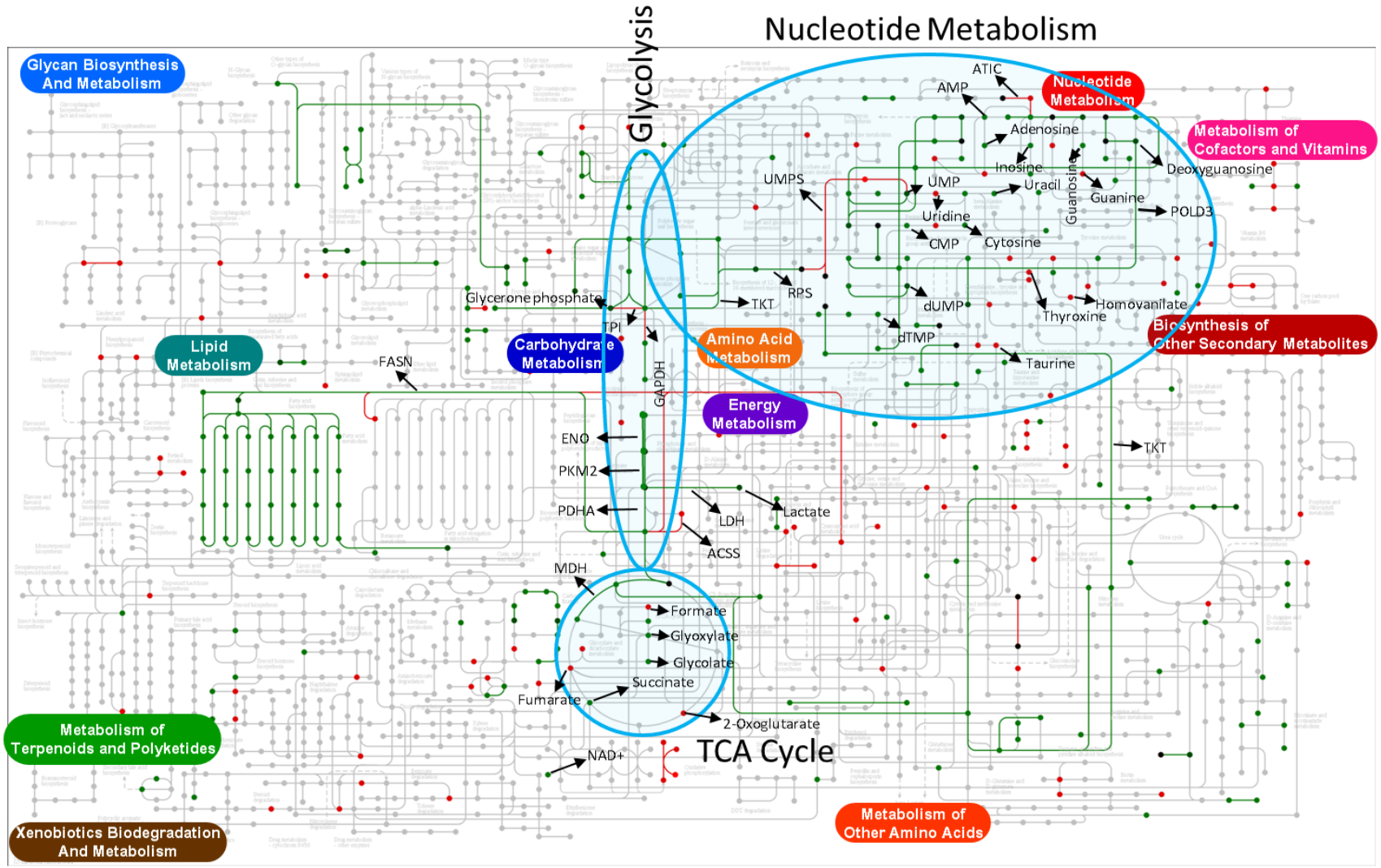

Figure 2.13: Integrated "omic" analysis reveals global metabolic changes. KEGG "search&color pathway" analysis for phosphoproteins and metabolites overlaid on the human metabolic reference map (hsa01100). Phosphoproteomic data from one biological replicate of the SU-DHL-1 was used while metabolomics data from four averaged biological replicates of SU-DHL-1 cells was used. Metabolites that changed (T-test, $p<0.1$) in response to CEP treatment were used. Green and red represent decrease and increase, respectively. Lines represent phosphoprotein and dots represent metabolites. Blue shading over Glycolysis, TCA cycle and nucleotide metabolism serve to highlight pathways that are highly represented.

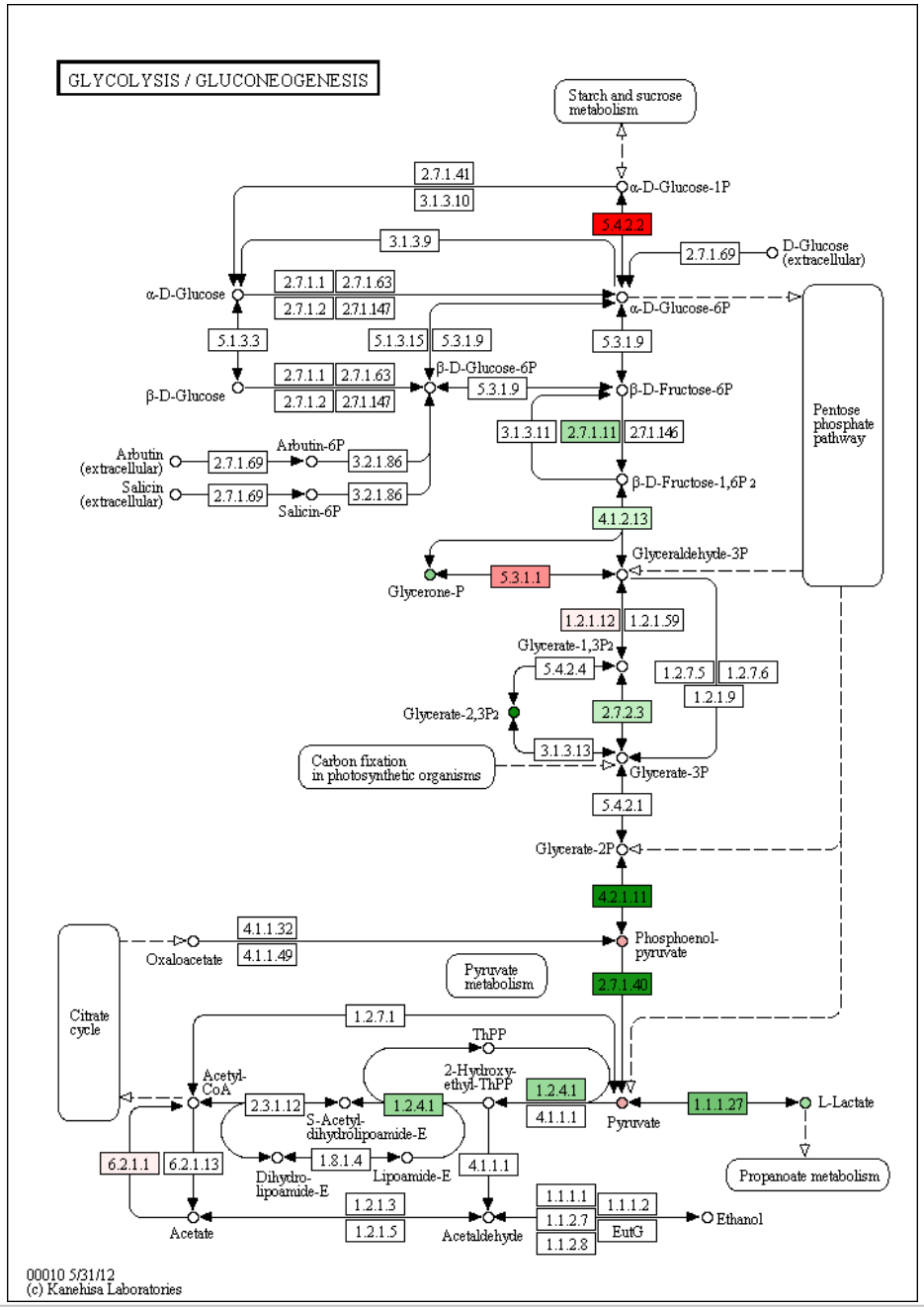

Figure 2.14: Integrated "omic" analysis of glycolysis. KEGG Search&Color Pathway Mapper was used to a generate pathway map of glycolysis for the proteins whose phosphorylation changed in response to NPM-ALK inhibition from the phosphoproteomic studies. The proteomics data represents the merged pS/T (MOAC) and pY (pY-IP) datasets from one biological replicate of SU-DHL-1 cells. The proteins identified are represented by the green and red rectangular boxes. Green represents decrease and red represents increase in phosphoprotein spectral counts following NPM-ALK inhibition. The color intensity of the box corresponds to the extent of change. The metabolomics data was integrated onto these maps and are represented as circles. Color and intensity of the circles follow the same parameters as the boxes.

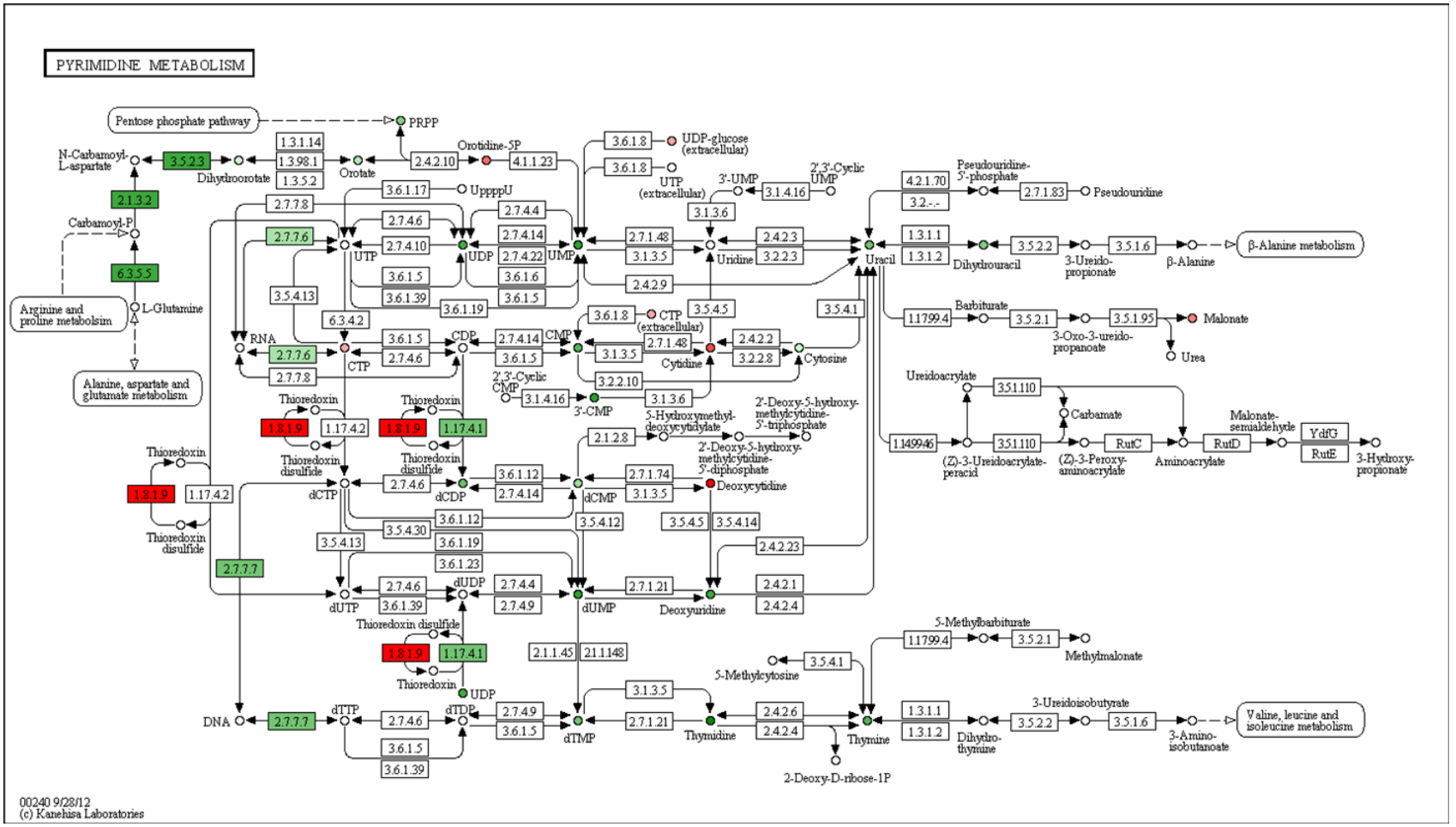

Figure 2.15: Integrated "omic" analysis of pyrimidine metabolism. KEGG Search&Color Pathway Mapper was used to a generate pathway map of pyrimidine metabolism for the proteins whose phosphorylation changed in response to NPM-ALK inhibition from the phosphoproteomic studies. The proteomics data represents the merged pS/T (MOAC) and pY (pY-IP) datasets from one biological replicate of SU-DHL-1 cells. The proteins identified are represented by the green and red rectangular boxes. Green represents decrease and red represents increase in phosphoprotein spectral counts following NPM-ALK inhibition. The color intensity of the box corresponds to the extent of change. The metabolomics data was integrated onto these maps and are represented as circles. Color and intensity of the circles follow the same parameters as the boxes.

Metabolic flux analysis reveals NPM-ALK-regulated metabolic shift

Phosphoproteomic and metabolomic profiling highlighted global changes reflecting NPM-ALK induced steady state alterations in cellular metabolism. Specifically, the metabolomic analysis showed significant reduction in lactate (21.4% SD ± 5.6% of control, $p<0.01$) following NPM-ALK inhibition using area under the curve calculation to determine abundance (Figure 2.16), suggesting that NPM-ALK drives increased lactate production.

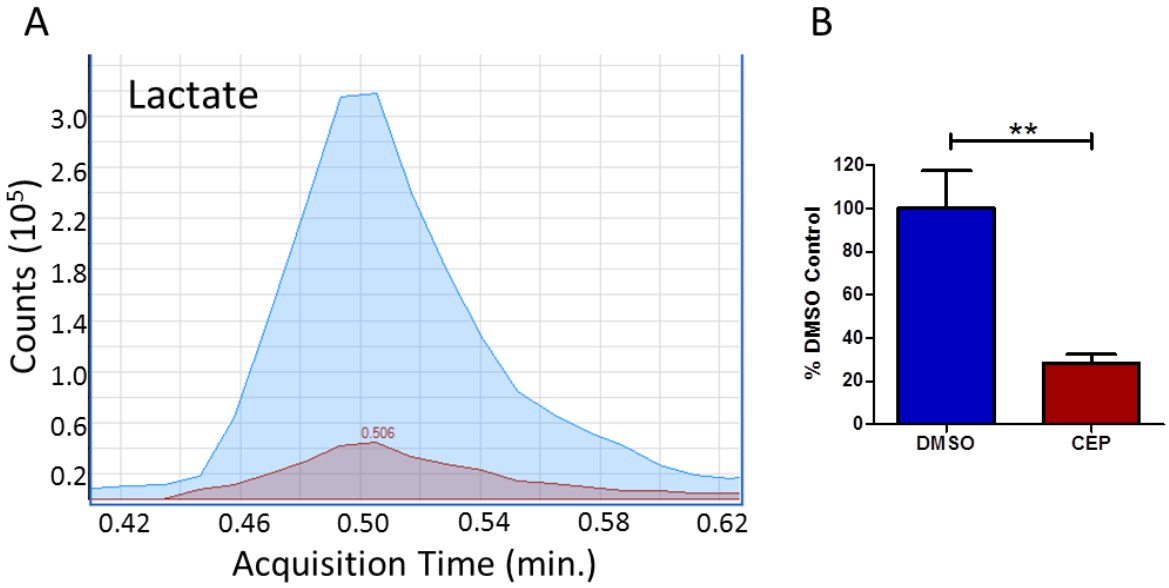

Figure 2.16: NPM-ALK activity drives lactate production. (A) Quantitation of lactate levels from the metabolomics analysis. Representative spectra for DMSO (Blue) and CEP (Red) treated cells. (B) The quantitation of lactate based on four replicates. **p<0.01

All of the metabolomic data to this point represents a snapshot of steady state metabolite levels and does not provide information regarding flux through metabolic pathways. Metabolism is a very dynamic process and to understand how the cells are utilizing the available nutrients is necessary for understanding their metabolic

demands. To address this question we investigated the kinetics of glucose metabolism by determining the flux of glucose carbons through different metabolic pathways. ALCL-derived cell lines were cultured in ^{13}C-glucose and exposed to the ALK inhibitor. [^{13}C]-isotopomers of various metabolites were determined by LC-MS. After 30 minutes of growth in [U-^{13}C]-glucose, the majority of the lactate appeared as fully labeled [m+3] demonstrating that it was derived directly from glucose (Figure 2.17A). Interestingly, NPM-ALK inhibition resulted in a significant reduction (52 ± 19% of control, $p<0.05$) of glycolytic flux to lactate. Similarly, flux of other key metabolites was also impacted by NPM-ALK. Glucose flux to glucose 6-phosphate+fructose 6-phosphate (G6P+F6P) showed a significant reduction (63% of control, $p<0.01$) following NPM-ALK inhibition (Figure 2.17B). Since generation of G6P from glucose represents the first step in glycolysis after glucose entry into the cell, the reduced flux to G6P can be attributed to a reduced glucose uptake rate. Similarly 6-labeled [m+6] fructose 1,6 bisphosphate (FBP) and 3 labeled [m+3] phosphoenolpyruvate (PEP) were also significantly reduced following NPM-ALK inhibition (79% of control, $p<0.05$) (Figure 2.17C-D). Since FBP is an intermediate metabolite and PEP is toward the end of glycolysis, this indicates that NPM-ALK regulates glycolytic flux.

Interestingly, ribose 5-phosphate+xylose 5-phosphate (R5P+X5P) which are key metabolites within the pentose phosphate shunt and supply the sugar backbone for nucleotide biosynthesis also showed a significant reduction of m+5 labeling after NPM-ALK inhibition (61% of control, $p<0.01$) (Figure 2.17E). These data indicate

that NPM-ALK activity increases the flux of glucose metabolism and the pentose phosphate shunt favoring pathways that lead to biomass synthesis.

Importantly, when total pools (all ^{13}C labeled and unlabeled species combined) of ADP and ATP were evaluated after NPM-ALK inhibition, a shift in energy balance was observed. NPM-ALK inhibition induced a 133% (SD ± 33%, $p<0.01$) increase in ATP levels while reducing ADP levels by 72% (SD ± 33%, $p<0.01$) (Figure 2.17F). These data suggest that ALK activity results in a metabolic shift away from energy production favoring biomass production. Importantly, ATP levels are often used as a surrogate for cell health and viability[249]. Thus, the resulting decrease in glycolytic flux in response to NPM-ALK inhibition is not attributable to a loss in viability, but represents a metabolic shift toward energy production.

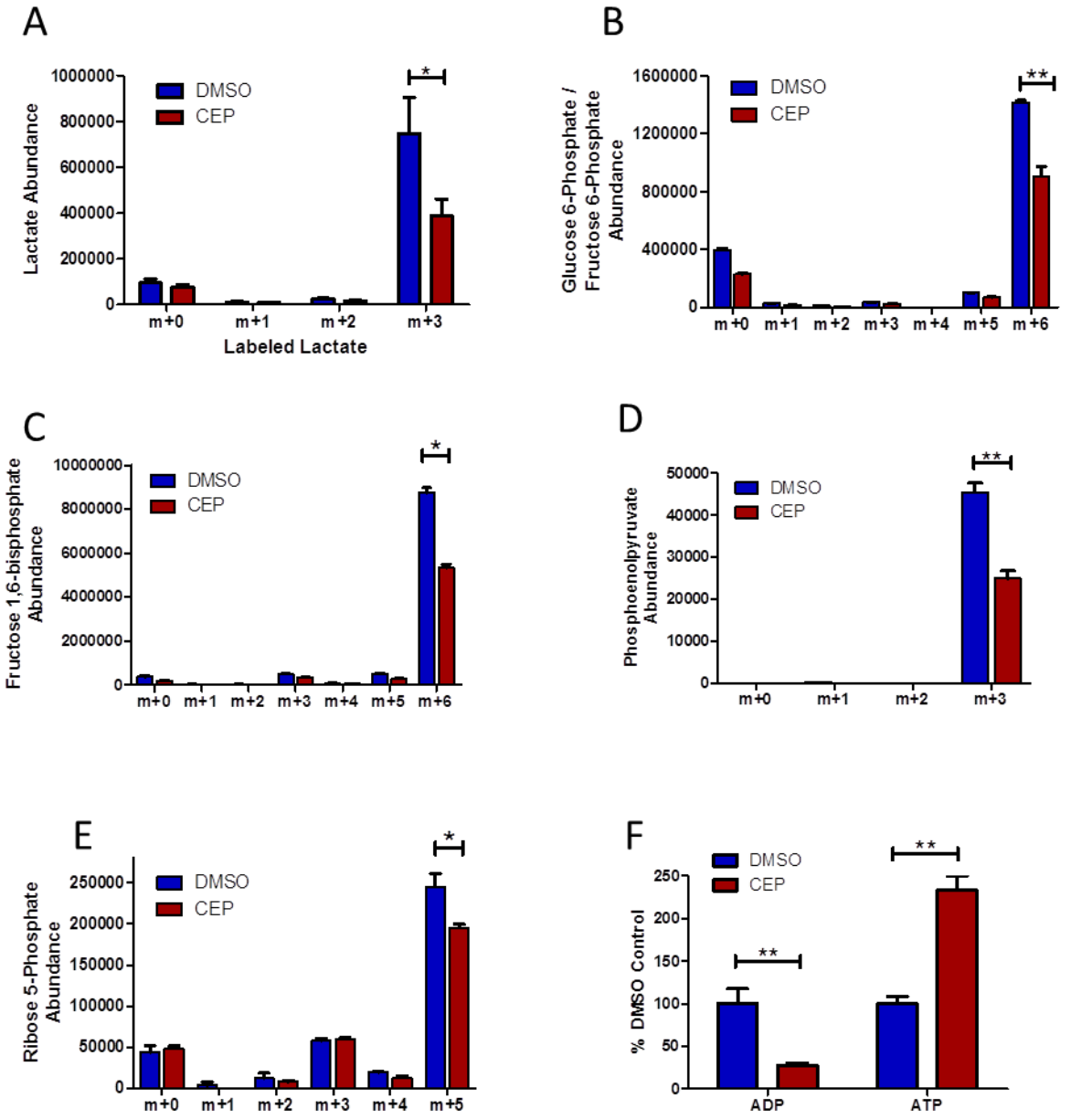

Figure 2.17: Metabolic flux analysis reveals NPM-ALK driven shift toward biomass production. (A) Metabolic flux analysis of lactate in SU-DHL-1 cells following 300nM CEP treatment and 30 minutes treatment with ^{13}C-glucose. All species of labeled lactate are shown. Mass = m. Flux analysis for fully labeled glucose 6-phosphate/fructose 6-phosphate (G6P/F6P) (B), fructose bisphosphate (FBP) (C), phosphoenolpyruvate (D), and ribose 5-phosphate/xylose 5-phosphate (R5P/X5P) (E) are shown in the presence of DMSO or ALK inhibitor. (F) Total pool abundance (all labeled and unlabeled species combined) for ADP and ATP in the presence of DMSO or NPM-ALK inhibitor. Data are mean ± SD, *p<0.05, **p<0.01

In order to quantify NPM-ALK induced changes in metabolic reprogramming for subsequent studies, we measured ATP and lactate levels using biochemical assays. A significant decrease in lactate was detected after ALK inhibition in two ALCL-derived cell lines (18% (SD ± 2.6%, $p<0.01$) decrease in DEL cells and 35% (SD ± 2.9%, $p<0.01$) in SU-DHL-1 cells). There was an increase in ATP levels after ALK inhibition in both DEL (15% (SD ± 4.3%, $p<0.05$) and SU-DHL-1 cells (48% (SD ± 5.9%, $p<0.01$), while no changes in lactate or ATP levels were observed in Jurkat (ALK negative T-cell leukemia) cells (Figure 2.18). Taken together, these data highlight a metabolic shift driven by ALK characterized by an increase in biomass production and a decrease in energy production.

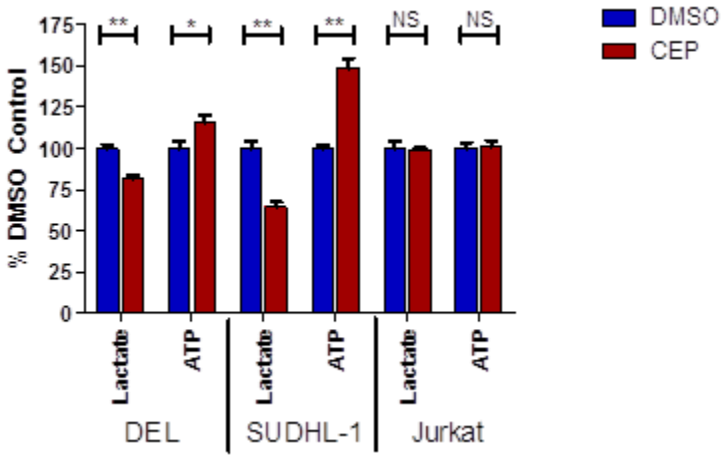

Figure 2.18: NPM-ALK drives metabolic shift away from energy production. Biochemical assays for Lactate (from conditioned media) and ATP (from cell lysates) after 300 nM CEP for 6hrs. Three cell lines were evaluated. Data are mean ± SD, *$p<0.05$, **$p<0.01$

DISCUSSION

Integrated analysis of the phosphoproteomic and metabolomic data identified a novel role of NPM-ALK in the regulation of cellular metabolism. Proteins and metabolites within glycolysis, the pentose phosphate shunt, and pyrimidine metabolic pathways were significantly regulated by the tyrosine kinase activity of NPM-ALK. The observations indicate that oncogenic signaling of NPM-ALK results in an increase in biomass production by re-routing glycolytic intermediates. Our studies represent the first to integrate these powerful screening tools to address the question of metabolic regulation by an oncogenic kinase.

While we were able to identify key metabolic characteristics of ALK kinase activity, this study also points out the limitations of utilizing and integrating large-scale datasets. First, the tools to conduct this level of integration (metabolite and protein phosphorylation) are very limited. Also, the complexity of the data and the variability between cell lines yield difficulties in funneling the data into clear and concise conclusions.

We were able to identify key metabolic and protein phosphorylation changes in numerous biomass producing pathways and map these changes on the KEGG metabolic pathway maps. However, the final interpretation of these landscape images must be considered in the context of the role of each protein phosphorylation. While, several glycolytic proteins are known to be phosphorylated and this phosphorylation alters the enzymatic activity[198,214,218,250,251], many of the phosphorylation sites we identified are novel and may play an activating or inhibitory

role. Therefore, to gain a complete understanding of the metabolic signature of ALK expression, investigation of each protein phosphorylation is necessary.

Phosphoproteomic and metabolomic analysis also indicated that lipid metabolism, amino acid metabolism and nucleotide synthesis metabolism were regulated by NPM-ALK. (Table S1 and S2). Tyrosine phosphorylation or transcriptional regulation of key metabolic enzymes involved in these pathways such as lactate dehydrogenase A (LDHA)[209,218], mitochondrial pyruvate dehydrogenase kinase 1 (PDHK1)[250], phosphoglycerate mutase 1 (PGAM1)[216], have been implicated in mediating an oncogenic metabolic switch. Furthermore, recent studies highlighting the importance of citrate metabolism or impaired TCA cycle function in cancer cells support the notion that metabolic adaption is a hallmark of oncogenesis[252]. Accordingly, future studies to elucidate the molecular mechanisms underlying ALK-dependent regulation of proteins and metabolites within lipid metabolism, nucleotide synthesis and amino acid metabolism are warranted.

Our metabolomic studies identified significant changes in glycine, serine and threonine metabolism in response to ALK inhibition (Figure 2A). Recent studies have demonstrated that PKM2 may regulate *de novo* serine synthesis from the glycolytic intermediate 3-phosphoglycerate (3-PG)[226,253]. The amino acid serine contributes to increased cellular biomass as well as the activation of mTORC1[253]. Given the previously demonstrated effect of NPM-ALK in the activation of mTORC1[165], our results provide a potential link between NPM-ALK and serine synthesis through PKM2.

FUTURE DIRECTIONS

The generation and integration of the phosphoproteomic and metabolomic data led to novel discoveries regarding the role of NPM-ALK in the regulation of cellular metabolism. These large-scale datasets serve as unique resources for the identification of novel ALK substrates. The subsequent chapters (3 and 4) utilize the data obtained through phosphorylation and metabolic analysis to identify novel substrates of ALK and pursue the in depth biochemical and biological consequence of this relationship. However, these datasets provide a rich opportunity to discover additional important signaling mechanisms driven by ALK that are not covered in this dissertation.

Specifically, the role of ALK signaling in regulating glutamine metabolism is unknown. Through our metabolomics analysis we identified glutamine concentrations to be altered upon ALK inhibition in all of our ALCL cell lines (Table 2.2). Glutamine metabolism plays an important role in mediating biomass production and the Warburg effect through c-Myc activation[254]. Since NPM-ALK is known to activate c-Myc[124], it is likely that NPM-ALK signaling also results in alterations within glutamine metabolism to drive the Warburg effect.

Additionally, the integrated analysis revealed alterations in lipid metabolism that were regulated by ALK. Specifically, ALK was found to regulate ACLY through our phosphoproteomic analysis (Table 2.1). Additionally, the metabolomic analysis reveals changes in several lipid metabolism components (Table 2.3). Since cancer

cells must double their membrane size in order to progress through mitosis, the generation of lipids is a metabolic priority[255]. A future project could use these data as rationale for exploring the mechanisms behind ALK regulated lipid metabolism, possibly via the phosphorylation of ACLY.

CHAPTER 3

NPM-ALK Phosphorylates PKM2 Resulting in Metabolic Reprogramming and Increased Tumorigenesis

ABSTRACT

The integrated phosphoproteomic and metabolomic studies identified an NPM-ALK mediated metabolic shift. We identified ALK regulated changes in glycolysis and its derivative biomass producing pathways. We also identified PKM2 to be differentially phosphorylated upon ALK inhibition. Therefore, we hypothesized that NPM-ALK regulates the metabolic shift through the phosphorylation of PKM2. NPM-ALK was found to directly phosphorylate PKM2 at the Y105 residue which consequently reduced its enzymatic activity. Small molecule activation of PKM2 or expression of an Y105F PKM2 mutant led to reversal of the metabolic switch with increased oxidative phosphorylation and reduced lactate production. Increased PKM2 activity and decreased phosphorylation resulted in decreased lymphoma cell viability, colony formation and reduced tumor growth in an *in vivo* xenograft model. Our studies show that PKM2 is a novel substrate of NPM-ALK and plays a critical role in mediating the metabolic shift towards biomass production and tumorigenesis. Small molecule activators of PKM2 may represent novel therapeutic agents for ALCLs.

INTRODUCTION

Global metabolic changes that coordinated with phosphoproteomic changes were characteristic of NPM-ALK expression and activity (Chapter 2). Many of these metabolic and proteomic changes were centered on glycolysis and its derivative biomass producing pathways (the pentose phosphate pathway, pyrimidine metabolism, and purine metabolism). Interrogation of these data led to the identification of PKM2 as a novel mediator of NPM-ALK signaling and a candidate effector molecule in the metabolic phenotype orchestrated by NPM-ALK.

PKM2 has been implicated in the Warburg effect and has been shown to be necessary for tumorigenesis[256]. Through differential splicing mechanisms PKM2 becomes the predominate PK isoform in proliferating cells[257]. Expression of the PKM2 isoform over the PKM1 isoform allows for the regulation of the last step in glycolysis. Phosphorylation of PKM2 as well as the lack of binding of the allosteric activator fructose bisphosphate (FBP) results in dimerization and loss of activity[214]. The inactivity of PK at the end of glycolysis coupled with the general increase in glucose uptake and glycolytic flux seen in many cancer cells, results in the backup of the glycolytic intermediates that serve as starting material for biomass production[190]. Another result of this metabolic reprogramming is the increased lactate production which is necessary to maintain redox balance when driving a metabolism based mainly on glycolysis.

We hypothesized that NPM-ALK phosphorylates PKM2 at Y105 to drive the metabolic shift observed in Chapter 2. The objective of this study was to

characterize the functional relationship of NPM-ALK and PKM2 as well as to determine the role of PKM2 in ALCL tumorigenesis. This study identified PKM2 as a novel substrate of NPM-ALK and that mediated the Warburg effect in NPM-ALK+ ALCL. We showed that NPM-ALK directly phosphorylates PKM2 at Y105 and caused a decrease in its enzymatic activity. Small molecule activators of PKM2 or expression of a PKM2 mutant (Y105F PKM2) resulted in a reversal of the NPM-ALK induced metabolic shift and decreased tumorigenesis of NPM-ALK+ ALCL cells. These studies reveal a novel role of NPM-ALK in the regulation of cellular metabolism via the phosphorylation of PKM2 and offer a rationale for PKM2 activators as potential therapeutic agents for NPM-ALK+ ALCL.

MATERIALS AND METHODS

Cell Lines: Stable PKM2 expressing cell lines were generated with lentiviral transduction from 293FT transfected cell cultured media. Viral packaging plasmid psPAX2 and envelope plasmid pMD2.G were used to generate viral particles while PKM2 was cloned into pRSV-Puro with an N-terminal Flag tag. Stable cell lines were established with puromycin selection.

Western Blotting: Proteins from cell lysates were extracted with lysis buffer (25 mM Tris-Base, 2% SDS, pH 7.4) followed by sonication and centrifugations (16,000 rpm for 10 min). Protein concentrations were determined by BCA assay (Thermo Scientific, Rockford, IL). Twenty µl of protein was separated by SDS-PAGE and transferred to nitrocellulose membranes. Western blotting was performed using the

following antibodies: ALK (Invitrogen, Carlsbad, CA), pY1604-ALK, PKM2 and pY105-PKM2 (Cell Signaling Technologies, Danvers, MA).

In vitro kinase assay: GFP-tagged WT NPM-ALK and K210R NPM-ALK were transfected in 293T cells using lipofectamine 2000 (Invitrogen, Carlsbad, CA) and cells were lysed 48 hours later. Immunoprecipitation using GFP antibody and Protein A/G agarose beads was used to purify NPM-ALK. His-tagged full-length PKM2 (WT, Y105F and Y390F) were expressed in E. coli using isopropyl β-D-1-thiogalactopyranoside (IPTG) induction. Proteins were purified using Ni-nitrilotriacetic acid (NTA) resin, washed 5 times and eluted with 250 mM imidazole (pH 8.0). PKM2 elution was added to NPM-ALK agarose beads along with 10X kinase buffer and 10 mM ATP. Following 30 minute incubation at room temperature, 6X laemmli buffer was added and the samples were boiled for 5 minutes. The reactions were then loaded onto and SDS-PAGE gel and western blots were performed.

PKM2 Activity: PKM2 activity assays were performed as previously described[214]. Briefly, cell lysates (source of PKM2) were incubated with 1mM ADP, 0.5 mM PEP, 0.3 mM NADH and 8 U of LDH. The kinetics of oxidation of NADH is measured by absorbance at 340 nm every 5 minutes until completion of reaction. The slope of the decrease in absorbance was calculated by linear regression analysis and reported as PKM2 activity.

Metabolic Assays: Lactate and ATP was measured in conditioned media and cell lysates, respectively using commercially available kits (BioVision, Milpitas, CA). Cell

lysates were used for ATP analysis and conditioned culture media was used for lactate measurements.

Proliferation and Colony Formation Assays: Proliferation was determined by trypan blue stain and measured on the TC10 Automated Cell Counter (Bio-Rad, Hercules, CA). Cells were seeded at 50,000 cells/ml on day 0. Colony formation assays were performed with Methocult H4230 (Vancouver, BC) per manufactures instructions. Colonies were grown for 14 days before staining with p-iodonitrotetrazolium chloride (Sigma-Aldrich, St. Louis, MO). Initial seeding density was 200 cells/ml.

Xenograft Experiments: Shaved (severe combined immune-deficient) SCID-Biege mice (Charles River, Wilmington, MA) were injected (using 27G needle) with 6 million cells in the subcutaneous flank. 100 µl injection volume containing 50% BD Matrigel (BD, San Jose, CA) was used. Tumors were measured with calipers and the tumor volumes determined through the following equation: $V = (0.5)*(L*W^2)$. During necropsy, tumors were divided for protein extracts and histology. Samples for protein extracts were flash frozen in LN_2, ground into a powder and stored at -80°C. Samples for histology were fixed in 10% formalin. Samples were paraffin embedded and sectioned for Hematoxylin and eosin (H&E) staining.

RESULTS

PKM2 is a substrate of NPM-ALK

Based on the integrated proteomic/metabolomic analysis (Chapter 2) and the results of the metabolic flux analysis which demonstrated the effect of ALK on glycolysis, we pursued the hypothesis that the NPM-ALK directed changes in cellular metabolism were mediated through phosphorylation of PKM2. Our phosphoproteomic analysis identified phospho-PKM2 (p-PKM2) to be significantly reduced following ALK inhibition (z=-1.1) (Figure 2.4). The MS data showed two unique tyrosine phosphorylated peptides of PKM2 decreased upon NPM-ALK inhibition (the peptides contained Y105 and Y390). The representative tandem mass spectra for the peptides containing pY105 (Figure 3.1A) and pY390 (Figure 3.1D) PKM2 are shown. Both peptides were identified with an adjusted probability greater than 0.99. The adjusted probability reflects the probability that the identified peptide actually corresponds to PKM2.

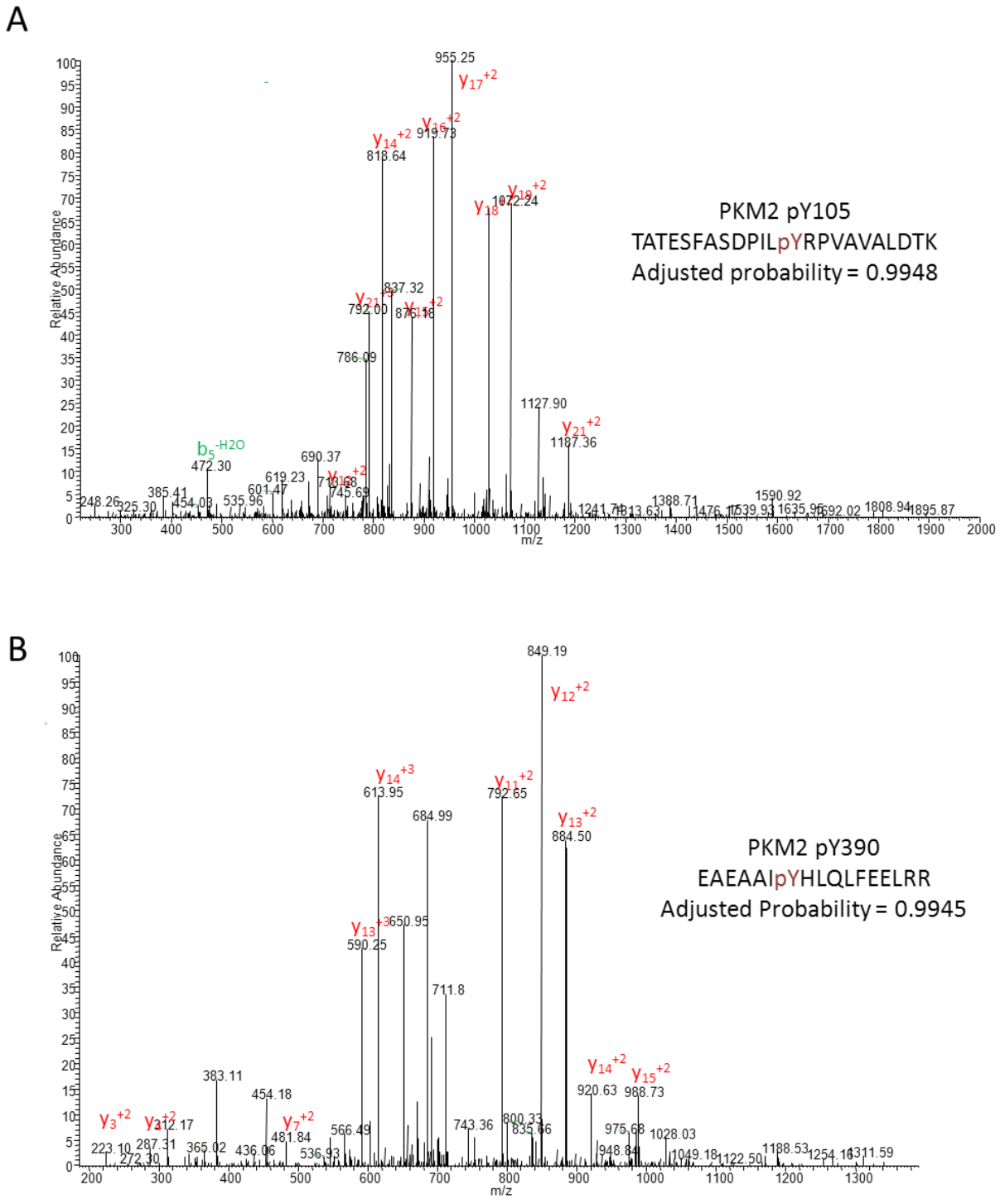

Figure 3.1: Mass spectrometry identification of phosphorylated PKM2. (A) A representative tandem mass spectrum of the PKM2 peptide containing the pY105 residue. (B) A representative tandem mass spectrum of the PKM2 peptide containing the pY390 residue. Identified b and y ions are indicated.

Figure 3.2A tabulates the spectral counts of phosphopeptides of ALK and PKM2 that were determined in a representative experiment in which SU-DHL-1 cells were exposed to DMSO or CEP. There was a significant reduction of spectral counts of ALK-derived phospho-Tyr peptides (76 in DMSO to 0 in CEP), suggesting that the CEP treatment was effective at inhibiting ALK autophosphorylation. Similarly, the spectral counts for peptides containing pY105 PKM2 were reduced from 9 (DMSO) to 2 (CEP treated), while those for the pY390 residue were reduced from 3 to 1. These data provided the rationale to pursue subsequent studies to characterize PKM2 as a mediator of ALK-regulated switch in cellular metabolism. Given the role for pY105-PKM2 in the regulation of its enzymatic activity, we decided to pursue this residue in subsequent studies in NPM-ALK+ ALCL cell lines.

Additionally, we analyzed nine T-cell lymphoma derived cell lines using phosphoproteomic analysis, the results of which are provided in Figure 3.2B. Phosphorylated peptides derived from PKM2 were identified in all four of the ALK+ ALCL cell lines as well as the natural killer/T-cell lymphomas (NK/T-NHL) but not in the ALK negative ALCL (ALK- ALCL), Sézary syndrome (SS) and mycosis fungoides (MF) cells. Western blot analysis corroborated the proteomic results and revealed that the levels of pY105-PKM2 were highest in the ALK+ ALCL cell lines (SU-DHl-1, SUPM2 and Karpas299) and the YT cell line while the rest of the cell lines expressed negligible levels of pY105-PKM2 (Figure 3.2C). In contrast, there was no difference in the expression of total PKM2 or GAPDH. These data indicate that there is an increase in Y105 phosphorylation of PKM2 in ALK+ ALCL cells.

A

SUDHL-1

		DMSO	CEP
	ALK	76	0
PKM2	pY105	9	2
	pY390	3	1

B

	ALK+ALCL				ALK-ALCL	SS	MF	NKTL	
	DEL	Karpas299	SUDHL-1	SUPM2	MAC1	HUT78	HH	NK92	YT
Peptides	8	9	6	11	0	0	0	3	4
Spec Counts	63	34	56	63	0	0	0	19	20

C

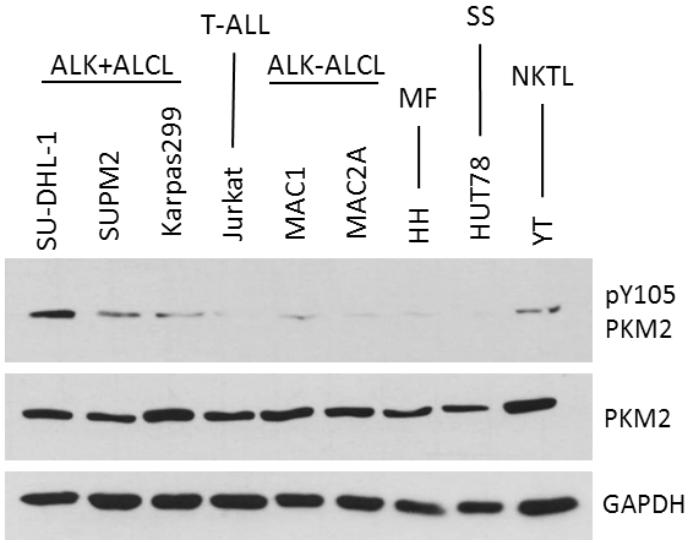

Figure 3.2: pY105-PKM2 is regulated by NPM-ALK and shows differential expression across other T-cell derived lymphoma. (A) Spectral count changes in p-ALK (all phosphorylated peptides) and the two identified PKM2 phosphopeptides in response to NPM-ALK inhibition. (B) Phosphoproteomic data from nine different T-cell lymphoma derived cell lines. Data shows the number of peptides and the spec counts for the identification of PKM2 across the different disease entities. C) Western blot analysis of different T-cell lymphoma derived cell lines for phosphorylated and total PKM2. Mycosis fungoides (MF), Sézary syndrome (SS), Natural killer/T-cell lymphoma (NKTL).

To confirm the phosphoproteomic data suggesting that pY105-PKM2 is regulated by NPM-ALK, western blot analysis of ALCL-derived cells were performed in the presence of DMSO or CEP (Figure 3.3A). CEP treatment (6hrs, 300nM) resulted in inhibition of ALK (as evidenced by abrogation of pY1604 ALK) and a marked reduction of pY105-PKM2 (56% of control) without a change in total PKM2. To verify that these effects are not cell line dependent or a result of selectivity of the CEP compound, we utilized another specific inhibitor of ALK (Crizotinib)[181] in two additional ALCL-derived cell lines. Crizotinib treatment for 16 hours resulted in a significant decrease in Y105 phosphorylation of PKM2 in a dose dependent manner (Figure 3.3B). Crizotinib (100nM) resulted in reduction of pY105-PKM2 levels to 53% and 24% of control in SUPM2 and DEL cells, respectively, while 300nM Crizotinib reduced the levels of pY105-PKM2 to 62% and 15% of control. Furthermore, transfection of 293T cells with WT NPM-ALK resulted in an increase in Y105 PKM2 (average 140%) compared to those transfected with a kinase deficient mutant, K210R NPM-ALK (Figure 3.3C). These results suggest that the kinase activity of NPM-ALK regulates the phosphorylation of PKM2 at the Y105 residue.

Additionally, BA/F3 cells stably transfected with either empty vector (EV) or WT NPM-ALK were analyzed for pY105-PKM2 levels via western blotting. BA/F3 cells are a murine pre-B-cell line that is IL-3 growth dependent[258]. This is a powerful model for determining the transforming potential of oncogenes, as NPM-ALK expression is able to make these cells IL-3 independent[235]. Figure 3.3D shows that pY105-PKM2 was present in both EV and WT NPM-ALK conditions under the presence of IL-3. Upon removal of IL-3 the pY105 was lost from PKM2 in a time

dependent manner in the EV expressing cells (44% after 4 hours). However, WT NPM-ALK expression stabilized pY105 levels of PKM2 with no loss of signal after 4 hours of IL-3 removal. These data suggest that NPM-ALK (and possibly IL-3) regulates the phosphorylation of Y105-PKM2.

In order to determine whether PKM2 is a direct substrate of NPM-ALK kinase activity and not a distant downstream signaling molecule, we carried out *in vitro* kinase assays using immunoaffinity-purified WT or K210R GFP-NPM-ALK and His-tagged WT, Y105F and Y390F PKM2 purified from E. coli. After incubation of both proteins with ATP, western blot analysis was used to detect pY105-PKM2 (Figure 3.3E). Since NPM-ALK is capable of autophosphorylation, pY1604-ALK was used as a positive control. As shown in Figure 3.3D, WT NPM-ALK was autophosphorylated in contrast to the K210R NPM-ALK mutant which showed no p-ALK. WT PKM2 was phosphorylated at the Y105 residue in the presence of active NPM-ALK, but not when it was incubated with K210R NPM-ALK. Also, pY105-PKM2 was not detected when Y105F PKM2 was incubated with WT NPM-ALK. The Y390F PKM2 mutant was also phosphorylated at the Y105 residue by WT NPM-ALK. These data show that NPM-ALK directly phosphorylates PKM2 at the Y105 residue.

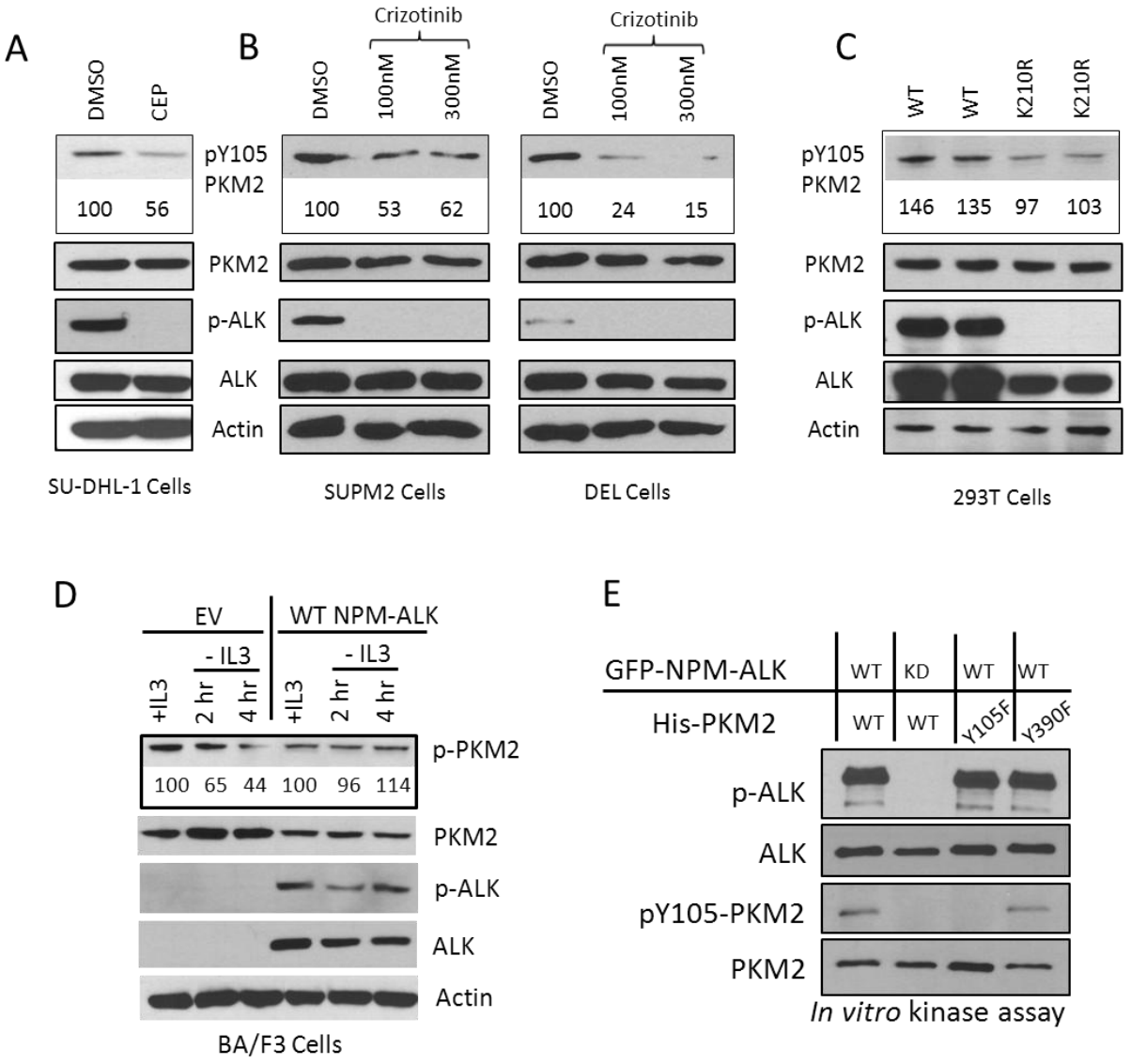

Figure 3.3: NPM-ALK directly phosphorylates pY105-PKM2. (A) Immunoblots of lysates from SU-DHL-1 cells following CEP treatment for 6hrs at 300nM CEP. (B) Immunoblots of SUPM2 and DEL cell lysates after treatment with 100nM and 300nM Crizotinib for 16 hours. (C) Immunoblots of 293T lysates that were transiently transfected with either WT NPM-ALK or K210R NPM-ALK (samples in duplicate). (D) Immunoblots from BA/F3 cells stably transfected with either empty vector (EV) or WT NPM-ALK. Cells were lysed following 0, 2 or 4 hours of IL3 removal from media. (E) *In vitro* kinase assay with purified His-PKM2 (WT, Y105F or Y390F) and ALK immunoprecipitation using GFP-NPM-ALK (WT or K210R).

NPM-ALK regulates PKM2 activity via Y105 phosphorylation

We next sought to determine the effect of NPM-ALK mediated phosphorylation of PKM2 on its enzymatic activity using an assay that measures the conversion of phosphoenolpyruvate (PEP) to pyruvate with subsequent LDH-catalyzed conversion of pyruvate to lactate. The consumption of NADH by LDH is measured by optical density (OD) at 340nm and the kinetics are calculated (Figure 3.4A, schematic)[214]. Based on a series of experiments to optimize the dose and duration, we evaluated cell lysates of ALCL cell lines to quantitate PKM2 activity after a 4-hour exposure to CEP (100 nM). Figure 3.4B shows the raw kinetic data for this experiment. The positive control contains purified PK, while the negative control contains no PK source. The slope of the OD decay was calculated using linear regression analysis and is plotted at the PKM2 activity rate in Figure 3.4C. Inhibition of ALK resulted in a significant increase in PKM2 enzymatic activity (159% of control, $p<0.01$), suggesting that NPM-ALK reduces PKM2 activity. Similarly, 293T cells transfected with WT NPM-ALK showed reduction of PKM2 activity by 14% (SD ± 2.9%) compared to mock transfected cells and those transfected with a kinase-deficient K210R NPM-ALK mutant (Figure 3.4D-E). Interestingly, the levels of PKM2 activity correlated with the levels of Y105-PKM2 phosphorylation under varying NPM-ALK activity/expression conditions (Figures 3.3A and 3.3C). These data provide evidence for the negative regulation of PKM2 activity by NPM-ALK.

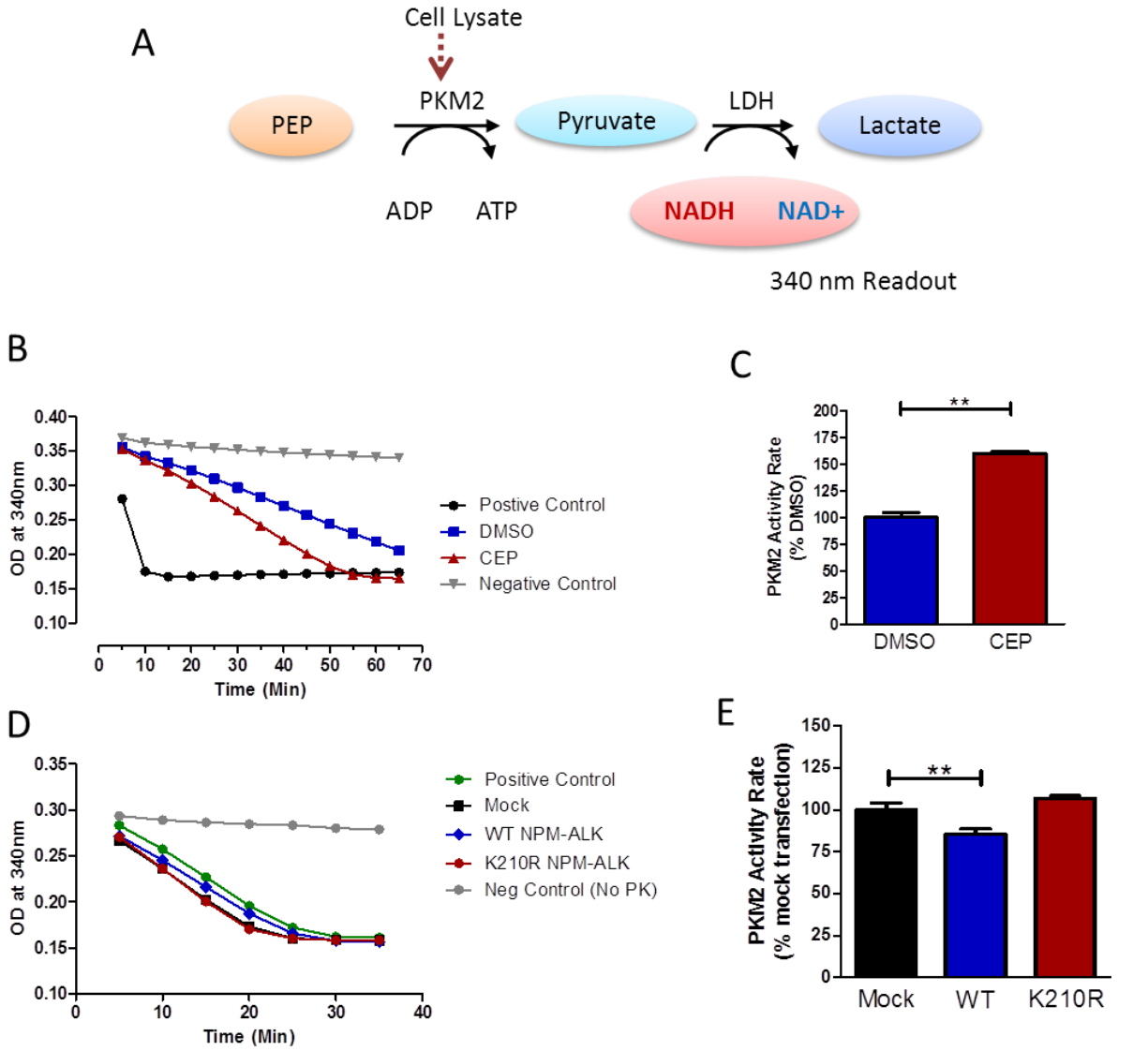

Figure 3.4: NPM-ALK regulates the activity of PKM2. (A) Schematic representation of PKM2 activity assay. PEP, ADP, NADH and LDH are added to the reaction in excess. PKM2 is supplied from cell lysates. Activity is determined by the slope of decay of 340nm optical absorbance. (B) PKM2 activity assay timecourse for SUPM2 cells treated with DMSO or CEP 100nM for 4 hours. Positive control contains purified PKM2 protein, negative control contains no PKM2. (C) Quantification of PKM2 activity rate from (B) by calculating slope. (D) PKM2 activity assay timecourse on lysates from 293T cells transfected with mock, WT NPM-ALK or K210R NPM-ALK. (E) Quantification of PKM2 activity rate from (D) by calculating slope. Data are mean ± SD, **p<0.01

In order to directly evaluate the function of the pY105-PKM2 in ALK expressing cell lines, we generated cell lines stably expressing a non-phosphorylatable Y105F-PKM2 mutation. Expression of flag-Y105F-PKM2 and flag-WT-PKM2, are shown in Figure 3.5A. As shown in Figure 3.5B, DEL cells which express Y105F-PKM2 displayed increased PKM2 activity, 68% (SD ± 6%, $p<0.01$) compared to WT control. Together, these data demonstrated that phosphorylation of PKM2 by NPM-ALK results in inhibition of its enzymatic activity.

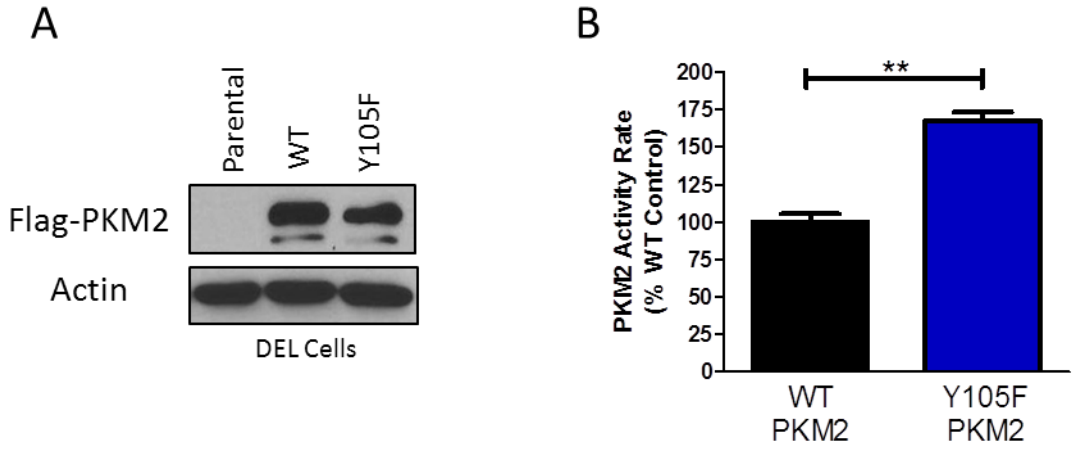

Figure 3.5: pY105-PKM2 reduces its enzymatic activity. (A) Stable expression of Flag-PKM2 in DEL cells. B) PKM2 activity assay of DEL cells stably expressing WT or Y105F PKM2. Data are mean ± SD, **$p<0.01$

Phosphorylation of PKM2 alters cellular metabolism

In order to assess the biological implications of NPM-ALK mediated phosphorylation of PKM2 and consequent inhibition of its enzymatic activity, we utilized two small molecule activators of PKM2 and evaluated their effect on cellular metabolism of ALCL-derived cell lines. The two compounds (NCGC00186528

(TEPP-46), and NCGC00186527 (NCGC-527)) were derived from the chemical class thieno-[3,2-b]pyrrole[3,2-d]pyridazinone and differ only by a change in one side-group (Figure 3.6A)[225]. Anastasiou et al. reported the PKM2 activating capabilities of these compounds (Figure 3.6B). Treatment of SU-DHL-1 cells with 30 μM of the two activators (NCGC-527 and TEPP-46) for 16 hours, resulted in a significant increase, 52% (SD ±11%, $p<0.01$) and 57% (SD ± 11%, $p<0.01$) respectively, in PKM2 activity (Figure 3.6C). These compounds as well as the Y105F-PKM2 expressing cells provided us with valuable tools to investigate the role of PKM2 activity and phosphorylation in NPM-ALK expressing cells.

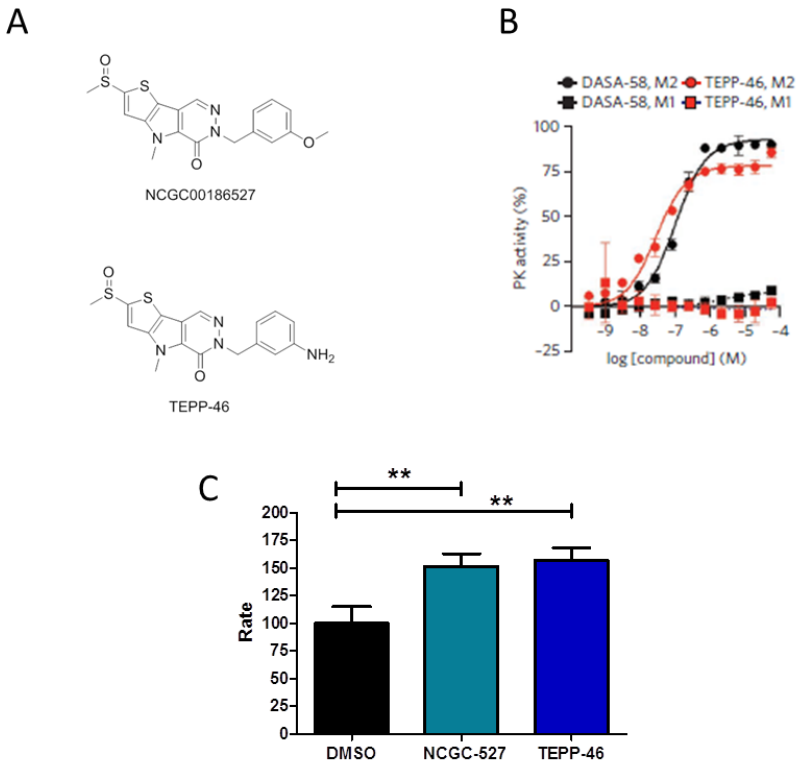

Figure 3.6: PKM2 activator compounds increase PKM2 enzymatic activity. (A) Chemical structures of NCGC00186527 (top) and TEPP-46 (bottom). (B) TEPP-46 and DASA-58 (not used in this dissertation) effects on PKM1 (M1) and PKM2 (M2) activity. Data from collaborators (Anastasiou et al. 2012). (C) PKM2 activity assay using SU-DHL-1 treated with 10μM NCGC-527 or TEPP-46 for 24 hours. Data are mean ± SD, **$p<0.01$

The activation of PKM2 by NCGC-527 led to a significant decrease in lactate production, 20% (SD ± 6.4%, $p<0.01$) in Karpas299 cells and 23% (SD ± 5.1%, $p<0.01$) in DEL cells (Figure 3.7A). This was associated with a corresponding increase in ATP levels with a 67% (SD ± 12%, $p<0.01$) increase in Karpas299 cells and a 19% (SD ± 1%, $P<0.01$) increase in DEL cells. Jurkat cells (ALK negative) did not show a significant change in lactate or ATP levels following PKM2 activation by either compound. Similarly, DEL cells stably expressing Y105F-PKM2 also exhibited a metabolic shift compared to WT-PKM2 expressing cells (Figure 3.7B). The mutant Y105F-PKM2 expressing cells produced 42% (SD ± 7.7%, $p<0.01$) less lactate and 69% (SD ± 3.2%, $p<0.01$) more ATP than their WT counterpart. These data indicate that NPM-ALK expression results in phosphorylation of PKM2 with consequent inhibition of its activity and altered cellular metabolism. The metabolic shift, driven by NPM-ALK causes increased lactate production, a known marker of the Warburg effect. Furthermore, this shift in metabolism decreases ATP production likely because much of the carbon sources are diverted to biomass producing pathways.

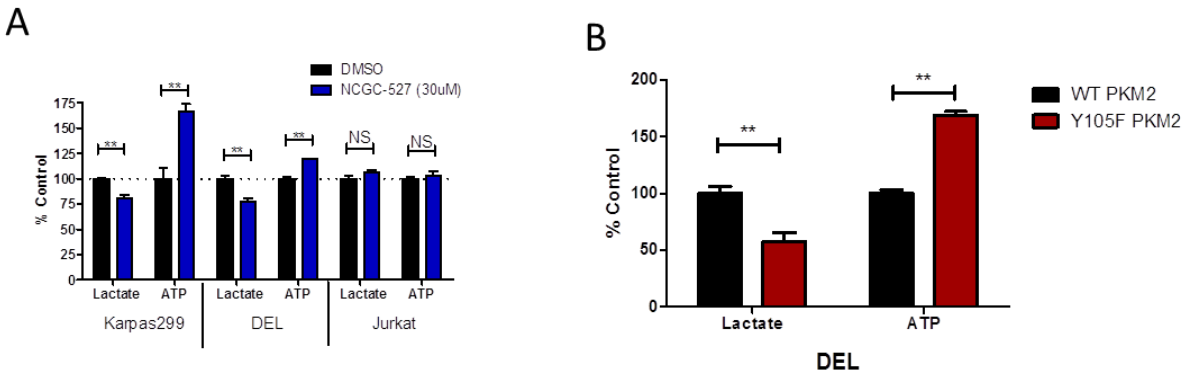

Figure 3.7: PKM2 activity and phosphorylation induce a metabolic shift. (A) Lactate and ATP assays using conditioned media and cell lysates (respectively) on Karpas299, DEL and Jurkat cells following 6 hour treatment with 30µM NCGC-527. C) Lactate and ATP assays on DEL cells stably expressing Flag-PKM2 WT on Flag-PKM2 Y105F.

Phosphorylation of PKM2 regulates cell proliferation

Next, we investigated the effect of PKM2 phosphorylation on cell proliferation. DEL cells were treated with increasing concentrations of PKM2 activator (NCGC-527) and cell proliferation was monitored over 72 hours by trypan blue staining under both normoxic (21% O_2) and hypoxic (3% O_2) conditions to determine their sensitivity in differing oxygenated environments. There was reduction of cell proliferation in a dose dependent manner in both normoxic and hypoxic conditions (Figure 3.8A). At 72 hours, cells exposed to PKM2 activator NCGC-527 (30µM) showed a 54% (SD ± 8.6%, $p<0.01$) reduction in proliferation in normoxic conditions compared to DMSO. At the same concentration of NCGC-527 cells in hypoxic conditions showed a 69% (SD ± 5%, $p<0.01$) reduction in proliferation. Interestingly, under normoxic conditions the cells still maintained greater than 85% viability (as

determined by trypan blue staining) under the highest concentration of NCGC-527 (Figure 3.8B). In contrast, cells exposed to PKM2 activation under hypoxic conditions demonstrated a dose dependent decrease in cell viability with only 49% (SD ± 11%, $p<0.01$) viable cells remaining after 72 hours with 30 μM NCGC-527. These data suggest that chemical activation of PKM2 results in a metabolic shift from anaerobic glycolysis to oxidative phosphorylation. While PKM2 activation decreases proliferation, it does not induce cell death under normoxic conditions. However, the cells grown in hypoxic conditions die as a result of PKM2 activation. This suggests that cells with active PKM2 are reliant on oxidative phosphorylation for survival.

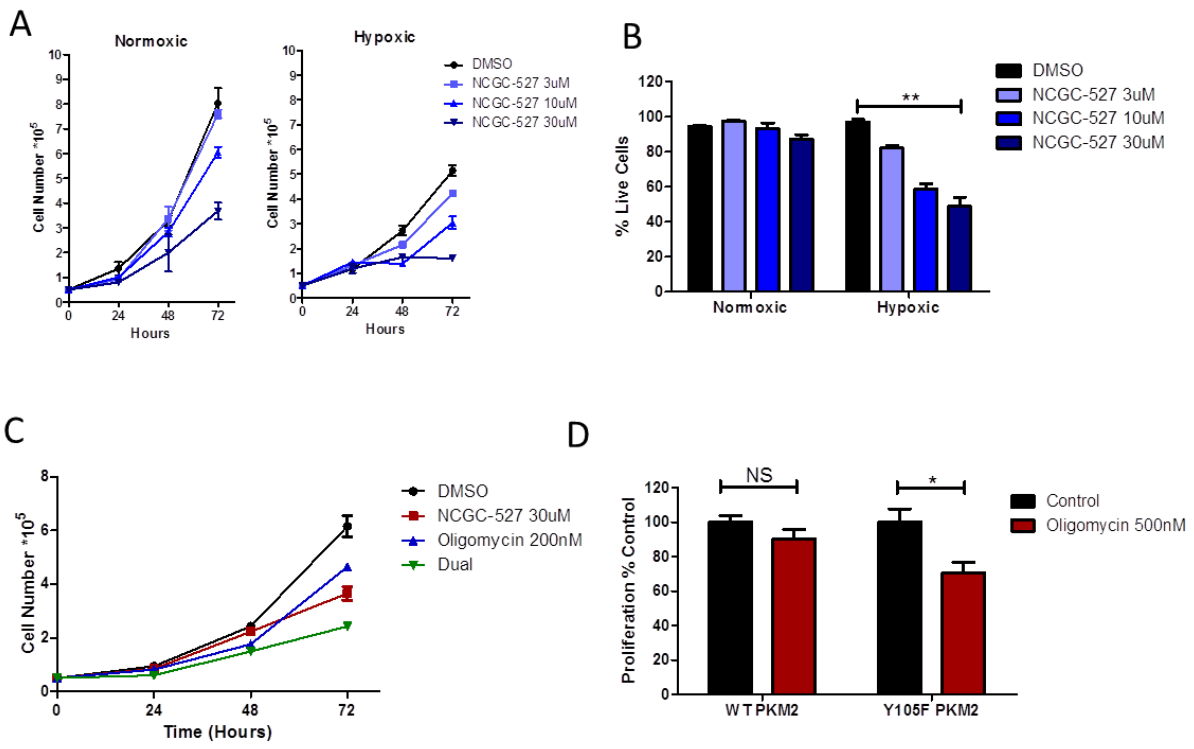

Figure 3.8: PKM2 regulates ALCL proliferation. (A) Cellular proliferation measured by trypan blue staining of DEL cells treated with indicated concentrations of NCGC-527. Cells were maintained in either normoxic or hypoxic (3% O_2) conditions. (B) Viability data from (A) 72 hour time point showing the % live cells under the indicated conditions. (C) Cell proliferation of DEL cells treated with NCGC-527, oligomycin or both (dual). (D) Cell proliferation of DEL cells stably expressing Flag-PKM2 and treated with DMSO or 500nM oligomycin for 48 hours. Counts were normalized to each control (DMSO) condition. Data are mean ± SD, *p<0.05, **p<0.01, not significant (NS)

Similarly, when DEL cells were exposed to both the PKM2 activator and oligomycin (ATP synthase inhibitor)[259] under normoxic conditions, an additive decrease in cell proliferation was observed (39%, SD ± 4.7%, p<0.01 compared to DMSO control) (Figure 3.8C). Furthermore, DEL cells stably expressing Y105F-PKM2 were growth sensitive to oligomycin (72 hours) and resulted in a 30% (SD ± 12%, p<0.05) reduction in proliferation relative to DMSO control whereas oligomycin had minimal effect (91% of control, SD ± 11%, p=0.2) in DEL cells stably expressing

WT-PKM2 (Figure 3.8D). The increased sensitivity of Y105F-PKM2 expressing cells to ATP synthase inhibition suggests that these cells were more reliant on oxidative phosphorylation than their WT counterpart. These data support the role for phosphorylation and inhibition of PKM2 as a key regulatory mechanism for the metabolic switch towards anaerobic glycolysis and consequent impact on cell proliferation.

PKM2 regulates tumorigenesis

To investigate the role of PKM2 in tumorigenesis of NPM-ALK+ALCL, methylcellulose colony formation assays were conducted using PKM2 activating compounds as well as WT-PKM2 and Y105F-PKM2 stably expressing DEL cells. Activation of PKM2 using increasing doses of NCGC-527 resulted in a significant reduction in number of colonies formed after 14 days in a dose response manner (Figure 3.9A). The number of colonies under 10μM NCGC-527 was 107 (SD ± 7.2, $p<0.01$) which represented 24% reduction compared to DMSO treated cells. There were 39% (SD ± 2.2%, $p<0.01$) fewer colonies in cells exposed to 30μM NCGC-527 relative to DMSO treated cells. Furthermore, DEL cells expressing Y105F-PKM2 showed significantly reduced number of colonies as compared to WT-PKM2 (46%, SD ± 10.4%, $p<0.01$). These data indicate that the activity and phosphorylation of PKM2 contribute to the tumorigenic potential of ALK+ALCL cells *in vitro*.

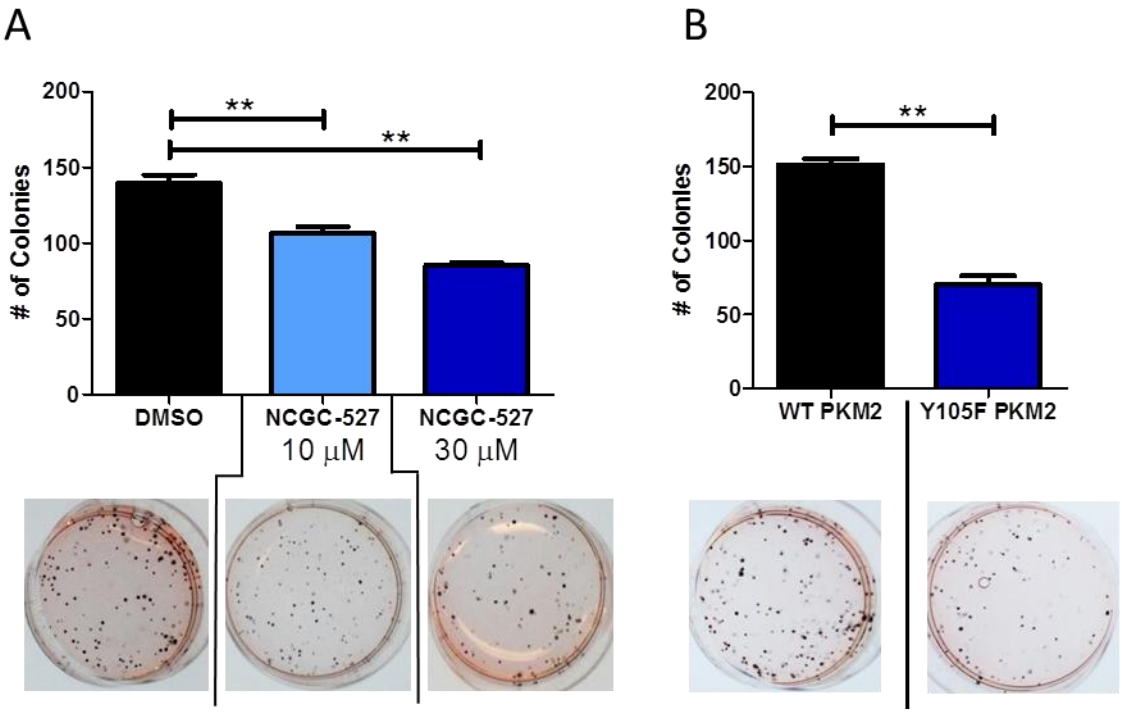

Figure 3.9: PKM2 regulates ALCL colony formation. (A) Methylcellulose colony formation assay using DEL cells treated with 10μM and 30μM NCGC-527 (A) and DEL cells stably expressing Flag-PKM2 WT and Y105F (B). Samples analyzed in triplicate with a representative image shown below each bar. Data are mean ± SD. *p<0.05, **p<0.01

In order to determine the role of PKM2 in ALK+ALCL tumorigenesis *in vivo*, we evaluated the tumorigenic potential of PKM2 activators and the WT-PKM2 and Y105F-PKM2 in xenografted tumors in mice. TEPP-46 was used for this study based on the availability of the compound and the similarity of the *in vitro* effect on PKM2 activity and cell proliferation between NCGC-527 and TEPP-46 (Figure 3.6C and data not shown). SCID-Beige mice (n=7) were implanted with DEL cells (6 million cells per injection in 100μl injection volume containing 50% matrigel in the subcutaneous flank) and orally treated with either vehicle (0.5% methylcellulose + 0.1% Tween 80) or TEPP-46 (50 mg/kg, B.I.D.) on the day of tumor injection. Tumor

volume was assessed on a daily basis until day 14 when maximal diameter exceeded 1cm and animals were sacrificed. As shown in Figure 3.10A, 14 days after tumor injection, the vehicle treated mice showed significant tumor growth (359 mm^3, SEM ± 63 mm^3) while the TEPP-46 treated mice showed marked retardation in tumor growth and development with mean tumor volume of 56 mm^3 (SEM ± 27 mm^3, $p<0.01$) with 3 of the 7 mice developing no measurable tumors. Figure 3.10B shows the gross images of three representative tumors from each group of vehicle treated (upper panel) and TEPP-46 treated mice (lower panel).

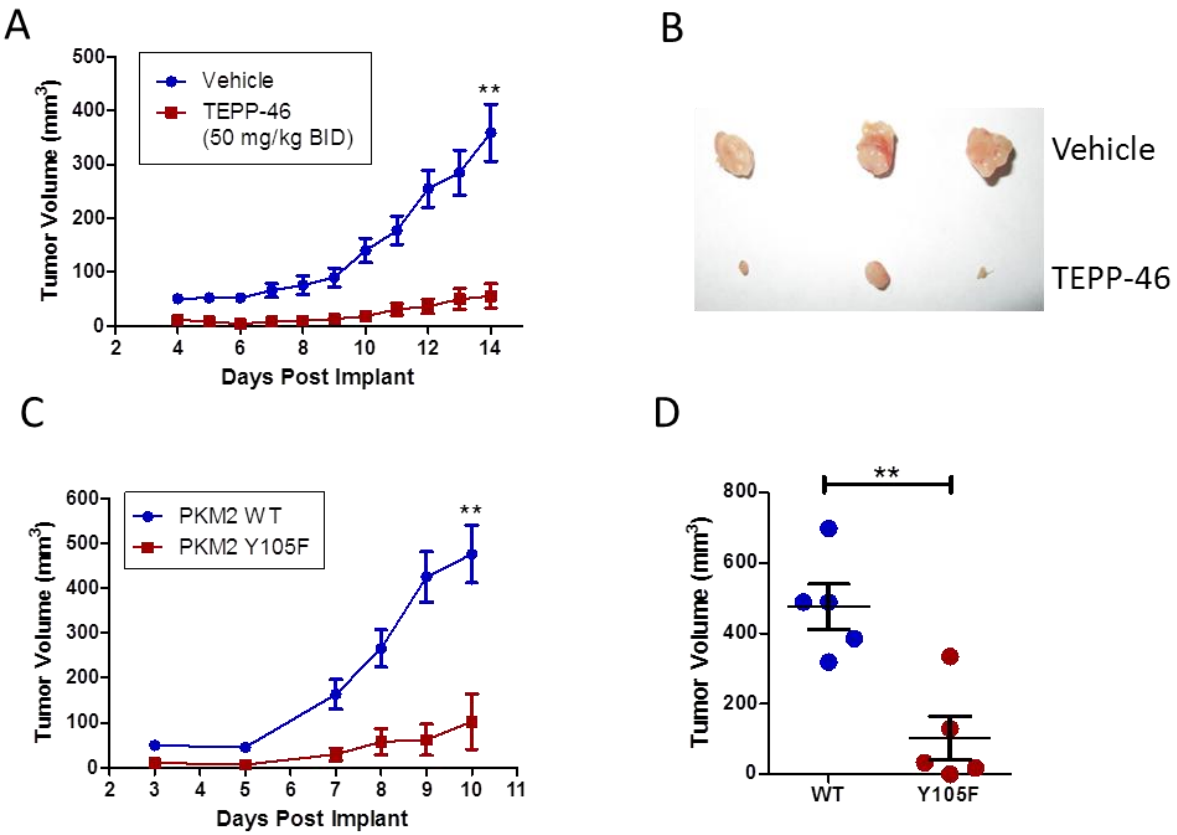

Figure 3.10: PKM2 regulates ALCL tumorigenesis. (A) Tumor volumes of DEL xenograft tumors treated with TEPP-46 (50mg/kg, BID) by oral dose from day of tumor implantation for a duration of 14 days (n=7). (B) Representative images of tumors at day 14. (C) Tumor volumes of xenografted DEL cells stably expressing WT or Y105F-PKM2 (n=5). (D) Scatter plot of day 10 tumor volumes. Data are mean ± SEM, **p<0.01

DEL cells stably expressing WT or Y105F PKM2 were implanted in the subcutaneous flank of SCID-Beige mice (n=5) and tumor volumes were measured over 10 days (Figure 3.10C). Mice xenografted with cells expressing Y105F PKM2 showed significant reduction in tumor volume compared to WT after 10 days ($p<0.01$). The average tumor volume for the WT-PKM2 was 476 mm^3 (SEM ± 64 mm^3) while the Y105F-PKM2 tumors averaged 103 mm^3 (SEM ± 62 mm^3) (Figure 3.10D).

To assess the level of exogenous Flag-PKM2 expressed in the resulting tumors, western blots were performed to compare expression in the implanted cells vs. the resulting tumors (Figure 3.11A). Cells stably expressing WT and Y105F-PKM2 showed strong Flag expression while the DEL parental cells did not. Lysates derived from WT tumors showed Flag expression at comparable levels to the WT cell lines. However, tumors in the Y105F-PKM2 group lost expression of the mutant PKM2 vector compared to the cell lines. Importantly, the two Y105F-PKM2 tumors shown in Figure 3.11A were the only tumors in this group that were large enough to produce protein extracts. These data suggest that the WT-PKM2 expression has no effect on tumor formation, but in Y105F-PKM2 expressing cells, tumor growth is contingent on the ability of these cells to lose expression of the mutant gene, as previously reported[225].

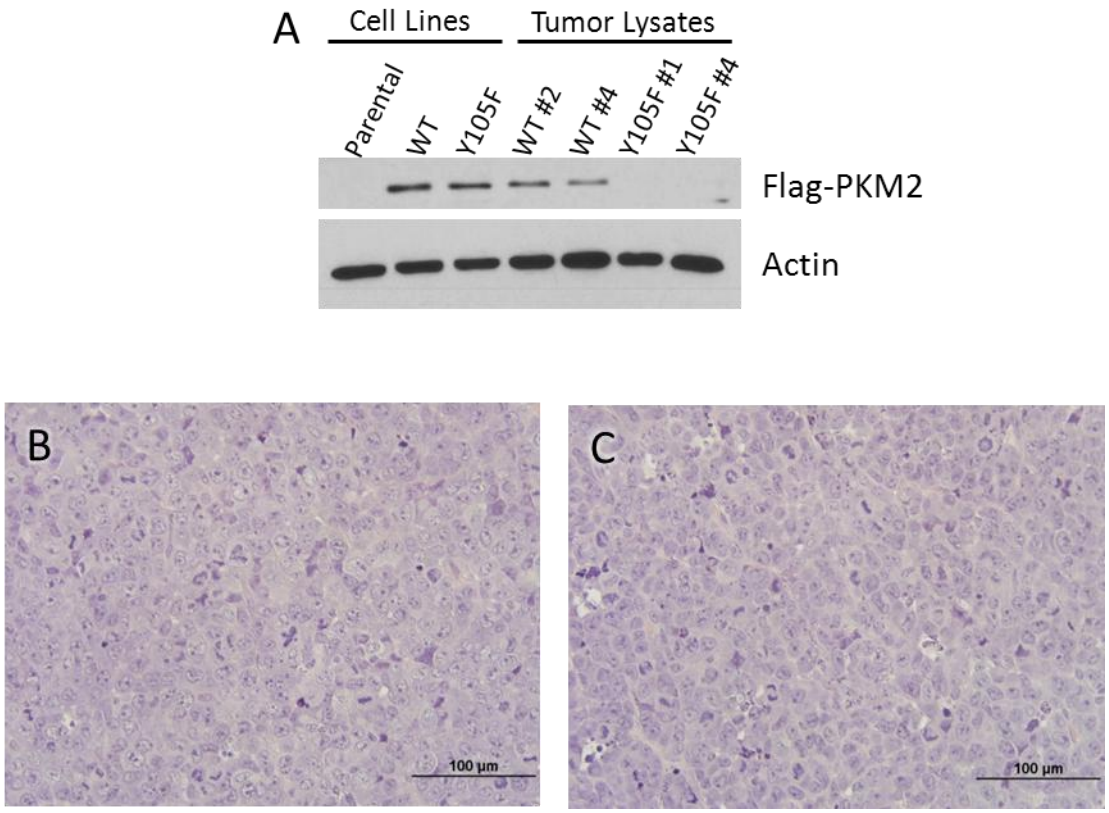

Figure 3.11: *Ex vivo* analysis of PKM2 mutant tumors. (A) Western blot analysis of cell lines used for tumor injections and tumor lysates from several of the developed tumors from (Figure 3.10 C-D). (B) H&E staining of a tumor section for WT PKM2 expressing DEL cells. (C) H&E staining of a tumor section for WT PKM2 expressing DEL cells.

Furthermore, histology sections from the WT and Y105F-PKM2 expressing tumors were taken and stained with H&E (Figure 3.11B-C). Tumors from both conditions displayed the characteristic cells of ALCL including large cells with abundant cytoplasm and kidney shaped nuclei. Many mitoses were also identified in both conditions suggesting aggressive tumor growth. No differences in cell size were observed. Importantly, the Y105F expressing tumor (Figure 3.11C) was one of the two tumors large enough to take sections for histology. Also, this tumor was shown to have lost expression of the Y105F-PKM2 gene (Figure 3.11A, lane 6).

Therefore, these data substantiate the idea that the Y105F-PKM2 expressing cells will not undergo tumorigenesis unless the expression of this mutant gene is lost. The results from this study suggest that phosphorylation of PKM2 at the Y105 residue plays a major role in promoting ALCL tumorigenesis. Taken together, these data indicate that the phosphorylation and inhibition of PKM2 is an important aspect of NPM-ALK regulated tumorigenesis in ALCL.

DISCUSSION

This study reveals that PKM2 mediates the NPM-ALK directed metabolic shift towards a Warburg effect (Figure 3.12). Inhibition of PKM2 via Y105 phosphorylation reprograms the cellular metabolism to generate biomass which is necessary for tumorigenesis. We show that through chemical activation of PKM2 or the mutation of the Y105-PKM2 residue, the cellular metabolism is diverted back to a more “normal” metabolism that is dependent on oxidative phosphorylation and not conducive to tumorigenesis.

PKM2 is a key regulator of aerobic glycolysis. As the last enzyme in glycolysis, the PKM2 isoform of pyruvate kinase is frequently expressed in tumors and proliferating cells[256]. The enzymatic activity of PKM2 has been shown to be regulated by tyrosine phosphorylation and phosphorylated peptide binding[214,223] with consequent diversion of glycolytic intermediates toward biomass production. Our data provide evidence that tyrosine phosphorylation of Y105 PKM2 by NPM-ALK may represent a mechanism by which lymphoma cells acquire a metabolic advantage that facilitates tumor growth. Pharmacological activation of PKM2 and

the expression of Y105F-PKM2 were effective in reversing the metabolic switch and subsequent proliferation and tumorigenesis. Our data substantiates the role of PKM2 in metabolic reprogramming in lymphoid cells and expands the spectrum of oncogenic tyrosine kinases that regulates its activity.

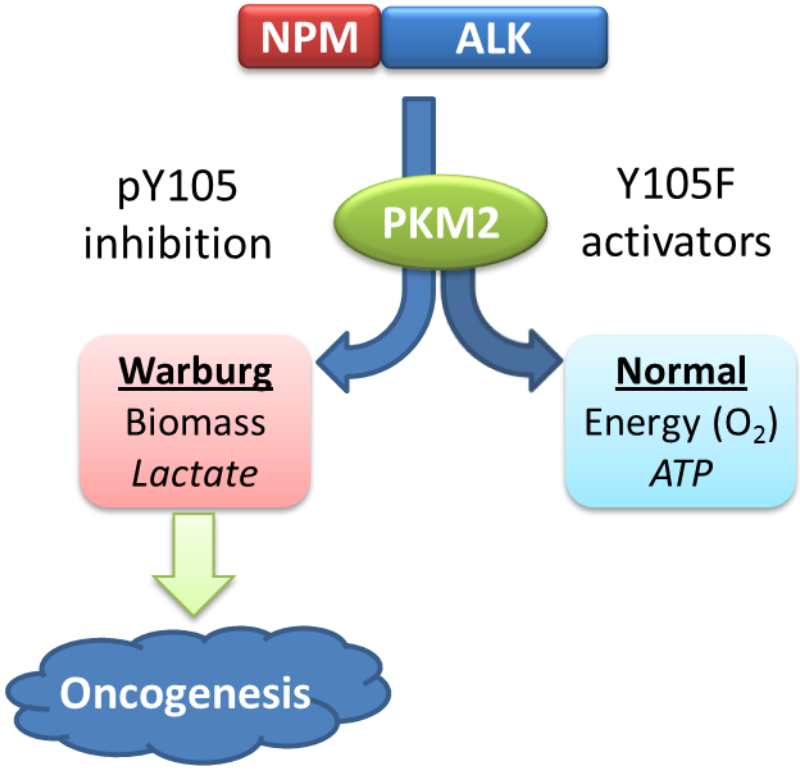

Figure 3.12: Working model for NPM-ALK regulation of metabolism through PKM2. The phosphorylation of PKM2 by NPM-ALK results in inhibition of its enzymatic activity and the shift toward Warburg effect. This metabolic program generates biomass needed from proliferation and produces lactate as a byproduct. Mutating the Y105 residue or using PKM2 activating compounds, the metabolism is shift back to a "normal" metabolism which is driven to produce ATP and consumes O_2 as a result. This form of metabolism is not conducive for rapid proliferation or oncogenesis.

Our data also indicates that activation of PKM2 controls the shift to a metabolic framework that is more reliant on oxidative phosphorylation and energy production. This is highlighted in Figure 3.8 where activation of PKM2 had no effect

on cell viability under normal oxygen conditions. This suggests that oxidative phosphorylation is not conducive to tumor formation as seen by the reduced colony formation and tumor growth in xenograft studies.

Our findings suggest that PKM2 may serve as a therapeutic target in ALCL. NPM-ALK is an oncogenic tyrosine kinase that activates numerous growth-promoting signaling pathways in ALCLs. ALCLs are aggressive lymphomas and although most patients respond well to aggressive chemotherapeutic agents, many patients experience relapses and recurrence[260]. Recently developed small molecular inhibitors of ALK have shown promising early responses for patients with NPM-ALK+ ALCL. However, a subset of patients develops resistance to kinase inhibitors highlighting the need to expand on therapeutic options for these patients. Combination therapies that target multiple signaling pathways including NPM-ALK-mediated metabolic changes may provide additional benefit and are worth investigating in clinical trial settings.

The results of our study show for the first time that NPM-ALK regulates cellular metabolism to increase aerobic glycolysis, decrease oxidative phosphorylation and enhance biosynthesis and tumorigenesis. We identify PKM2 as a new substrate of NPM-ALK and provide the mechanistic rationale for the use of PKM2 activators as therapeutic agents in NPM-ALK+ ALCL.

FUTURE DIRECTIONS

This study identifies PKM2 as a novel substrate of NPM-ALK and defines its role in reprogramming cellular metabolism in ALCL cell lines. However, recent studies have greatly expanded the role of PKM2 in oncogenesis beyond metabolic reprogramming. Specifically, PKM2 has been shown to be necessary for transcriptional activation in several complexes. PKM2 translocates to the nucleus upon EGFR and ERK1/2 activation and phosphorylation of S37-PKM2[231,234]. Once inside the nucleus, PKM2 is necessary for the transactivation of transcriptional regulators such as β-catenin, HIF-1α, STAT3 and Oct4[230-234]. The PKM2 driven phosphorylation of STAT3 and Histone H3 leads to increased target gene expression. Interestingly, the role of PKM2 in regulating gene transcription seems to be mutually exclusive to its role in glycolysis. The dimer form of PKM2 is active in gene transcription, while the tetramer form of PKM2 is active in PEP to pyruvate conversion in glycolysis.

An interesting future project derived from this current study will be to address these transcriptional roles of PKM2 in the context of NPM-ALK and ALCL. Is the S37 phosphorylation and nuclear translocation of PKM2 driven by NPM-ALK signaling? Is PKM2 involved in transcriptional regulation in ALCL? How does the NPM-ALK regulated Y105-PKM2 phosphorylation affect the transcriptional regulatory role of PKM2? STAT3, β-catenin and HIF-1α have all been implicated in ALCL tumorigenesis, so it is plausible that PKM2 is involved in regulating these transcriptional complexes[113,130,261].

CHAPTER 4

NPM-ALK signals through GSK3β to promote oncogenesis

ABSTRACT

The mass spectrometry-based phosphoproteomic screen described in Chapter 2 identified GSK3β as a signaling mediator of NPM-ALK. Using a selective inhibitor of ALK, we demonstrated that the tyrosine kinase activity of ALK regulates the serine-9 phosphorylation of GSK3β. Expression of NPM-ALK in 293T cells led to an increase of pS^{9}-GSK3β compared to kinase-defective K210R mutant NPM-ALK but did not affect total GSK3β levels. Phosphorylation of pS^{9}-GSK3β by NPM-ALK was mediated by the PI3K/AKT signaling pathway. ALK inhibition resulted in degradation of GSK3β substrates Mcl-1, CDC25A and GYS which was recovered upon chemical inhibition of the proteasome (MG132). Furthermore, the degradation of Mcl-1 was recoverable with inhibition of GSK3β. ALK inhibition resulted in decreased glycogen stores within the cells. Decreased cell viability under ALK inhibition was rescued by GSK3β inhibition. Stable knockdown of GSK3β conferred resistance to the growth inhibitory effects of ALK inhibition, as seen by viability and colony formation assays. pS^{9}-GSK3β and CDC25A were selectively expressed in neoplastic cells of ALK+ ALCL tissue biopsies and showed a significant correlation

($p<0.001$). Conversely, ALK- ALCL tissue biopsies did not show significant correlation of pS^9-GSK3β and CDC25A expression ($p<0.2$). Our results demonstrate that NPM-ALK regulates the phosphorylation of S^9-GSK3β via PI3K/AKT. The subsequent inhibition of GSK3β activity results in accumulation of CDC25A, Mcl-1 and GYS which confers growth advantage and protection from apoptosis. These findings provide support for the role of GSK3β as a mediator of NPM-ALK oncogenesis.

INTRODUCTION

Our phosphoproteomics studies (Chapter 2) also aided us in the identification of GSK3β as a candidate mediator of NPM-ALK signaling. GSK3β is a serine/threonine kinase that is constitutively active in resting cells[262,263]. Upon growth factor signaling, GSK3β is phosphorylated at serine-9 which inhibits its ability to target key substrates for proteasomal degradation. The inhibition of GSK3β by serine-9 phosphorylation is the result of the amino terminal tail of the protein folding back on itself and pS9 residue binding to the active site. This active site occupation prevents substrates from entering. The resulting accumulation of substrates such as CDC25A and Mcl-1 that regulate the cell cycle and apoptosis contributes to the enhanced proliferative capacity of tumor cells[264-267]. GSK3β was originally discovered through its role in glucose metabolism and insulin signaling. Upon insulin receptor activation, AKT phosphorylates and inactivates GSK3β[268]. Under resting conditions GSK3β phosphorylates and inhibits glycogen synthase (GYS) preventing glycogen production. Therefore, insulin signaling removes that inhibitory pressure on GYS, allowing for increased glycogen production. GSK3β also plays a

key role in other signaling mechanisms. In the WNT signaling pathway, active GSK3β is associated with APC and Axin to form a destruction complex. Here GSK3β and CK1 phosphorylate β-catenin, targeting it for proteasomal degradation. Upon binding of WNT to its receptor Frizzled (FZ), the destruction complex is disrupted and β-catenin is free to translocate to the nucleus where it is drives WNT target gene expression.

Based on our phosphoproteomic studies we hypothesized that NPM-ALK regulates the phosphorylation of GSK3β to induce proliferative and metabolic phenotypes. The objective of this study was to define the functional relationship between NPM-ALK and GSK3β as well as investigate the role of GSK3β in ALCL oncogenesis. We showed that serine-9 phosphorylation of GSK3β is dependent on NPM-ALK kinase activity and the PI3K/AKT pathway. We provided evidence that NPM-ALK activity results in stabilization of Mcl-1 and CDC25A through GSK3β inhibition which in turn enhances cell viability, proliferation and oncogenic potential. Furthermore, tissue biopsies of ALK+ ALCLs express pS^{9}-GSK3β as well as CDC25A provided additional support for its functional significance in ALK+ ALCLs.

MATERIALS AND METHODS

Cell lines and inhibitors: SU-DHL-1, DEL, Karpas299 and SUPM2 cells were cultured in RPMI 1640 + 10% fetal bovine serum (FBS). 293T cells were cultured in DMEM +10% FBS. All cells were maintained in humidified incubators containing 5% CO_2. SU-DHL-1 cells stably expressing tetracycline inducible shRNA targeting ALK were generated as previously described[269]. Transient transfections were done with

Lipofectamine 2000 (Invitrogen, Carlsbad, CA). Stable GSK3β knockdown SU-DHL-1 and Karpas299 cells were generated by lentiviral transfection with MISSION shRNA sequence: CCGGCCCAAATGTCAAACTACCAAACTCGAGTTTGGTAGTTT GACATTTGGGTTTTT (Sigma-Aldrich, St. Louis, MO). The 7-amino-1,3,4,5,-tetrahydrobenzoazepinone derivative selective ALK inhibitor (Compound 15, Cephalon, Inc, Frazer, PA) was previously described[270]. CAL-101 was acquired from Chemietek (Indianapolis, IN). MG132 was acquired from Sigma-Aldrich (St. Louis, MO). GSK3 Inhibitor IX was acquired from Calbiochem (San Diego, CA). All compounds were dissolved in DMSO.

Phosphoproteomics: See Chapter 2.

Western Blotting and Antibodies: Cell lysates were resolved on 10% SDS-Page and transferred to nitrocellulose. Antibodies used: GSK3β, pS^{9}-GSK3β, p-ALK (Y1604), Mcl-1, AKT, p-AKT (S473), PARP (rabbit, 1:1000, Cell Signaling), ALK (mouse, 1:1000, Invitrogen), CDC25A (mouse, 1:200, Santa Cruz Biotechnology).

Glycogen Assay: Glycogen concentrations were measured cell lysates using commercially available kit (BioVision, Milpitas, CA).

WST-1, Colony Formation, Flow Cytometry: Cell proliferation and viability was assessed by WST-1 assay per manufacturer's protocol (Roche Applied Science, Indianapolis, IN). Cells were seeded with an initial density of 50,000 cells/ml and monitored by WST every day for 4 days. Colony formation assay was performed with MethoCult methylcellulose-based media per manufacturer's protocol (Stemcell Technologies, Vancouver, Canada). An initial seeding density of 200 cells/ml was

used. After 14 days, colonies were stained with iodonitrotetrazolium chloride (5 mg/ml in PBS) overnight and counted. Apoptosis and viability were assessed by flow cytometry following cell staining with Annexin V and propidium iodide (PI)[271].

Immunohistochemistry: Tissue samples were obtained from the archives of the Hematopathology Section, Department of Pathology, University of Michigan, with institutional approval (HUM00023256). IHC staining was conducted with the following antibodies: ALK (mouse, 1:100, Dako), pS^{9}-GSK3β (rabbit, 1:50, Cell Signaling Technology) and CDC25A (mouse, 1:500, Abcam).

GSK3 Interactome: GSK3β was cloned into the pGLUE expression vector and coupled with a tandem affinity purification tag (TAP-tag). Constructs were transfected in 293T cells using Lipofectamine 2000 (Invitrogen, Carlsbad, CA) and cell lysates were collected 48 hours later. Protein extracts were incubated in 100µl of packed streptavidin resin (Amersham, Piscataway, NJ) at 4°C overnight. Resin was washed five times and eluted with 2mM biotin. Eluents were separated by SDS-PAGE. Gel lanes were excised and cut into 16 slices. Upon reduction (10 mM DTT) and alklylation (50 mM iodoacetamide) of the cysteines, proteins were digested overnight with sequencing grade, modified trypsin (Promega). Resulting peptides were resolved on a nano-capillary reverse phase column (Picofrit column, New Objective) using a 1% acetic acid/acetonitrile gradient at 300 nl/min and directly introduced in to an ion-trap mass spectrometer (LTQ XL, ThermoFisher). Data-dependent MS/MS spectra on the 5 most intense ion from each full MS scan were collected (relative CE ~35%). Proteins were identified by searching the data against Human IPI database (v 3.41, 72,254 entries) appended with decoy (reverse)

sequences using X!Tandem/Trans-Proteomic Pipeline (TPP) software suite[272,273]. All proteins with a ProteinProphet probability score of >0.9 (error rate <2%) were considered positive identifications and manually verified.

RESULTS

Identification of phospho-GSK3β by mass spectrometry

Given the oncogenic role of constitutively active NPM-ALK tyrosine kinase in ALK+ ALCL, we hypothesized that NPM-ALK expressing cell lines would exhibit a phosphoproteomic signature that would reflect the signaling cascade regulated by the oncogene. To gain insight into these signaling pathways and to identify novel regulators of NPM-ALK induced oncogenesis, we used a phosphoproteomic approach[274] to evaluate the tyrosine phosphorylated proteins in the NPM-ALK expressing SUPM2 cell line. SUPM2 cell lysates were subjected to phosphopeptide enrichment using phosphotyrosine specific antibodies followed by tandem mass spectrometry. NPM-ALK-derived phosphotyrosine peptides in addition to numerous other phosphorylated proteins were identified (data not shown). Among this list was an eleven-amino acid tryptic peptide corresponding to GSK3β protein phosphorylated at Y216 (Figure 4.1A and B). Of note, this phosphotyrosine peptide has been identified in a similar study contributing to the confidence of this candidate protein[177]. Based on the known role of GSK3β in cellular signaling[262], we hypothesized that GSK3β may mediate the oncogenic properties of NPM-ALK. Since GSK3β activity is known to be regulated by growth factor signaling through

serine-9 phosphorylation, we hypothesized that NPM-ALK regulates the serine phosphorylation of GSK3β and inhibits its activity.

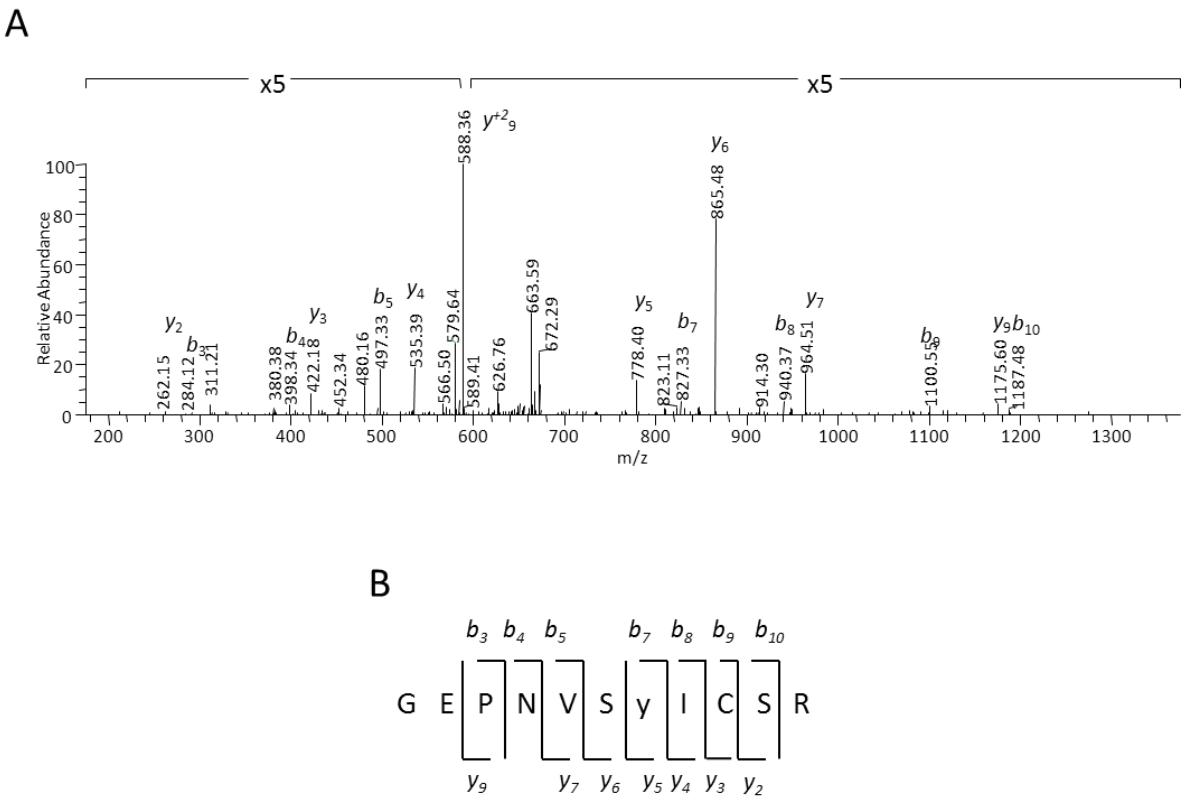

Figure 4.1: Identification of phosphorylated GSK3β in NPM-ALK expressing cells (A) SU-DHL-1 (ALK+ ALCL) cells were subjected to PhosphoScan (Cell Signaling Technologies, Danvers, MA) enrichment and tandem mass spectrometry. Representative MS/MS spectrum of phosphopeptide from GSK3β is shown. Identified *b* and *y* ions are indicated. (B) The sequence and cleavage sites for the identified GSK3β phosphopeptide.

NPM-ALK regulates the serine-9 phosphorylation of GSK3β

In order to determine whether serine phosphorylation of GSK3β is NPM-ALK dependent, we utilized a small molecule (CEP-26939, Compound 15) to inhibit ALK kinase[270]. Treatment of SU-DHL-1 cells with the ALK inhibitor for 2 and 6 hours

resulted in a marked decrease in the levels of phosphorylated NPM-ALK (Y1604) but not total NPM-ALK (Figure 4.2A). There was marked decrease of pS^9-GSK3β in both a dose and time dependent manner, while total GSK3β levels remained unaffected. After 6 hours of 300nM CEP treatment only 34% of the serine phosphorylated GSK3β remained. Three additional ALCL-derived cell lines (DEL, Karpas 299 and SUPM2) were treated with 300nM CEP for 6 hours (Figure 4.2B) and similar to the effect observed in SU-DHL-1 cells, pS^9-GSK3β was consistently reduced by ALK inhibition in all of the cell lines. Notably, in contrast to the marked decrease in ALK phosphorylation, the decrease in pS^9-GSK3β was not complete. This may be partially explained by the existence of other kinases that phosphorylate GSK3β independent of NPM-ALK. Alternatively, the time points used may not be representative of the maximal loss of pS^9-GSK3β. In addition, protein phosphatases that regulate pS^9-GSK3β may be weakly active in the context of NPM-ALK. Similarly, 293T cells that were transiently transfected with vectors encoding the kinase defective mutant (K210R) showed a 76% reduction in GSK3β serine phosphorylation compared to those that expressed the wild-type NPM-ALK (Figure 4.2C). Consistent with the previous observation, there was no effect on expression of total GSK3β protein levels. Next, we evaluated the effect of ALK knockdown using stable tetracycline inducible shRNA targeting NPM-ALK in SU-DHL-1 cells[269]. Successful knockdown of NPM-ALK, which was observed after 4 days of tetracycline treatment, led to a marked decrease (79%) in pS^9-GSK3β (Figure 4.2D), while the total GSK3β protein levels remained unchanged. These data demonstrate that NPM-ALK kinase activity is required for the serine-9 phosphorylation of GSK3β.

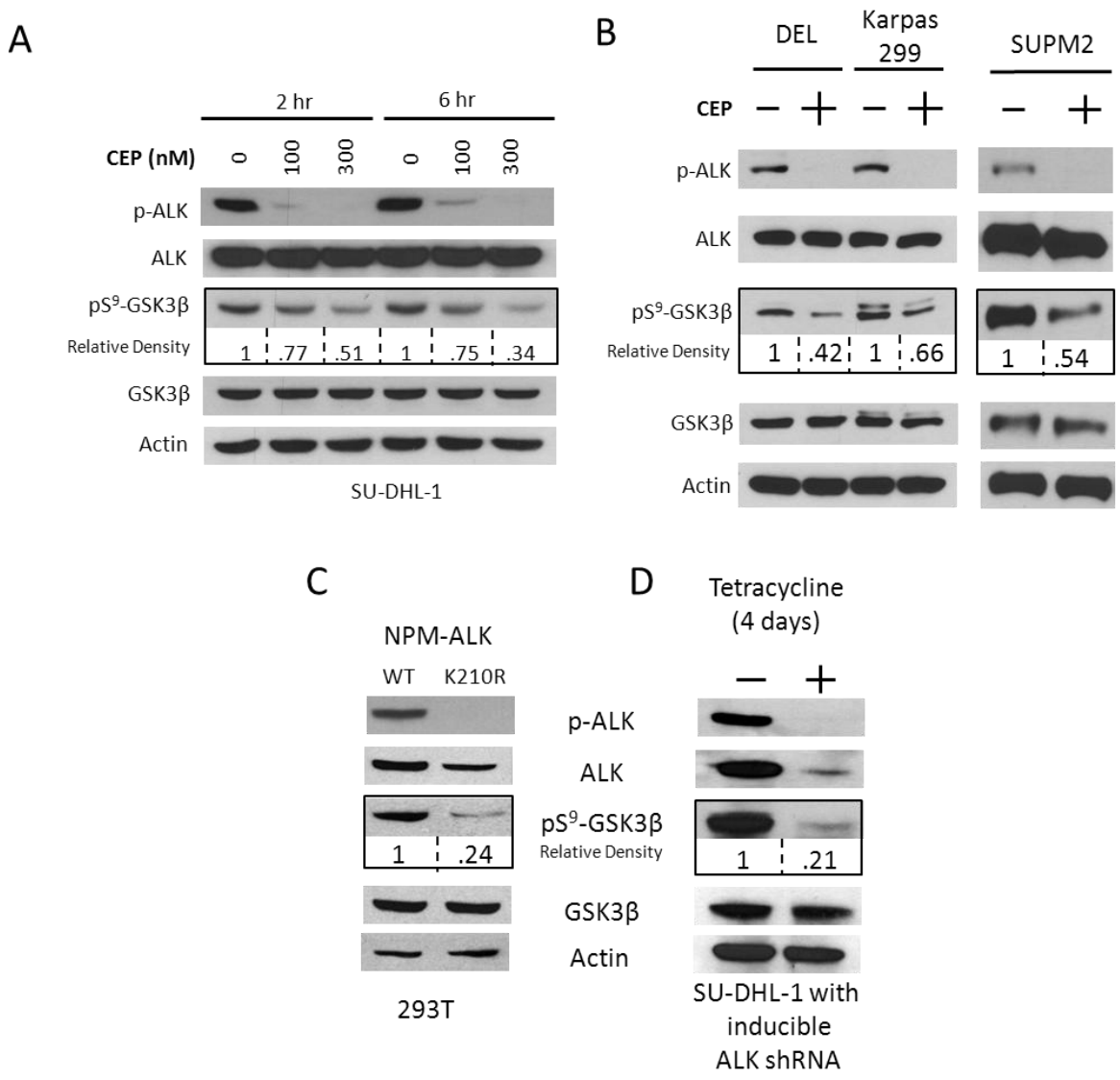

Figure 4.2: NPM-ALK regulates pS^{9}-GSK3β. (A) SU-DHL-1 cells were treated for 2 and 6 hours with the CEP (Compound 15, Cephalon, Inc, Frazer, PA) at indicated doses in 1% FBS media conditions. Cell lysates were resolved on SDS-Page gels and transferred to nitrocellulose membranes. Western blot analysis of GSK3β, pS^{9}-GSK3β, p-ALK (Y1604) (rabbit, 1:1000, Cell Signaling) and ALK (mouse, 1:1000, Invitrogen) are shown. Densitometry measurements were conducted with WCIF ImageJ software. (B) DEL, Karpas 299 and SUPM2 cells treated with DMSO or 300nM CEP for 6 hours. (C) 293T cells were transiently transfected with NPM-ALK WT or NPM-ALK K210R and harvested 48 hours later. Western blot analysis of cell lysates is shown. (D) SU-DHL-1 cells were stably transfected with tetracycline inducible shRNA against ALK. After 4 days of tetracycline treatment, cells were harvested and subjected to western blotting. Densitometry of pS^{9}-GSK3β is indicated as relative to control.

PI3K/AKT pathway mediates NPM-ALK phosphorylation of GSK3β

Interrogation of the phosphoproteomic data identified several serine kinases that are known to phosphorylate GSK3β (data not shown). These included the PI3K, PKC and PKA kinases. Since the PI3K/AKT pathway is known to be activated by NPM-ALK as well as responsible for GSK3β serine phosphorylation[275,276] we hypothesized that the regulation of pS^{9}-GSK3β by NPM-ALK is mediated by PI3K/AKT. We utilized a selective small molecule inhibitor against PI3K-δ (CAL-101)[277] to determine the effect of PI3K/AKT inhibition on pS^{9}-GSK3β in SU-DHL-1 cells. Exposure to CAL-101 for 24 hours at increasing concentrations resulted in decreased phosphorylation of pS^{9}-GSK3β and pS^{473}-AKT in a dose dependent manner (Figure 4.3). Importantly, p-ALK was not affected by CAL-101 mediated inhibition of PI3K/AKT. These data show that the PI3K/AKT pathway mediates the serine-9 GSK3β phosphorylation by NPM-ALK. However, this doesn't preclude the possibility that other pathways active in such as WNT [278] or PLCγ[279] also contribute to GSK3β phosphorylation.

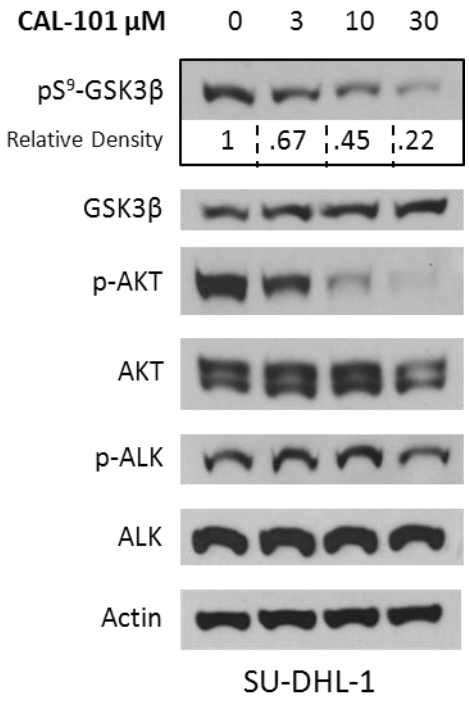

Figure 4.3: The PI3K/AKT pathway mediates ALK induced pS^{9}-GSK3β. SU-DHL-1 cells treated with CAL-101 for 24 hours in 1% DMSO. Levels of pS^{9}-GSK3β, GSK3β, p-AKT, AKT, p-ALK, ALK and actin were determined by western blot analysis.

pS^{9}-GSK3β protects CDC25A and Mcl-1 from proteasomal degradation

The serine-9 phosphorylation of GSK3β results in inhibition of its kinase activity[280]. Since active GSK3β is known to target a variety of proteins for proteasomal degradation, we hypothesized that two known substrates of GSK3β, CDC25A and Mcl-1, would be deregulated in ALCL cells. We evaluated the expression of CDC25A in SU-DHL-1 cells after inhibition of ALK at indicated time points following release from double thymidine block synchronization[281] (Figure 4.4A) . ALK inhibition resulted in significant reduction of CDC25A levels in a time dependent manner with only 30% of the protein remaining after 8 hours. In contrast,

CDC25A expression remained unchanged through the entire 8 hour time period in the DMSO control condition. These data suggest that NPM-ALK deregulates the normal cyclical expression of CDC25A and leads to stabilization and enhanced expression throughout the cell cycle[267]. Similarly, the expression of Mcl-1 and CDC25A were analyzed in SU-DHL-1 cells in the presence of CEP and/or proteasome inhibitor (MG132) after release from synchronization using double thymidine block. As shown in Figure 4.4B, inhibition of ALK resulted in significant down-regulation of Mcl-1 (47% of control) and CDC25A (14% of control) which was recoverable by simultaneous inhibition of the proteasome. These data suggest that NPM-ALK activity enhances the stability of Mcl-1 and CDC25A. Interestingly, MG132 treatment resulted in recovery of Mcl-1 and CDC25A levels that exceeded the expression in the DMSO control (120% and 358% respectively), suggesting that NPM-ALK does not provide complete proteasomal protection for these proteins.

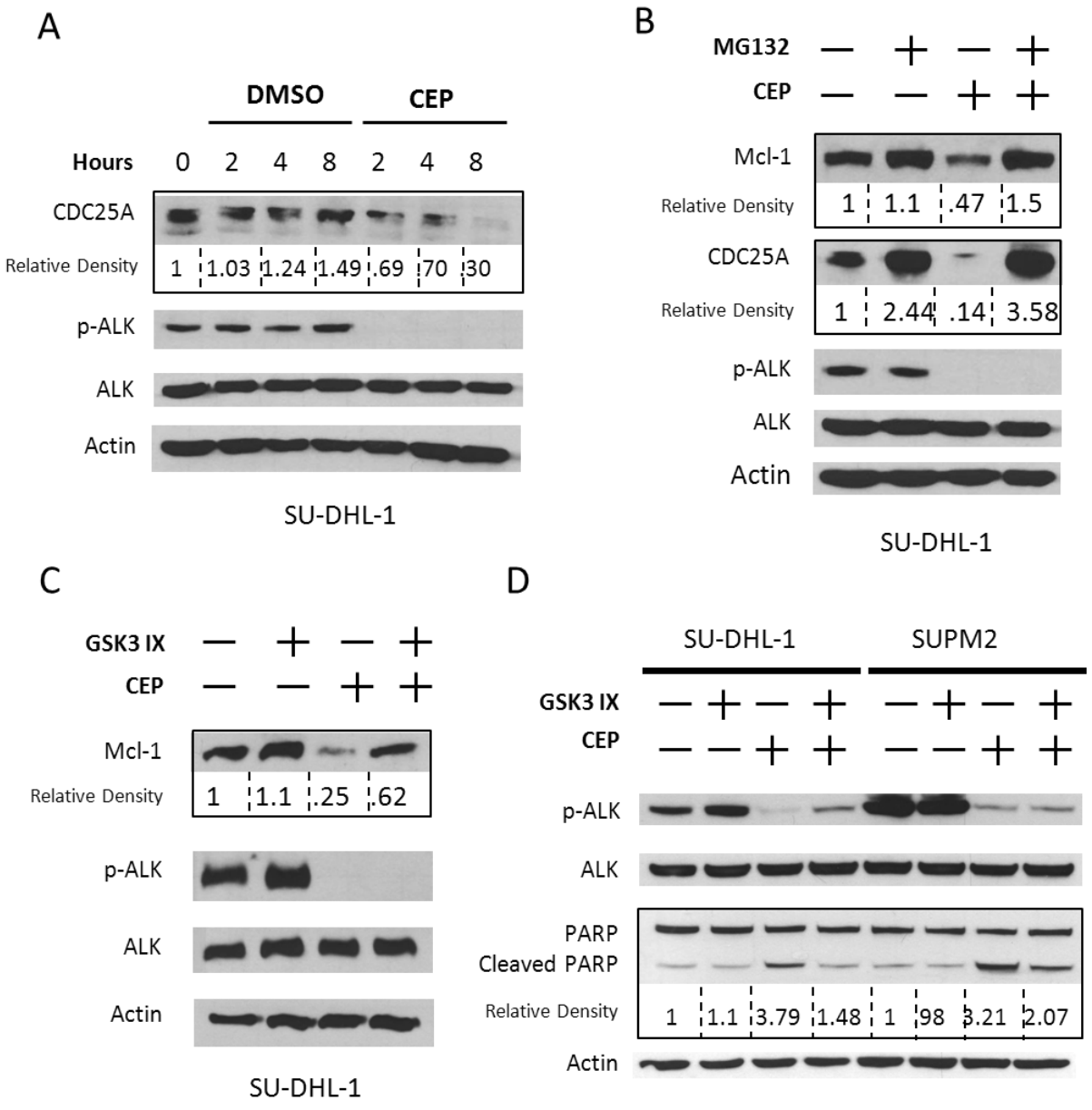

Figure 4.4: GSK3β regulates degradation of CDC25A and Mcl-1. (A) SU-DHL-1 cells were synchronized by double thymidine block. Upon release, cells were treated with DMSO or 300nM of CEP. Cells were lysed at indicated times following release. (B) SUPM2 cells were treated with CEP (300nM) and/or MG132 (10μM) for 6 hours. (C) SU-DHL-1 cells were treated with CEP (300nM) and/or GSK3 IX (Calbiochem, San Diego, CA) (100nM) for 6 hours. (D) SU-DHL-1 cells were treated with CEP (100nM) and/or GSK3 inhibitor IX (100nM) for 6 hours.

To determine the role of GSK3β in proteasomal degradation of Mcl-1, SU-DHL-1 cells were treated with the CEP and/or a GSK3 inhibitor (GSK3 IX) for 6 hours. As shown in Figure 4.4C, the decrease in Mcl-1 upon ALK inhibition was abrogated by GSK3 inhibition. Thus, NPM-ALK mediated inhibition of GSK3β results in protection of Mcl-1 from proteasomal degradation. These data provide evidence for the role of GSK3β in enhancing the stability of Mcl-1 in NPM-ALK expressing cells. Since Mcl-1 is a known anti-apoptotic protein[282], we asked whether NPM-ALK confers resistance to apoptosis via its inhibition of GSK3β. Western blot analyses were performed on SU-DHL-1 and SUPM2 cell lysates to evaluate PARP cleavage as a surrogate marker for apoptosis[283]. Cells treated with GSK3 IX alone resulted in no change in PARP cleavage, while ALK inhibition greatly reduced ALK phosphorylation and increased the cleavage of PARP (Figure 4.4D). Interestingly, when both enzymes were inhibited, PARP cleavage was significantly reduced compared to the ALK inhibitor alone. These data indicate that NPM-ALK leads to inhibition of GSK3β which provide protection against apoptosis.

pS^{9}-GSK3β regulates GYS stability and glycogen metabolism

GSK3β is also known to phosphorylate glycogen synthase (GYS) in the insulin signaling pathway[268]. This phosphorylation inhibits GYS and prevents the formation of glycogen. In order to determine the effects of NPM-ALK signaling through GSK3β on GYS, ALK was inhibited in SU-DHL-1 and SUPM2 cells using CEP (Figure 4.5A). Western blot analysis showed a decrease in both pS^{641}-GYS and total GYS in response to ALK inhibition. This reduction corresponds with a reduction in p-ALK levels and pS^{9}-GSK3β. Given the decrease in both pS^{641}-GYS

and total GYS, it is likely that the majority of the difference is accounted for by changes in total protein levels. To determine whether this decrease in GYS is regulated by GSK3β SU-DHL-1 cells were treated with combination of CEP, GSK3 IX and MG132. As shown in Figure 4.5B, ALK phosphorylation and GSK3β phosphorylation are decreased when CEP is present. Inhibition of ALK results in a decrease in pS^{641}-GYS levels which is recoverable upon inhibition of the proteasome. This suggests that ALK protects GYS from proteasomal degradation. Similarly, GYS levels are most elevated when GSK3β is chemically inhibited, further supporting this notion. In order to determine the effects of GYS regulation on cellular glycogen levels, Karpas299 and SU-DHL-1 cells were treated with CEP for 6 hours following glycogen quantification (Figure 4.5C). ALK inhibition resulted in a decrease of glycogen stores with only 32% (SD ± 0.54%, $p<0.01$) and 27% (SD ± 1.2%, $p<0.01$) remaining in Karpas299 and SU-DHL-1 cells, respectively.

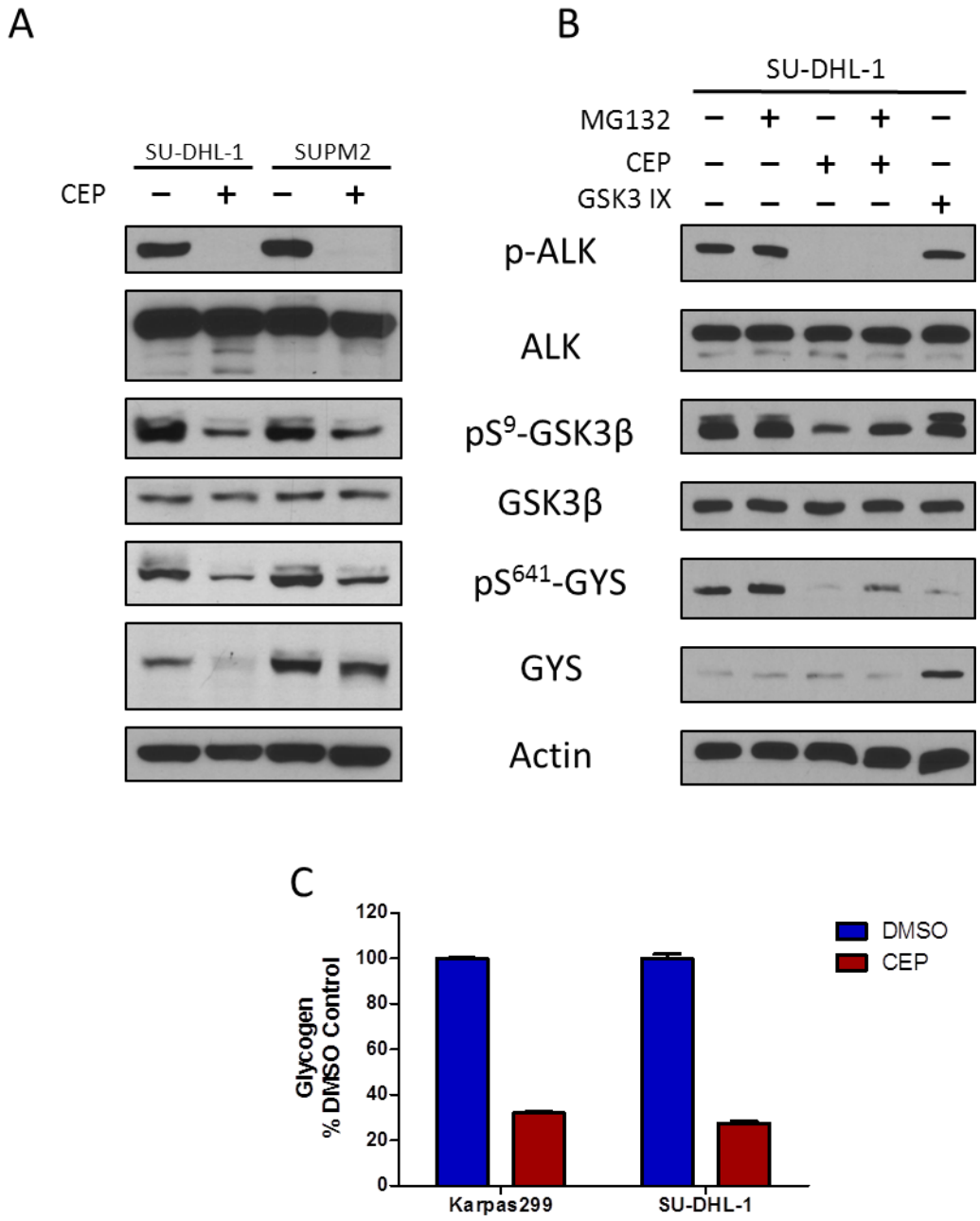

Figure 4.5: GSK3β regulates phosphorylation and degradation of GYS. (A) Immunoblots of SU-DHL-1 and SUPM2 cell lysates following 6 hours CEP 300nM treatment. (B) Immunoblots from SU-DHL-1 cell lysates treated for 6 hours with the indicated inhibitors. MG132 (10μM), CEP (300nM), GSK3IX (100nM). (C) Glycogen assay (BioVision) on Karpas299 and SU-DHL-1 cell lysates following 6 hours CEP 300nM treatment.

GSK3β mediates NPM-ALK driven oncogenesis

To determine whether GSK3β is a key mediator of NPM-ALK induced oncogenesis, we assessed the effect of inhibitor IX on cell viability of two ALCL-derived cell lines. An effective dose of 100nM of GSK3 IX was selected because it represents a concentration well above the IC_{50} for GSK3β but below the IC_{50} for other serine/threonine kinases[284]. As expected, CEP (100nM) resulted in a dramatic reduction of cell viability as determined by WST-1 (4-[3-(4-iodophenyl)-2-(4-nitrophenyl)-2H-5-tetrazolio]-1,3-benzene disulfonate) assay (Figure 4.6A) to approximately 35% of control in both cell lines. Treatment of ALCL-derived cell lines, SU-DHL-1 and SUPM2 with the GSK3 inhibitor IX (100nM) did not affect viability after 24 hours. Notably, exposure to both compounds simultaneously (Dual) resulted in a viability of 55% and 47% compared to control in SU-DHL-1 and SUPM2 cells, respectively. This represents a significant recovery of viability compared to ALK inhibition ($p<.01$). Importantly, Jurkat cells (ALK negative T-lymphoblastic leukemia) were not responsive to either GSK3 IX or CEP and there was no recovery in cellular viability. To corroborate the results of ALK and GSK3β inhibition on cell proliferation, we carried out flow cytometry-based Annexin V and propidium iodide (PI) staining to quantitatively assess cell viability (Figure 4.6B). Similar to the results of the WST-1 assay, inhibition of NPM-ALK resulted in a drastic reduction (80%) in the percent of live (Annexin V and PI negative) cells compared to the DMSO control. Treatment with the GSK3β inhibitor alone did not have an effect on the percentage of live cells. However, inhibition of both GSK3β and NPM-ALK (Dual) resulted in

significant increase in the percentage of live cells compared to ALK inhibition alone (34%).

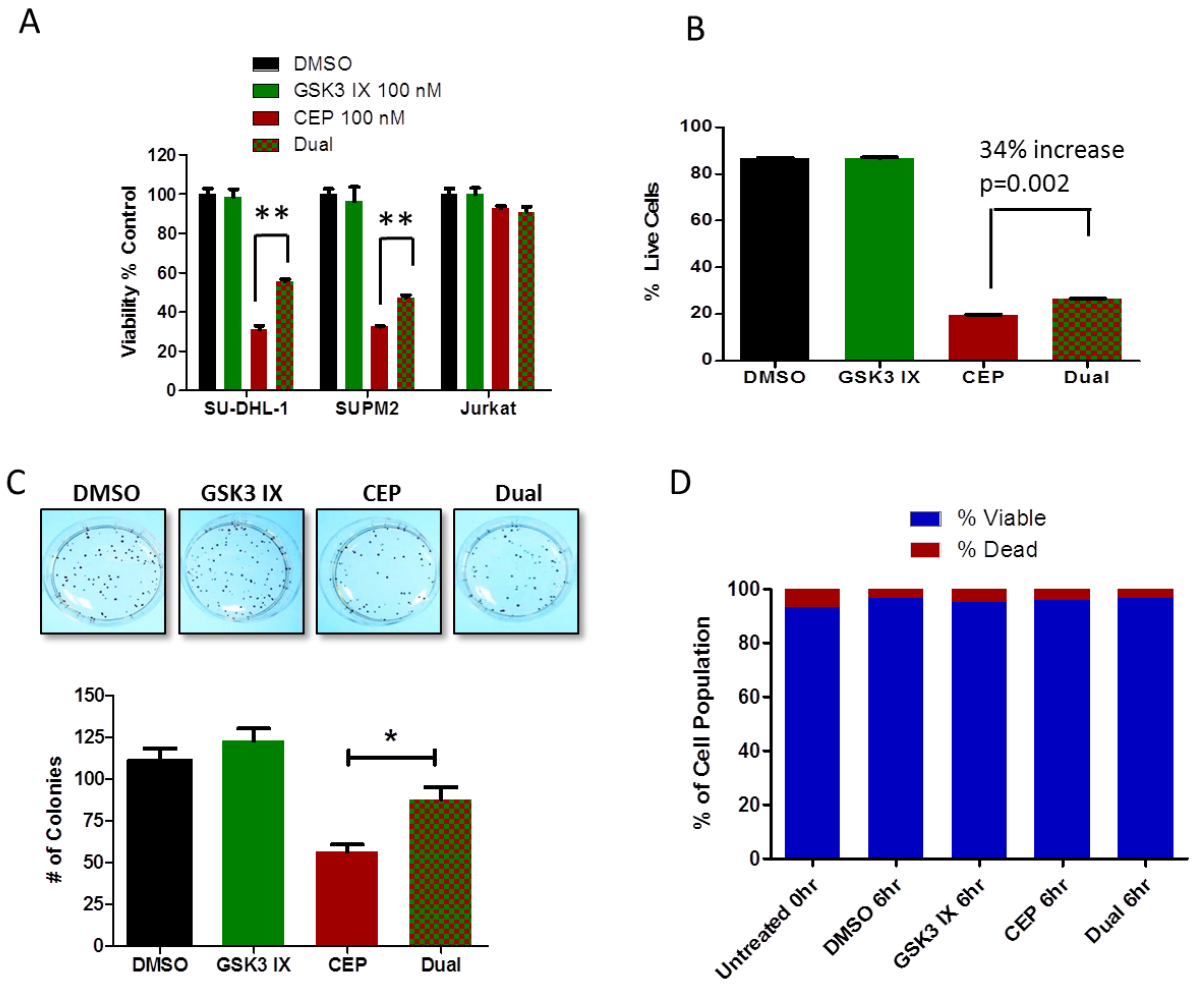

Figure 4.6: pS^{9}-GSK3β confers growth advantage for ALCL cells. (A) SU-DHL-1 (ALK+ALCL), SUPM2 (ALK+ ALCL) and Jurkat (ALK- ALL) cells were treated with ALK inhibitor and/or Inhibitor IX (GSK3 inhibitor) for 24 hours followed by WST-1 assay. (B) SU-DHL-1 cells were treated with indicated inhibitors (100nM) for 24 hours. After 15 min incubation with PI and Annexin V, cells were subjected to flow cytometric quantification of live cells (PI negative and Annexin V negative). (C) Karpas 299 cells were pre-treated with indicated inhibitors (100nM) for 6 hours then seeded in to methylcellulose media (MethoCult, Stemcell Technologies, Vancouver, Canada). After 14 days, colonies were stained with iodonitrotetrazolium chloride overnight and counted. (D) After 6 hour drug treatment but prior to seeding into methylcellulose media, Karpas 299 cell viability was assessed by trypan blue staining. (* $p < 0.05$, ** $p < 0.01$)

To address the role of GSK3β in oncogenic potential of ALCL cells, Karpas299 cells were treated with the CEP and GSK3 IX for 6 hours prior to seeding into methylcellulose media for colony formation. After 14 days, colonies were stained and enumerated (Figure 4.6C). While inhibition of ALK led to significant reduction of the number of colonies compared to control (51%), dual inhibition of both GSK3β and ALK caused a recovery in the number of colonies (79% compared to DMSO). We verified that 6 hour pre-treatment did not affect viability prior to seeding into the methylcellulose media by trypan blue staining. This showed that the same number of viable cells were seeded for all conditions that were evaluated (Figure 4.6D).

To further evaluate the role of GSK3β in NPM-ALK mediated oncogenesis, stable GSK3β knockdown cell lines were created by lentiviral transfection of shRNA targeted against GSK3β (Figure 4.7A) in two ALCL-derived cell lines. SU-DHL-1 and Karpas 299 cells stably expressing scramble or shGSK3β vectors were subjected to WST-1 assay following treatment with the ALK inhibitor (Figure 4.7B). Both cell lines expressing scramble shRNA showed a decrease in viability upon ALK inhibition (about 60% in both cell lines, $p<0.01$). In contrast, the cells with knockdown of GSK3β (shGSK3β) were resistant to the growth inhibitory effect of ALK inhibition ($p<0.01$). SU-DHL-1 cells with GSK3β knockdown showed a 12% (SD ± 2.9%) reduction in viability following CEP treatment, while Karpas299 showed a 29.5% (SD ± 1.8%) reduction. Similarly, cells expressing scramble shRNA displayed a 25% (SD ± 7.2%) reduction in number of colonies following ALK inhibition, while those with knockdown of GSK3β (shGSK3β) were resistant to ALK

inhibition and showed more colonies (92%, SD ± 6.7%) (Figure 4.7C). These data support the hypothesis that NPM-ALK mediated phosphorylation of GSK3β promotes proliferation and oncogenic transformation.

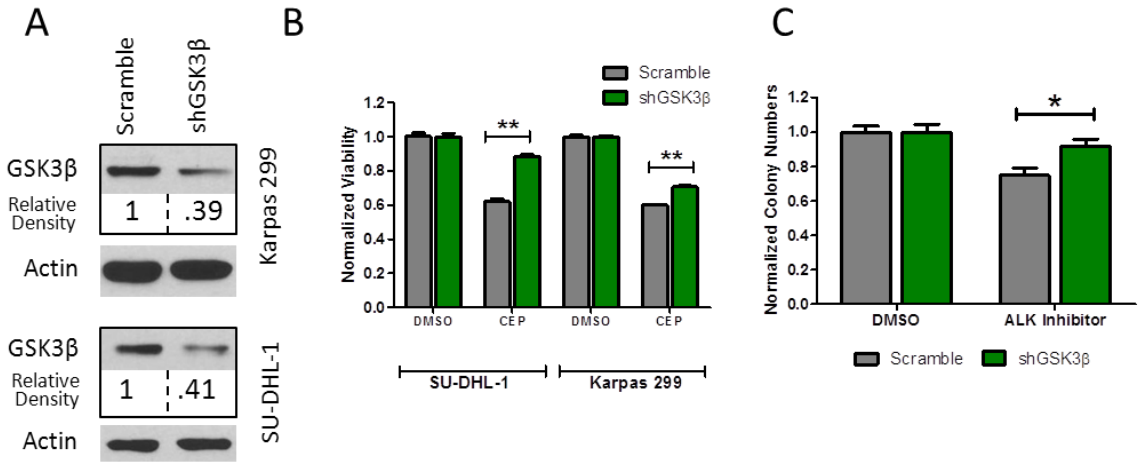

Figure 4.7: GSK3β knockdown yeild resistance to ALK inhibition. (A) Validation of GSK3β stable knockdown in Karpas 299 and SU-DHL-1 cells. (B) WST-1 assay after 48 hour treatment with 300nM ALK inhibitor in SU-DHL-1 and Karpas 299 cells with or without GSK3β knockdown Each ALK inhibitor condition normalized to its DMSO control. (C) Karpas 299 cells with or without GSK3β knockdown was subjected to methylcellulose colony formation assay after treatment with ALK inhibitor for 6 hours. Colony numbers normalized to DMSO for each cell condition. (* $p < 0.05$, ** $p < 0.01$)

pS^{9}-GSK3β is expressed in ALK+ ALCL tumors

Immunohistochemistry (IHC) was performed on 16 ALK positive ALCL (ALK+ ALCL) tissue biopsies and 16 ALK negative ALCL (ALK- ALCL) tissue biopsies. ALK+ALCL samples showed strong staining for ALK in both the cytoplasm and nucleus of neoplastic cells (Figure 4.8A), while ALK- ALCL samples show not expression of ALK (Figure 4.8E). Fourteen of the 16 ALK+ ALCL samples showed

strong expression of pS^{9}-GSK3β in the neoplastic cells with weak expression in adjacent endothelial cells (Figure 4.8B and D). Additionally, 13/16 ALK+ ALCL cases also showed expression of CDC25A highlighting the nuclear membranes of the neoplastic cells (Fig 4C). Reactive lymphocytes did not express significant levels of pS^{9}-GSK3β (Figure 4.8B) or CDC25A (Figure 4.8C). Using chi squared distribution to test if the observed distribution is statistically different from the expected randomized distribution, we found that the ALK+ ALCL cases displayed a significant correlation of pS^{9}-GSK3β and CDC25A expression ($p < 0.001$) (Fig. 4.8D). In contrast, only 5/16 of the ALK- ALCL cases showed expression of pS^{9}-GSK3β in the neoplastic cells while the infiltrating neutrophils showed strong expression (Figure 4.8F and H). CDC25A expression in ALK- ALCL was present in 11/16 cases. Figure 4G shows a representative case of ALK- ALCL lacking CDC25A expression. In contrast to the ALK+ ALCL cases, the ALK- ALCL cases displayed a lack of significant correlation of pS^{9}-GSK3β and CDC25A expression distribution ($p < 0.2$) (Figure 4.8H). Reactive tonsillar tissues demonstrated weak expression of pS^{9}-GSK3β in epithelial cells and scattered interfollicular activated T-lymphocytes (Figure 4.8I). CDC25A expression was strongly expressed in the epithelial cells and in scattered interfollicular activated T-lymphocytes (Figure 4.8J). These findings confirm the presence of the inhibited form of GSK3β and the accumulation of one of its downstream substrates in human ALCL tumor samples. Overexpression of CDC25A transcript has been observed in various lymphomas including ALK+ ALCLs[285], however its expression in ALCL tumor tissue samples using immunohistochemistry has not been reported previously.

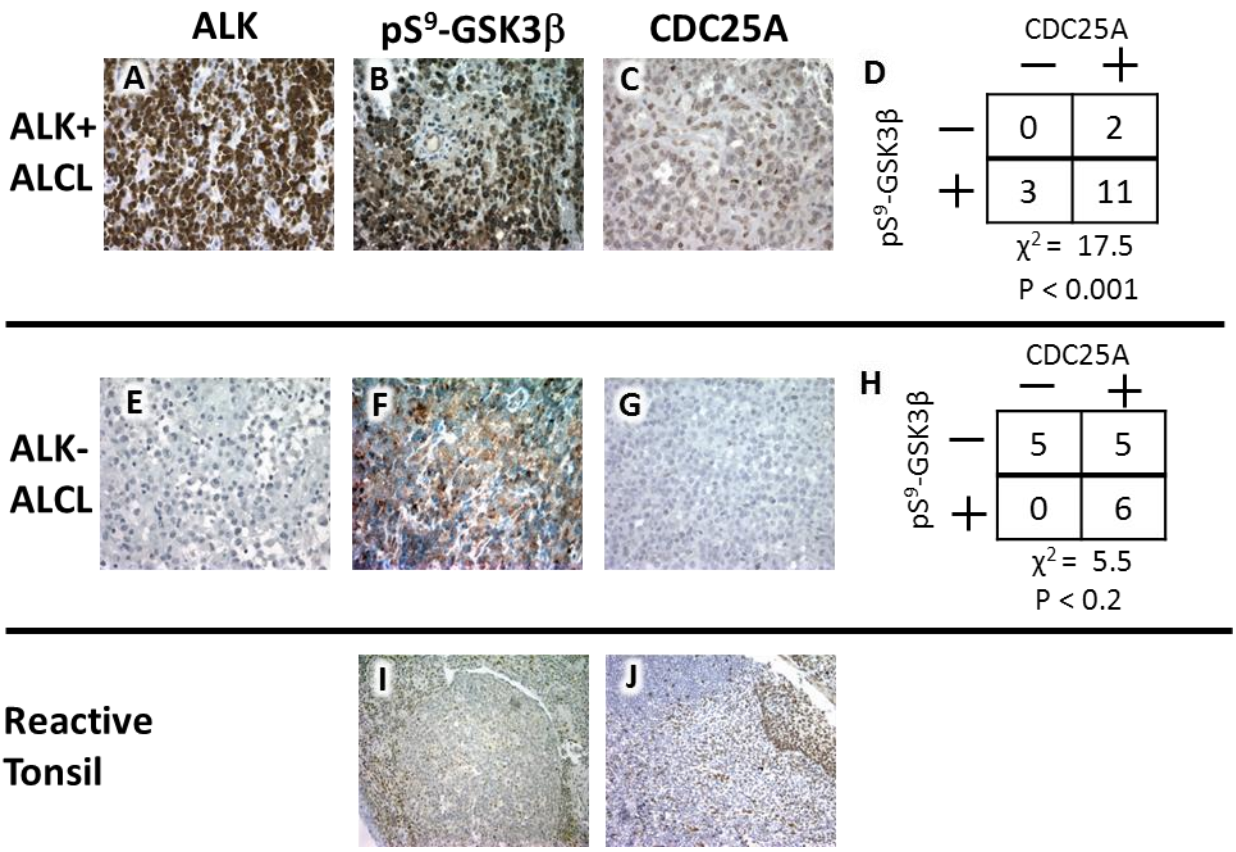

Figure 4.8: pS^{9}-GSK3β and CDC25A are expressed in human tumors. ALK+ ALCL tissue samples were obtained from the archives of the Hematopathology Section, Department of Pathology, University of Michigan, with institutional approval (HUM00023256). (A,B,C) Representative case of ALK+ ALCL. (E,F,G) Representative case of ALK- ALCL. (I,J) Reactive tonsil. (A,E) IHC staining for ALK (mouse, 1:100, Dako). (B,F,I) IHC staining for pS^{9}-GSK3β (rabbit, 1:50, Cell Signaling Technology). (C,G,J) IHC staining for CDC25A (mouse, 1:500, Abcam). (D) Tabulated results for 16 ALK+ ALCL tumor samples analyzed for immunohistochemical staining for CDC25A and pS^{9}-GSK3β. Immunohistochemistry results were evaluated using parameters of staining intensity (0-3) and percentage of immunoreactive neoplastic cells. Positivity was defined by 30% or more of neoplastic cells showing reactivity. (H) Tabulated results for 16 ALK- ALCL tumor samples analyzed for immunohistochemical staining for CDC25A and pS^{9}-GSK3β.

Phosphoproteomic analysis of pY216-GSK3β

A retrospective analysis of the phosphoproteomic data from chapter 2 was conducted to identify changes in GSK3β tyrosine phosphorylation in response to ALK inhibition. Table 4.1 depicts the spectral counts identified for pY216-GSK3β in DMSO or CEP treated conditions. Representative replicates from three ALCL-derived cell lines are shown. In each case, the amount of pY216-GSK3β increases in response to ALK inhibition. These data correlate well with our previous biochemical findings. The tyrosine phosphorylation of GSK3β is thought to be an autophosphorylation site and positively correlates with its enzymatic activity[286-288]. We show that NPM-ALK induces the serine-9 phosphorylation of GSK3β and therefore inhibits its ability to regulate the degradation of its downstream substrates. The decreased GSK3β activity driven by ALK would therefore correlate with an increased serine phosphorylation and a decreased tyrosine phosphorylation. Also, since more tyrosine phosphorylation is present after ALK inhibition, these data strengthen the observations that GSK3β is more active under these conditions (Figures 4.4-4.6).

Table 4.1: Spectral counts of pY216-GSK3β in ALCL cell lines

	SUDHL-1		SUPM2		Karpas299	
	DMSO	CEP	DMSO	CEP	DMSO	CEP
pY216 GSK3β	10	21	8	12	21	35

GSK3β Interactome

We next wanted to expand this study to the identification of novel GSK3β interacting proteins. To this aim, we pursued a mass spectrometry based GSK3β interactome study. We cloned GSK3β into a pGLUE expression vector containing a tandem affinity purification tag (TAP-Tag) (Figure 4.9A)[289]. This TAP-Tag allows for purification of the bait protein (GSK3β) using two independent approaches including streptavidin binding and calmodulin binding for the high purity of complexes and low background. However, based on validation experiments we utilized only the streptavidin purification because of loss of bait during the tandem purification (data not shown). Figure 4.9BB shows the purification of TAP-Tag-GSK3β via western blot analysis. Here, the TAP-Tag vector was expressed in 293T cells and lysed after 48 hours. The streptavidin beads achieved high level of binding (lane 2 and 3) of the TAP-Tag-GSK3β protein. While the elution was not 100% efficient (lane 4), a large amount of the protein was recovered in the final product (lane 5). SDS-PAGE and coomassie stain of the final product is shown in Figure 4.9C. GSK3β was present as a large band, while other interacting protein bands were visible. The empty vector contained no visible bands suggesting a low background.

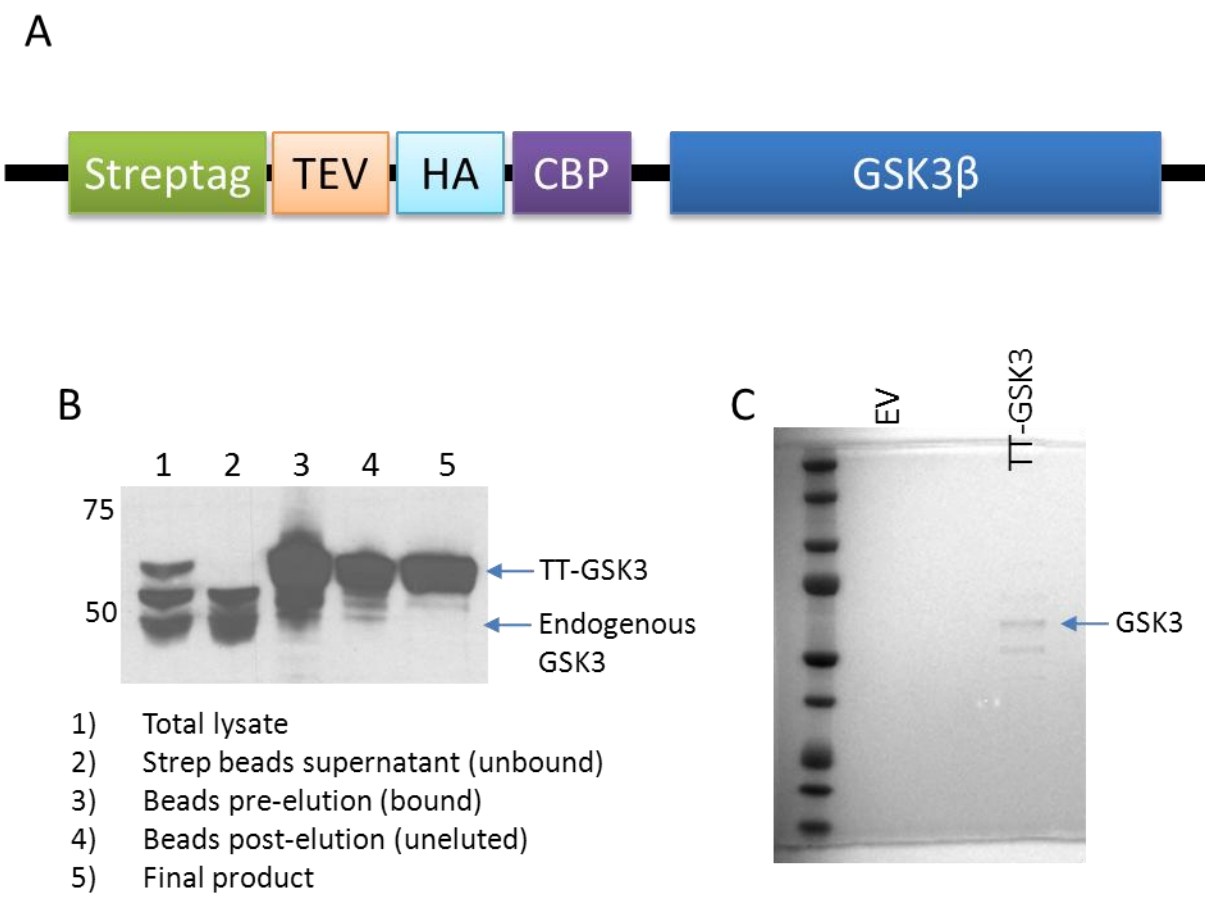

Figure 4.9: GSK3 interactome. (A) Representation TAP-Tag vector within the pGLUE expression vector. Streptavidin (streptag) and calmodulin binding affinity tags surround an HA tag for protein detection and protease TEV recognition site for cleavage of streptag. (B) GSK3 western blot from 293T cell lysates expressing the TAP-Tag-GSK3β. (C) Coomassie stained SDS-PAGE gel of the final product from empty vector and TAP-Tag-GSK3β expressing 293T cells.

Following in-gel digest, LC-MS/MS was used to identify proteins interacting with GSK3β. Table 4.2 shows the results of GSK3β interactome. GSK3β was the most abundantly identified protein in this analysis with 31 peptides identified with 159 spectral counts. We also identified GSK3β interaction protein (GSKIP) in the interactome with 2 peptides identified with 8 spectral counts. Since GSKIP is a known interacting protein with GSK3β, this serves as an internal positive control for

the analysis[290]. Therefore this list of proteins represents candidate GSK3β interacting proteins and may have a role in NPM-ALK driven oncogenesis or a broader role in other GSK3β biology.

We selected C1QBP to validate as a novel GSK3β interacting protein. As shown in Figure 4.10, C1QBP interacts with TAP-Tag-GSK3β in the streptavidin pull-down experiment. Here, TAP-Tag-GSK3β was capable of pulling down C1QBP while the empty vector was not. These data provide confidence in the interaction between GSK3β and C1QBP as well as the GSK3β interactome in general. However, further work is warranted to confirm this interaction in an endogenous setting and determine the functional consequence of the interaction. C1QBP (complement component 1, q subcomponent binding protein) (also known as p32) localizes to the mitochondrial membrane and is thought to be involved in oxidative phosphorylation[291]. Interestingly, this protein has been implicated in cancer metabolism as its disruption results in a shift toward aerobic glycolysis[292]. The novel interaction between GSK3β and C1QBP could yield another link between GSK3β and the regulation of cancer metabolism. This has implications in ALK signaling and a variety of other pathological scenarios involving GSK3β.

Table 4.2: GSK3 interacting proteins by mass spectrometry

Protein ID	Peptides	Spec Counts	Define	
P49841	31	159	GSK3B	(Glycogen synthase kinase-3 beta)
P04350	22	68	TBB4	(Tubulin beta-4 chain)
P02538	11	44	K2C6A	(Keratin, type II cytoskeletal 6A)
Q9BUF5	12	38	TBB6	(Tubulin beta-6 chain)
P62820	2	29	RAB1A	(Ras-related protein Rab-1A)
Q16543	6	13	CDC37	(Hsp90 co-chaperone Cdc37)
P27708	6	11	PYR1	(Dihydroorotase)
P05023	5	9	AT1A1	(Sodium/potassium-transporting ATPase subunit alpha-1)
Q9H1R3	1	9	MYLK2	(Myosin light chain kinase 2, skeletal/cardiac muscle)
Q13451	5	8	FKBP5	(Peptidyl-prolyl cis-trans isomerase FKBP5)
Q9Y230	5	8	RUVB2	(RuvB-like 2)
Q9Y265	4	8	RUVB1	(RuvB-like 1)
P31689	3	8	DNJA1	(DnaJ homolog subfamily A member 1)
Q9P0R6	2	8	GSKIP	(GSK3-beta interaction protein)
Q9HAN4	2	8	TRY1	(Alpha-trypsin chain 2)
Q9UME3	6	7	PRKDC	(DNA-dependent protein kinase catalytic subunit)
P40227	5	6	TCPZ	(T-complex protein 1 subunit zeta)
O60884	2	6	DNJA2	(DnaJ homolog subfamily A member 2)
Q96HK3	4	5	CALM	(Calmodulin)
O15020	4	5	SPTN2	(Spectrin beta chain, brain 2)
P53985	3	5	MOT1	(Monocarboxylate transporter 1)
P31948	3	4	STIP1	(Stress-induced-phosphoprotein 1)
P78371	2	4	TCPB	(T-complex protein 1 subunit beta)
Q07021	2	4	C1QBP	(Complement component 1 Q subcomponent-binding protein)
Q5JWF2	2	4	GNAS1	(Guanine nucleotide-binding protein G(s) subunit alpha)
Q13263	2	4	TIF1B	(Transcription intermediary factor 1-beta)
P19338	2	4	NUCL	(Nucleolin)
P12956	2	3	KU70	(ATP-dependent DNA helicase 2 subunit 1)
P63010	2	3	AP2B1	(AP-2 complex subunit beta)
P62241	2	3	RS8	(40S ribosomal protein S8)
Q14980	2	3	NUMA1	(Nuclear mitotic apparatus protein 1)
Q99615	2	3	DNJC7	(DnaJ homolog subfamily C member 7)
O00165	2	2	HAX1	(HCLS1-associated protein X-1)
P45880	2	2	VDAC2	(Voltage-dependent anion-selective channel protein 2)
P62829	2	2	RL23	(60S ribosomal protein L23)
O43795	2	2	MYO1B	(Myosin-Ib)
P25685	2	2	DNJB1	(DnaJ homolog subfamily B member 1)
P35613	2	2	BASI	(Basigin)
O95831	2	2	AIFM1	(Apoptosis-inducing factor 1, mitochondrial)
P21796	2	2	VDAC1	(Voltage-dependent anion-selective channel protein 1)
P35232	1	2	PHB	(Prohibitin)
P08754	1	2	GNAI3	(Guanine nucleotide-binding protein G(k) subunit alpha)
Q9NP68	1	2	P53	(Cellular tumor antigen p53)
P61421	1	2	VA0D1	(V-type proton ATPase subunit d 1)
Q15293	1	2	RCN1	(Reticulocalbin-1)
P26373	1	2	RL13	(60S ribosomal protein L13)

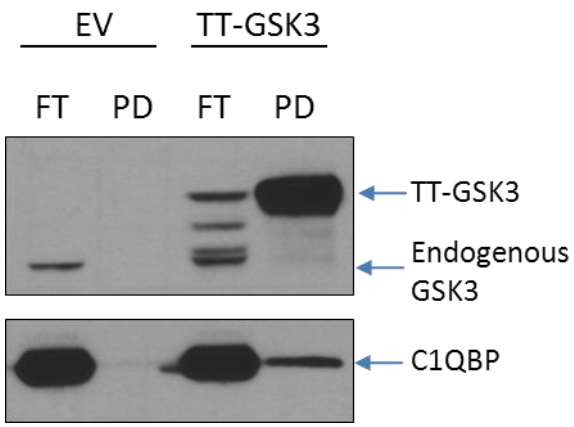

Figure 4.10: Validation of C1QBP and GSK3 interaction. 293T cells were transfected with either empty vector (EV) or TAP-Tag-GSK3β (TT-GSK3). After 48 hours the cell lysates were subjected to streptavidin purification. The flow through (FT) and pull-down (PD) were analyzed by western blot.

DISCUSSION

These studies provide insight in to a novel mechanism of NPM-ALK mediated oncogenesis and demonstrate the utility of phosphoproteomics in the identification of novel kinase signaling mechanisms. We provide evidence for the NPM-ALK directed serine-9 phosphorylation of GSK3β through the PI3K/AKT pathway (Figure 4.11). The resulting inhibition of GSK3β causes the accumulation of CDC25A, Mcl-1 and GYS, providing increased proliferation, survival and metabolic support.

Our work identifies a role for NPM-ALK in driving glycogen production. It is known that insulin signaling increases GYS activity and glycogen production[293]. Given the overlap between insulin receptor signaling and other growth factor receptor signaling, it is possible that NPM-ALK employs similar mechanisms to drive

glycogen production. Cancer cells have a highly increased appetite for glucose as evident by increased glucose uptake and rapid glycolysis[190]. The ability to uptake and store glucose is within the metabolic requirements for cells with rapid glycolytic turnover.

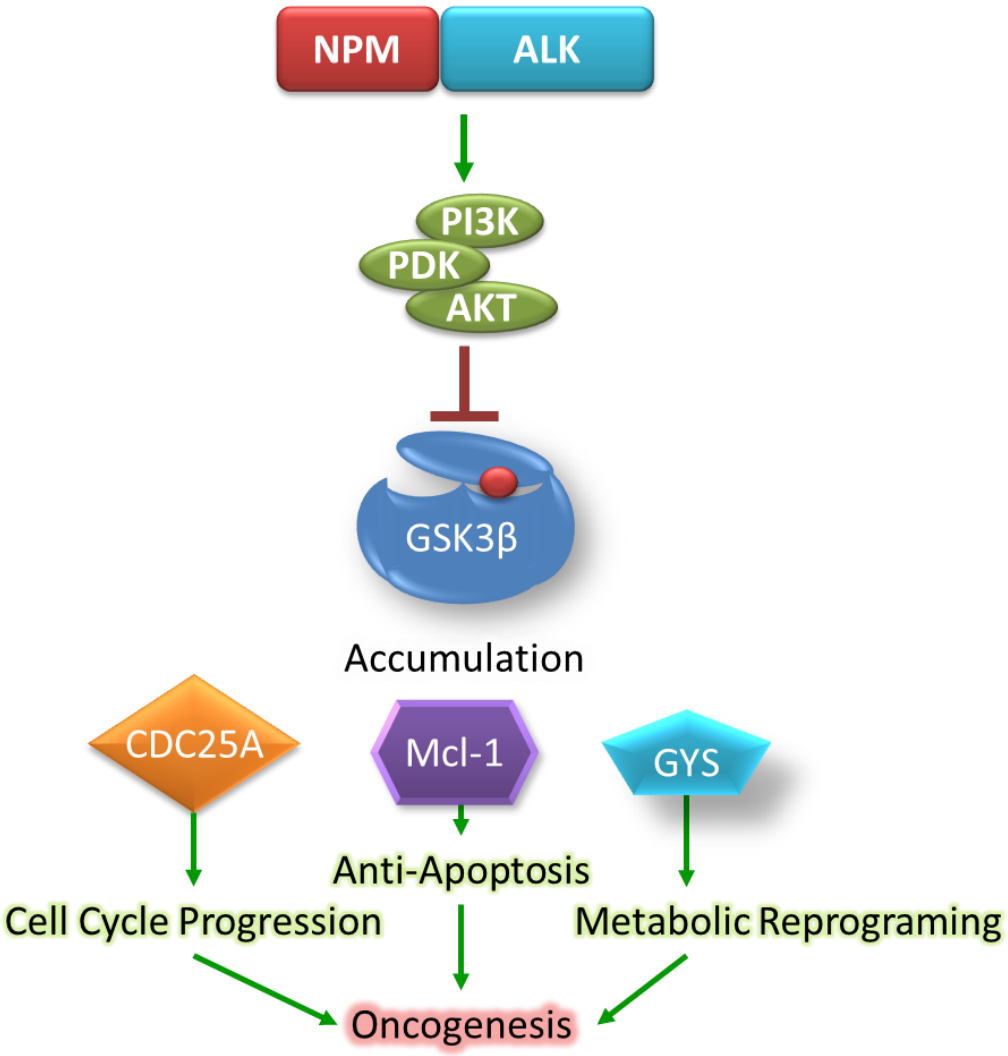

Figure 4.11: Model for NPM-ALK regulation of GSK3β and it downstream substrates. NPM-ALK regulates the inhibitory serine-9 phosphorylation of GSK3β through the activation of the PI3K/AKT pathway. The inhibited GSK3 is unable to regulate the protein levels of CDC25A, Mcl-1 and GYS. The accumulated downstream substrates drive oncogenesis through cell cycle progression, survival and metabolic reprogramming.

NPM-ALK signaling through GSK3β provides one mechanism through which NPM-ALK exerts its oncogenic potential. This was seen by the rescue in proliferation when both NPM-ALK and GSK3β are inhibited (4.6). This also accounts for the resistance to ALK inhibition when GSK3β is knocked down (Figure 4.7). However, the rescue mediated by inhibition of GSK3β was not complete. This may be due to the presence of several GSK3β-independent signaling pathways that are regulated by NPM-ALK such as JAK/STAT or ERK [294-296]. This idea is also evident in the observation that pS^{9}-GSK3β was not completely abolished by ALK inhibition (Figure 4.2A-B), yet a dramatic decrease in cell viability was observed. NPM-ALK activates many downstream signaling pathways which can all be disrupted by inhibiting NPM-ALK. We can reconstitute one of these pathways through the chemical inhibition or knockdown of GSK3β. However, all other pathways remain "off" accounting for the less than 100% recovery in proliferation and colony formation.

In conclusion, our data show that NPM-ALK regulates the inhibitory serine phosphorylation of GSK3β in ALCL cells, providing a growth advantage and the maintenance of a proliferative phenotype. Our studies uncover a novel mechanism of NPM-ALK mediated oncogenesis. Detailed elucidation of such deregulated signaling events may be exploited in the design of targeted and combinatorial therapeutic strategies for the treatment of ALK-driven neoplasia.

FUTURE DIRECTIONS

The mass spectrometric characterization of the GSK3β interactome introduces numerous directions to take future projects. Many of the proteins identified could have implications in GSK3β and ALK signaling. Specifically, the investigation of the GSK3β-C1QBP interaction will lead to novel discoveries about the regulation of cancer metabolism. C1QBP has been shown to be upregulated in many cancer types[297-300]. Therefore, several hypotheses could be made about the role of GSK3 in the regulation of C1QBP and its effects on cancer metabolism and tumorigenesis.

CHAPTER 5

Concluding Remarks

Alterations in the *ALK* gene are seen in a broad spectrum of human cancers. Understanding how ALK and its fusion products regulate oncogenesis is a necessary step in the development of therapeutics against these cancers. We aimed to identify novel phenotypes and signaling molecules regulated by ALK through the use of powerful screening approaches followed by in depth functional validation. The work presented in this dissertation provides the following scientific contributions:

- ALK drives global phosphoproteomic changes with many novel substrates identified.
- ALK induces metabolic reprogramming to meet the biomass requirements for proliferation.
- PKM2 is a novel substrate of ALK and mediates the observed metabolic switch.
- PKM2 is promising new therapeutic target in ALCL.

- GSK3β is a novel mediator of ALK signaling and drives broad oncogenic phenotypes including cell cycle progression, survival, and metabolic alterations.
- This study is the first of its kind to integrate phosphoproteomics and metabolomics for the identification of candidate metabolic regulators.

The work in this dissertation contributes significant advances in our understanding of ALK induced oncogenesis. Additionally, this work serves as a foundation for future studies. The phosphoproteomic and metabolic data sets are rich with novel discoveries about ALK signaling and oncogenesis. The thorough investigation of these candidate signaling molecules and metabolites will likely yield additional important discoveries. Investigation into the non-metabolic roles of PKM2 will offer opportunities to link the NPM-ALK regulation of pY105-PKM2 to gene regulation. Finally, the GSK3β interactome provides additional avenues of research through the characterization of novel mediators of GSK3β signaling dependent or independent of ALK. The continued investigation of ALK signaling will identify additional therapeutic targets that may provide options for controlling these aggressive diseases and allow us to be better equipped to treat resistant tumors.

REFERENCES

1 Morris, S. W. *et al.* ALK, the chromosome 2 gene locus altered by the t(2;5) in non-Hodgkin lymphoma, encodes a novel neural receptor tyrosine kinase that is highly related to leukocyte tyrosine kinase (LTK). *Oncogene* **14**, 2175-2188, doi:10.1038/sj.onc.1201062 (1997).

2 Iwahara, T. *et al.* Molecular characterization of ALK, a receptor tyrosine kinase expressed specifically in the nervous system. *Oncogene* **14**, 439-449, doi:10.1038/sj.onc.1200849 (1997).

3 Stoica, G. E. *et al.* Identification of anaplastic lymphoma kinase as a receptor for the growth factor pleiotrophin. *J Biol Chem* **276**, 16772-16779, doi:10.1074/jbc.M010660200 M010660200 [pii] (2001).

4 Loren, C. E. *et al.* Identification and characterization of DAlk: a novel Drosophila melanogaster RTK which drives ERK activation in vivo. *Genes Cells* **6**, 531-544, doi:gtc440 [pii] (2001).

5 Koduri, V. & Blacklow, S. C. Folding determinants of LDL receptor type A modules. *Biochemistry* **40**, 12801-12807, doi:bi011344k [pii] (2001).

6 Yamamoto, T. *et al.* The human LDL receptor: a cysteine-rich protein with multiple Alu sequences in its mRNA. *Cell* **39**, 27-38, doi:0092-8674(84)90188-0 [pii] (1984).

7 Esser, V., Limbird, L. E., Brown, M. S., Goldstein, J. L. & Russell, D. W. Mutational analysis of the ligand binding domain of the low density lipoprotein receptor. *J Biol Chem* **263**, 13282-13290 (1988).

8 Donella-Deana, A. *et al.* Unique substrate specificity of anaplastic lymphoma kinase (ALK): development of phosphoacceptor peptides for the assay of ALK activity. *Biochemistry* **44**, 8533-8542, doi:10.1021/bi0472954 (2005).

9 Tartari, C. J. *et al.* Characterization of some molecular mechanisms governing autoactivation of the catalytic domain of the anaplastic lymphoma

kinase. *J Biol Chem* **283**, 3743-3750, doi:M706067200 [pii] 10.1074/jbc.M706067200 (2008).

10 Wang, P. *et al.* Functional characterization of the kinase activation loop in nucleophosmin (NPM)-anaplastic lymphoma kinase (ALK) using tandem affinity purification and liquid chromatography-mass spectrometry. *J Biol Chem* **285**, 95-103, doi:M109.059758 [pii] 10.1074/jbc.M109.059758 (2010).

11 Lee, C. C. *et al.* Crystal structure of the ALK (anaplastic lymphoma kinase) catalytic domain. *Biochem J* **430**, 425-437, doi:BJ20100609 [pii] 10.1042/BJ20100609 (2010).

12 Weiss, J. B., Suyama, K. L., Lee, H. H. & Scott, M. P. Jelly belly: a Drosophila LDL receptor repeat-containing signal required for mesoderm migration and differentiation. *Cell* **107**, 387-398, doi:S0092-8674(01)00540-2 [pii] (2001).

13 Englund, C. *et al.* Jeb signals through the Alk receptor tyrosine kinase to drive visceral muscle fusion. *Nature* **425**, 512-516, doi:10.1038/nature01950 nature01950 [pii] (2003).

14 Lee, H. H., Norris, A., Weiss, J. B. & Frasch, M. Jelly belly protein activates the receptor tyrosine kinase Alk to specify visceral muscle pioneers. *Nature* **425**, 507-512, doi:10.1038/nature01916 nature01916 [pii] (2003).

15 Yang, H. L. *et al.* The ligand Jelly Belly (Jeb) activates the Drosophila Alk RTK to drive PC12 cell differentiation, but is unable to activate the mouse ALK RTK. *J Exp Zool B Mol Dev Evol* **308**, 269-282, doi:10.1002/jez.b.21146 (2007).

16 Stoica, G. E. *et al.* Midkine binds to anaplastic lymphoma kinase (ALK) and acts as a growth factor for different cell types. *J Biol Chem* **277**, 35990-35998, doi:10.1074/jbc.M205749200 M205749200 [pii] (2002).

17 Bowden, E. T., Stoica, G. E. & Wellstein, A. Anti-apoptotic signaling of pleiotrophin through its receptor, anaplastic lymphoma kinase. *J Biol Chem* **277**, 35862-35868, doi:10.1074/jbc.M203963200 M203963200 [pii] (2002).

18 Powers, C., Aigner, A., Stoica, G. E., McDonnell, K. & Wellstein, A. Pleiotrophin signaling through anaplastic lymphoma kinase is rate-limiting for glioblastoma growth. *J Biol Chem* **277**, 14153-14158, doi:10.1074/jbc.M112354200 M112354200 [pii] (2002).

19 Muramatsu, T. Midkine and pleiotrophin: two related proteins involved in development, survival, inflammation and tumorigenesis. *J Biochem* **132**, 359-371 (2002).

20 Dirks, W. G. *et al.* Expression and functional analysis of the anaplastic lymphoma kinase (ALK) gene in tumor cell lines. *Int J Cancer* **100**, 49-56, doi:10.1002/ijc.10435 (2002).

21 Mathivet, T., Mazot, P. & Vigny, M. In contrast to agonist monoclonal antibodies, both C-terminal truncated form and full length form of Pleiotrophin failed to activate vertebrate ALK (anaplastic lymphoma kinase)? *Cell Signal* **19**, 2434-2443, doi:S0898-6568(07)00226-4 [pii] 10.1016/j.cellsig.2007.07.011 (2007).

22 Moog-Lutz, C. *et al.* Activation and inhibition of anaplastic lymphoma kinase receptor tyrosine kinase by monoclonal antibodies and absence of agonist activity of pleiotrophin. *J Biol Chem* **280**, 26039-26048, doi:M501972200 [pii] 10.1074/jbc.M501972200 (2005).

23 Motegi, A., Fujimoto, J., Kotani, M., Sakuraba, H. & Yamamoto, T. ALK receptor tyrosine kinase promotes cell growth and neurite outgrowth. *J Cell Sci* **117**, 3319-3329, doi:10.1242/jcs.01183 117/15/3319 [pii] (2004).

24 Miyake, I. *et al.* Activation of anaplastic lymphoma kinase is responsible for hyperphosphorylation of ShcC in neuroblastoma cell lines. *Oncogene* **21**, 5823-5834, doi:10.1038/sj.onc.1205735 (2002).

25 Perez-Pinera, P., Zhang, W., Chang, Y., Vega, J. A. & Deuel, T. F. Anaplastic lymphoma kinase is activated through the pleiotrophin/receptor protein-tyrosine phosphatase beta/zeta signaling pathway: an alternative mechanism of receptor tyrosine kinase activation. *J Biol Chem* **282**, 28683-28690, doi:M704505200 [pii] 10.1074/jbc.M704505200 (2007).

26 Mourali, J. *et al.* Anaplastic lymphoma kinase is a dependence receptor whose proapoptotic functions are activated by caspase cleavage. *Mol Cell Biol* **26**, 6209-6222, doi:26/16/6209 [pii] 10.1128/MCB.01515-05 (2006).

27 Bredesen, D. E., Mehlen, P. & Rabizadeh, S. Apoptosis and dependence receptors: a molecular basis for cellular addiction. *Physiol Rev* **84**, 411-430, doi:10.1152/physrev.00027.2003 84/2/411 [pii] (2004).

28 Pulford, K. *et al.* Detection of anaplastic lymphoma kinase (ALK) and nucleolar protein nucleophosmin (NPM)-ALK proteins in normal and

neoplastic cells with the monoclonal antibody ALK1. *Blood* **89**, 1394-1404 (1997).

29 Loren, C. E. *et al.* A crucial role for the Anaplastic lymphoma kinase receptor tyrosine kinase in gut development in Drosophila melanogaster. *EMBO Rep* **4**, 781-786, doi:10.1038/sj.embor.embor897 embor897 [pii] (2003).

30 Cheng, L. Y. *et al.* Anaplastic lymphoma kinase spares organ growth during nutrient restriction in Drosophila. *Cell* **146**, 435-447, doi:S0092-8674(11)00715-X [pii] 10.1016/j.cell.2011.06.040 (2011).

31 Kalaany, N. Y. & Sabatini, D. M. Tumours with PI3K activation are resistant to dietary restriction. *Nature* **458**, 725-731, doi:nature07782 [pii] 10.1038/nature07782 (2009).

32 Gouzi, J. Y. *et al.* The receptor tyrosine kinase Alk controls neurofibromin functions in Drosophila growth and learning. *PLoS Genet* **7**, e1002281, doi:10.1371/journal.pgen.1002281 PGENETICS-D-11-00724 [pii] (2011).

33 Lasek, A. W. *et al.* An evolutionary conserved role for anaplastic lymphoma kinase in behavioral responses to ethanol. *PLoS One* **6**, e22636, doi:10.1371/journal.pone.0022636 PONE-D-10-06421 [pii] (2011).

34 Bilsland, J. G. *et al.* Behavioral and neurochemical alterations in mice deficient in anaplastic lymphoma kinase suggest therapeutic potential for psychiatric indications. *Neuropsychopharmacology* **33**, 685-700, doi:1301446 [pii] 10.1038/sj.npp.1301446 (2008).

35 Weiss, J. B. *et al.* Anaplastic lymphoma kinase and leukocyte tyrosine kinase: functions and genetic interactions in learning, memory and adult neurogenesis. *Pharmacol Biochem Behav* **100**, 566-574, doi:S0091-3057(11)00353-4 [pii] 10.1016/j.pbb.2011.10.024 (2012).

36 Brown, J. P. *et al.* Transient expression of doublecortin during adult neurogenesis. *J Comp Neurol* **467**, 1-10, doi:10.1002/cne.10874 (2003).

37 Stein, H. *et al.* The expression of the Hodgkin disease associated antigen Ki-1 in reactive and neoplastic lymphoid tissue: evidence that Reed-Sternberg cells and histiocytic malignancies are derived from activated lymphoid cells. *Blood* **66**, 848-858 (1985).

38 Benharroch, D. *et al.* ALK-positive lymphoma: a single disease with a broad spectrum of morphology. *Blood* **91**, 2076-2084 (1998).

39 Stein, H. *et al.* CD30(+) anaplastic large cell lymphoma: a review of its histopathologic, genetic, and clinical features. *Blood* **96**, 3681-3695 (2000).

40 Amin, H. M. & Lai, R. Pathobiology of ALK+ anaplastic large-cell lymphoma. *Blood* **110**, 2259-2267, doi:blood-2007-04-060715 [pii] 10.1182/blood-2007-04-060715 (2007).

41 Swerdlow, S. H. *WHO classification of tumours of haematopoietic and lymphoid tissues*. Vol. 2 (World Health Organization, 2008).

42 Savage, K. J. *et al.* ALK- anaplastic large-cell lymphoma is clinically and immunophenotypically different from both ALK+ ALCL and peripheral T-cell lymphoma, not otherwise specified: report from the International Peripheral T-Cell Lymphoma Project. *Blood* **111**, 5496-5504, doi:blood-2008-01-134270 [pii] 10.1182/blood-2008-01-134270 (2008).

43 Fischer, P. *et al.* A Ki-1 (CD30)-positive human cell line (Karpas 299) established from a high-grade non-Hodgkin lymphoma, showing a 2;5 translocation and rearrangement of the T-cell receptor beta-chain gene. *Blood* **72**, 234-240 (1988).

44 Kaneko, Y. *et al.* A novel translocation, t(2;5)(p23;q35), in childhood phagocytic large T-cell lymphoma mimicking malignant histiocytosis. *Blood* **73**, 806-813 (1989).

45 Rimokh, R. *et al.* A translocation involving a specific breakpoint (q35) on chromosome 5 is characteristic of anaplastic large cell lymphoma ('Ki-1 lymphoma'). *Br J Haematol* **71**, 31-36 (1989).

46 Mason, D. Y. *et al.* CD30-positive large cell lymphomas ('Ki-1 lymphoma') are associated with a chromosomal translocation involving 5q35. *Br J Haematol* **74**, 161-168 (1990).

47 Morris, S. W. *et al.* Fusion of a kinase gene, ALK, to a nucleolar protein gene, NPM, in non-Hodgkin lymphoma. *Science* **263**, 1281-1284 (1994).

48 Grisendi, S., Mecucci, C., Falini, B. & Pandolfi, P. P. Nucleophosmin and cancer. *Nat Rev Cancer* **6**, 493-505, doi:nrc1885 [pii] 10.1038/nrc1885 (2006).

49 Bischof, D., Pulford, K., Mason, D. Y. & Morris, S. W. Role of the nucleophosmin (NPM) portion of the non-Hodgkin lymphoma-associated

NPM-anaplastic lymphoma kinase fusion protein in oncogenesis. *Mol Cell Biol* **17**, 2312-2325 (1997).

50 Fujimoto, J. *et al.* Characterization of the transforming activity of p80, a hyperphosphorylated protein in a Ki-1 lymphoma cell line with chromosomal translocation t(2;5). *Proc Natl Acad Sci U S A* **93**, 4181-4186 (1996).

51 Lamant, L., Dastugue, N., Pulford, K., Delsol, G. & Mariame, B. A new fusion gene TPM3-ALK in anaplastic large cell lymphoma created by a (1;2)(q25;p23) translocation. *Blood* **93**, 3088-3095 (1999).

52 Siebert, R. *et al.* Complex variant translocation t(1;2) with TPM3-ALK fusion due to cryptic ALK gene rearrangement in anaplastic large-cell lymphoma. *Blood* **94**, 3614-3617 (1999).

53 Meech, S. J. *et al.* Unusual childhood extramedullary hematologic malignancy with natural killer cell properties that contains tropomyosin 4--anaplastic lymphoma kinase gene fusion. *Blood* **98**, 1209-1216 (2001).

54 Hernandez, L. *et al.* Diversity of genomic breakpoints in TFG-ALK translocations in anaplastic large cell lymphomas: identification of a new TFG-ALK(XL) chimeric gene with transforming activity. *Am J Pathol* **160**, 1487-1494, doi:S0002-9440(10)62574-6 [pii] 10.1016/S0002-9440(10)62574-6 (2002).

55 Hernandez, L. *et al.* TRK-fused gene (TFG) is a new partner of ALK in anaplastic large cell lymphoma producing two structurally different TFG-ALK translocations. *Blood* **94**, 3265-3268 (1999).

56 Touriol, C. *et al.* Further demonstration of the diversity of chromosomal changes involving 2p23 in ALK-positive lymphoma: 2 cases expressing ALK kinase fused to CLTCL (clathrin chain polypeptide-like). *Blood* **95**, 3204-3207 (2000).

57 Colleoni, G. W. *et al.* ATIC-ALK: A novel variant ALK gene fusion in anaplastic large cell lymphoma resulting from the recurrent cryptic chromosomal inversion, inv(2)(p23q35). *Am J Pathol* **156**, 781-789, doi:S0002-9440(10)64945-0 [pii] 10.1016/S0002-9440(10)64945-0 (2000).

58 Ma, Z. *et al.* Inv(2)(p23q35) in anaplastic large-cell lymphoma induces constitutive anaplastic lymphoma kinase (ALK) tyrosine kinase activation by fusion to ATIC, an enzyme involved in purine nucleotide biosynthesis. *Blood* **95**, 2144-2149 (2000).

59 Trinei, M. *et al.* A new variant anaplastic lymphoma kinase (ALK)-fusion protein (ATIC-ALK) in a case of ALK-positive anaplastic large cell lymphoma. *Cancer Res* **60**, 793-798 (2000).

60 Lamant, L. *et al.* Non-muscle myosin heavy chain (MYH9): a new partner fused to ALK in anaplastic large cell lymphoma. *Genes Chromosomes Cancer* **37**, 427-432, doi:10.1002/gcc.10232 (2003).

61 Tort, F. *et al.* Molecular characterization of a new ALK translocation involving moesin (MSN-ALK) in anaplastic large cell lymphoma. *Lab Invest* **81**, 419-426 (2001).

62 Tort, F., Campo, E., Pohlman, B. & Hsi, E. Heterogeneity of genomic breakpoints in MSN-ALK translocations in anaplastic large cell lymphoma. *Hum Pathol* **35**, 1038-1041, doi:S0046817704002874 [pii] (2004).

63 Cools, J. *et al.* Identification of novel fusion partners of ALK, the anaplastic lymphoma kinase, in anaplastic large-cell lymphoma and inflammatory myofibroblastic tumor. *Genes Chromosomes Cancer* **34**, 354-362, doi:10.1002/gcc.10033 (2002).

64 Gleason, B. C. & Hornick, J. L. Inflammatory myofibroblastic tumours: where are we now? *J Clin Pathol* **61**, 428-437, doi:jcp.2007.049387 [pii] 10.1136/jcp.2007.049387 (2008).

65 Coffin, C. M. *et al.* ALK1 and p80 expression and chromosomal rearrangements involving 2p23 in inflammatory myofibroblastic tumor. *Mod Pathol* **14**, 569-576, doi:10.1038/modpathol.3880352 (2001).

66 Cook, J. R. *et al.* Anaplastic lymphoma kinase (ALK) expression in the inflammatory myofibroblastic tumor: a comparative immunohistochemical study. *Am J Surg Pathol* **25**, 1364-1371 (2001).

67 Griffin, C. A. *et al.* Recurrent involvement of 2p23 in inflammatory myofibroblastic tumors. *Cancer Res* **59**, 2776-2780 (1999).

68 Lawrence, B. *et al.* TPM3-ALK and TPM4-ALK oncogenes in inflammatory myofibroblastic tumors. *Am J Pathol* **157**, 377-384, doi:S0002-9440(10)64550-6 [pii] 10.1016/S0002-9440(10)64550-6 (2000).

69 Debiec-Rychter, M., Marynen, P., Hagemeijer, A. & Pauwels, P. ALK-ATIC fusion in urinary bladder inflammatory myofibroblastic tumor. *Genes, Chromosomes and Cancer* **38**, 187-190 (2003).

70 Bridge, J. A. *et al.* Fusion of the ALK gene to the clathrin heavy chain gene, CLTC, in inflammatory myofibroblastic tumor. *Am J Pathol* **159**, 411-415, doi:S0002-9440(10)61711-7 [pii] 10.1016/S0002-9440(10)61711-7 (2001).

71 Debelenko, L. V. *et al.* Identification of CARS-ALK fusion in primary and metastatic lesions of an inflammatory myofibroblastic tumor. *Laboratory investigation* **83**, 1255-1265 (2003).

72 Ma, Z. *et al.* Fusion of ALK to the Ran-binding protein 2 (RANBP2) gene in inflammatory myofibroblastic tumor. *Genes, Chromosomes and Cancer* **37**, 98-105 (2003).

73 Takeuchi, K. *et al.* Pulmonary Inflammatory Myofibroblastic Tumor Expressing a Novel Fusion, PPFIBP1–ALK: Reappraisal of Anti-ALK Immunohistochemistry as a Tool for Novel ALK Fusion Identification. *Clinical Cancer Research* **17**, 3341-3348 (2011).

74 Panagopoulos, I. *et al.* Fusion of the SEC31L1 and ALK genes in an inflammatory myofibroblastic tumor. *International journal of cancer* **118**, 1181-1186 (2005).

75 Soda, M. *et al.* Identification of the transforming EML4–ALK fusion gene in non-small-cell lung cancer. *Nature* **448**, 561-566 (2007).

76 Koivunen, J. P. *et al.* EML4-ALK fusion gene and efficacy of an ALK kinase inhibitor in lung cancer. *Clinical Cancer Research* **14**, 4275-4283 (2008).

77 Choi, Y. L. *et al.* Identification of novel isoforms of the EML4-ALK transforming gene in non–small cell lung cancer. *Cancer research* **68**, 4971-4976 (2008).

78 Takeuchi, K. *et al.* Multiplex reverse transcription-PCR screening for EML4-ALK fusion transcripts. *Clinical Cancer Research* **14**, 6618-6624 (2008).

79 Sasaki, T., Rodig, S. J., Chirieac, L. R. & Jänne, P. A. The biology and treatment of EML4-ALK non-small cell lung cancer. *European Journal of Cancer* **46**, 1773-1780 (2010).

80 Wong, D. W. S. *et al.* The EML4-ALK fusion gene is involved in various histologic types of lung cancers from nonsmokers with wild-type EGFR and KRAS. *Cancer* **115**, 1723-1733 (2009).

81 Takeuchi, K. *et al.* KIF5B-ALK, a novel fusion oncokinase identified by an immunohistochemistry-based diagnostic system for ALK-positive lung cancer. *Clinical Cancer Research* **15**, 3143-3149 (2009).

82 Rikova, K. *et al.* Global survey of phosphotyrosine signaling identifies oncogenic kinases in lung cancer. *Cell* **131**, 1190-1203 (2007).

83 Togashi, Y. *et al.* KLC1-ALK: a novel fusion in lung cancer identified using a formalin-fixed paraffin-embedded tissue only. *PLoS One* **7**, e31323 (2012).

84 Jung, Y. *et al.* Discovery of ALK-PTPN3 gene fusion from human non-small cell lung carcinoma cell line using next generation RNA sequencing. *Genes, Chromosomes and Cancer* (2012).

85 Delsol, G. *et al.* A new subtype of large B-cell lymphoma expressing the ALK kinase and lacking the 2; 5 translocation. *Blood* **89**, 1483-1490 (1997).

86 Gascoyne, R. D. *et al.* ALK-positive diffuse large B-cell lymphoma is associated with Clathrin-ALK rearrangements: report of 6 cases. *Blood* **102**, 2568-2573 (2003).

87 Zhang, D., Denley, R. C., Filippa, D. A. & Teruya-Feldstein, J. ALK-positive diffuse large B-cell lymphoma with the t (2; 17)(p23; q23). *Applied Immunohistochemistry & Molecular Morphology* **17**, 172-177 (2009).

88 De Paepe, P. *et al.* ALK activation by the CLTC-ALK fusion is a recurrent event in large B-cell lymphoma. *Blood* **102**, 2638-2641 (2003).

89 Onciu, M. *et al.* ALK-positive plasmablastic B-cell lymphoma with expression of the NPM-ALK fusion transcript: report of 2 cases. *Blood* **102**, 2642-2644 (2003).

90 Takeuchi, K. *et al.* Identification of a novel fusion, SQSTM1-ALK, in ALK-positive large B-cell lymphoma. *haematologica* **96**, 464-467 (2011).

91 Bedwell, C. *et al.* Cytogenetically complex SEC31A-ALK fusions are recurrent in ALK-positive large B-cell lymphomas. *haematologica* **96**, 343-346 (2011).

92 Reichard, K. K., McKenna, R. W. & Kroft, S. H. ALK-positive diffuse large B-cell lymphoma: report of four cases and review of the literature. *Modern pathology* **20**, 310-319 (2007).

93 Kuefer, M. U. *et al.* Retrovirus-mediated gene transfer of NPM-ALK causes lymphoid malignancy in mice. *Blood* **90**, 2901-2910 (1997).

94 Lamant, L. *et al.* Expression of the ALK tyrosine kinase gene in neuroblastoma. *The American journal of pathology* **156**, 1711-1721 (2000).

95 Passoni, L. *et al.* Mutation-independent anaplastic lymphoma kinase overexpression in poor prognosis neuroblastoma patients. *Cancer research* **69**, 7338-7346 (2009).

96 Bagci, O., Tumer, S., Olgun, N. & Altungoz, O. Copy number status and mutation analyses of Anaplastic Lymphoma Kinase (< i> ALK</i>) gene in 90 sporadic neuroblastoma tumors. *Cancer letters* (2011).

97 Schönherr, C. *et al.* Anaplastic Lymphoma Kinase (ALK) regulates initiation of transcription of MYCN in neuroblastoma cells. *Oncogene* (2012).

98 Zhu, S. *et al.* Activated ALK collaborates with MYCN in neuroblastoma pathogenesis. *Cancer cell* **21**, 362-373 (2012).

99 Chen, Y. *et al.* Oncogenic mutations of ALK kinase in neuroblastoma. *Nature* **455**, 971-974 (2008).

100 George, R. E. *et al.* Activating mutations in ALK provide a therapeutic target in neuroblastoma. *Nature* **455**, 975-978 (2008).

101 Janoueix-Lerosey, I. *et al.* Somatic and germline activating mutations of the ALK kinase receptor in neuroblastoma. *Nature* **455**, 967-970 (2008).

102 De Brouwer, S. *et al.* Meta-analysis of neuroblastomas reveals a skewed ALK mutation spectrum in tumors with MYCN amplification. *Clinical Cancer Research* **16**, 4353-4362 (2010).

103 Cazes, A. *et al.* Characterization of rearrangements involving the ALK gene reveals a novel truncated form associated with tumor aggressiveness in neuroblastoma. *Cancer research* (2012).

104 Okubo, J. *et al.* Aberrant activation of ALK kinase by a novel truncated form ALK protein in neuroblastoma. *Oncogene* (2012).

105 Lin, E. *et al.* Exon array profiling detects EML4-ALK fusion in breast, colorectal, and non–small cell lung cancers. *Molecular Cancer Research* **7**, 1466-1476 (2009).

106 Lipson, D. *et al.* Identification of new ALK and RET gene fusions from colorectal and lung cancer biopsies. *Nat Med* **18**, 382-384, doi:10.1038/nm.2673 nm.2673 [pii] (2012).

107 Ren, H. *et al.* Identification of anaplastic lymphoma kinase as a potential therapeutic target in ovarian cancer. *Cancer Res* **72**, 3312-3323, doi:0008-5472.CAN-11-3931 [pii] 10.1158/0008-5472.CAN-11-3931 (2012).

108 Debelenko, L. V. *et al.* Renal cell carcinoma with novel VCL–ALK fusion: new representative of ALK-associated tumor spectrum. *Modern pathology* **24**, 430-442 (2010).

109 Perez-Pinera, P., Chang, Y., Astudillo, A., Mortimer, J. & Deuel, T. Anaplastic lymphoma kinase is expressed in different subtypes of human breast cancer. *Biochemical and Biophysical Research Communications* **358**, 399-403 (2007).

110 Zamo, A. *et al.* Anaplastic lymphoma kinase (ALK) activates Stat3 and protects hematopoietic cells from cell death. *Oncogene* **21**, 1038-1047, doi:10.1038/sj.onc.1205152 (2002).

111 Zhang, Q. *et al.* Multilevel dysregulation of STAT3 activation in anaplastic lymphoma kinase-positive T/null-cell lymphoma. *J Immunol* **168**, 466-474 (2002).

112 Amin, H. M. *et al.* Selective inhibition of STAT3 induces apoptosis and G(1) cell cycle arrest in ALK-positive anaplastic large cell lymphoma. *Oncogene* **23**, 5426-5434, doi:10.1038/sj.onc.1207703 1207703 [pii] (2004).

113 Chiarle, R. *et al.* Stat3 is required for ALK-mediated lymphomagenesis and provides a possible therapeutic target. *Nature medicine* **11**, 623-629 (2005).

114 Brierley, M. M. & Fish, E. N. Stats: multifaceted regulators of transcription. *Journal of interferon & cytokine research* **25**, 733-744 (2005).

115 Marzec, M. *et al.* Inhibition of ALK enzymatic activity in T-cell lymphoma cells induces apoptosis and suppresses proliferation and STAT3 phosphorylation independently of Jak3. *Laboratory investigation* **85**, 1544-1554 (2005).

116 Amin, H. M. *et al.* Inhibition of JAK3 induces apoptosis and decreases anaplastic lymphoma kinase activity in anaplastic large cell lymphoma. *Oncogene* **22**, 5399-5407 (2003).

117 Lai, R. *et al.* Jak3 activation is significantly associated with ALK expression in anaplastic large cell lymphoma. *Human pathology* **36**, 939-944 (2005).

118 Piva, R. *et al.* Functional validation of the anaplastic lymphoma kinase signature identifies CEBPB and BCL2A1 as critical target genes. *Journal of Clinical Investigation* **116**, 3171 (2006).

119 Anastasov, N. *et al.* C/EBPβ expression in ALK-positive anaplastic large cell lymphomas is required for cell proliferation and is induced by the STAT3 signaling pathway. *haematologica* **95**, 760-767 (2010).

120 Han, Y. *et al.* Loss of SHP1 enhances JAK3/STAT3 signaling and decreases proteosome degradation of JAK3 and NPM-ALK in ALK+ anaplastic large-cell lymphoma. *Blood* **108**, 2796-2803 (2006).

121 Coluccia, A. M. L. *et al.* Bcl-XL down-regulation suppresses the tumorigenic potential of NPM/ALK in vitro and in vivo. *Blood* **103**, 2787-2794 (2004).

122 Schlette, E. J., Medeiros, L. J., Goy, A., Lai, R. & Rassidakis, G. Z. Survivin expression predicts poorer prognosis in anaplastic large-cell lymphoma. *Journal of clinical oncology* **22**, 1682-1688 (2004).

123 Fawal, M. *et al.* A “liaison dangereuse” between AUF1/hnRNPD and the oncogenic tyrosine kinase NPM-ALK. *Blood* **108**, 2780-2788 (2006).

124 Raetz, E. A. *et al.* The nucleophosmin-anaplastic lymphoma kinase fusion protein induces c-Myc expression in pediatric anaplastic large cell lymphomas. *The American journal of pathology* **161**, 875-883 (2002).

125 Zhang, Q. *et al.* Oncogenic tyrosine kinase NPM-ALK induces expression of the growth-promoting receptor ICOS. *Blood* **118**, 3062-3071 (2011).

126 Gelebart, P. *et al.* Aberrant expression and biological significance of Sox2, an embryonic stem cell transcriptional factor, in ALK-positive anaplastic large cell lymphoma. *Blood Cancer Journal* **2**, e82 (2012).

127 Kasprzycka, M., Marzec, M., Liu, X., Zhang, Q. & Wasik, M. A. Nucleophosmin/anaplastic lymphoma kinase (NPM/ALK) oncoprotein induces the T regulatory cell phenotype by activating STAT3. *Proceedings of the National Academy of Sciences* **103**, 9964-9969 (2006).

128 Marzec, M. *et al.* Oncogenic kinase NPM/ALK induces through STAT3 expression of immunosuppressive protein CD274 (PD-L1, B7-H1). *Proceedings of the National Academy of Sciences* **105**, 20852-20857 (2008).

129 Dong, H. & Chen, L. B7-H1 pathway and its role in the evasion of tumor immunity. *Journal of molecular medicine* **81**, 281-287 (2003).

130 Anand, M., Lai, R. & Gelebart, P. β-catenin is constitutively active and increases STAT3 expression/activation in anaplastic lymphoma kinase-positive anaplastic large cell lymphoma. *haematologica* **96**, 253-261 (2011).

131 Armanious, H., Gelebart, P., Anand, M. & Lai, R. Identification of a novel crosstalk between casein kinase 2α and NPM-ALK in ALK-positive anaplastic large cell Lymphoma. *Cellular Signalling* (2012).

132 Hegazy, S. A. *et al.* Disheveled proteins promote cell growth and tumorigenicity in ALK-positive anaplastic large cell lymphoma. *Cellular Signalling* (2012).

133 Wang, P. *et al.* Serine phosphorylation of NPM–ALK, which is dependent on the auto-activation of the kinase activation loop, contributes to its oncogenic potential. *Carcinogenesis* **32**, 146-153 (2011).

134 Nieborowska-Skorska, M. *et al.* Role of signal transducer and activator of transcription 5 in nucleophosmin/ anaplastic lymphoma kinase-mediated malignant transformation of lymphoid cells. *Cancer Res* **61**, 6517-6523 (2001).

135 Ruchatz, H., Coluccia, A. M. L., Stano, P., Marchesi, E. & Gambacorti-Passerini, C. Constitutive activation of Jak2 contributes to proliferation and resistance to apoptosis in NPM/ALK-transformed cells. *Experimental hematology* **31**, 309-315 (2003).

136 Zhang, Q., Wang, H. Y., Liu, X. & Wasik, M. A. STAT5A is epigenetically silenced by the tyrosine kinase NPM1-ALK and acts as a tumor suppressor by reciprocally inhibiting NPM1-ALK expression. *Nature medicine* **13**, 1341-1348 (2007).

137 Khoury, J. D., Rassidakis, G. Z., Medeiros, L. J., Amin, H. M. & Lai, R. Methylation of SHP1 gene and loss of SHP1 protein expression are frequent in systemic anaplastic large cell lymphoma. *Blood* **104**, 1580-1581 (2004).

138 Zhang, Q., Raghunath, P. N., Vonderheid, E., Ødum, N. & Wasik, M. A. Lack of phosphotyrosine phosphatase SHP-1 expression in malignant T-cell lymphoma cells results from methylation of the SHP-1 promoter. *The American journal of pathology* **157**, 1137-1146 (2000).

139 Han, Y. *et al.* Restoration of shp1 expression by 5-AZA-2′-deoxycytidine is associated with downregulation of JAK3/STAT3 signaling in ALK-positive anaplastic large cell lymphoma. *Leukemia* **20**, 1602-1609 (2006).

140 Bard, J. D., Gelebart, P., Anand, M., Amin, H. M. & Lai, R. Aberrant expression of IL-22 receptor 1 and autocrine IL-22 stimulation contribute to tumorigenicity in ALK+ anaplastic large cell lymphoma. *Leukemia* **22**, 1595-1603 (2008).

141 Dien Bard, J. *et al.* IL-21 contributes to JAK3/STAT3 activation and promotes cell growth in ALK-positive anaplastic large cell lymphoma. *The American journal of pathology* **175**, 825-834 (2009).

142 Qiu, L. *et al.* Autocrine release of interleukin-9 promotes Jak3-dependent survival of ALK+ anaplastic large-cell lymphoma cells. *Blood* **108**, 2407-2415 (2006).

143 Zhang, Q. *et al.* IL-2R common γ-chain is epigenetically silenced by nucleophosphin–anaplastic lymphoma kinase (NPM-ALK) and acts as a tumor suppressor by targeting NPM-ALK. *Proceedings of the National Academy of Sciences* **108**, 11977-11982 (2011).

144 Carnero, A. The PKB/AKT pathway in cancer. *Current pharmaceutical design* **16**, 34-44 (2010).

145 Slupianek, A. *et al.* Role of phosphatidylinositol 3-kinase-Akt pathway in nucleophosmin/anaplastic lymphoma kinase-mediated lymphomagenesis. *Cancer research* **61**, 2194 (2001).

146 Bai, R. Y. *et al.* Nucleophosmin–anaplastic lymphoma kinase associated with anaplastic large-cell lymphoma activates the phosphatidylinositol 3-kinase/Akt antiapoptotic signaling pathway. *Blood* **96**, 4319-4327 (2000).

147 Maehama, T. & Dixon, J. E. The tumor suppressor, PTEN/MMAC1, dephosphorylates the lipid second messenger, phosphatidylinositol 3, 4, 5-trisphosphate. *Journal of Biological Chemistry* **273**, 13375-13378 (1998).

148 Üner, A. H. *et al.* PTEN and p27 expression in mature T-cell and NK-cell neoplasms. *Leukemia & lymphoma* **46**, 1463-1470 (2005).

149 McDonnell, S. R. P. *et al.* NPM-ALK signals through glycogen synthase kinase 3[beta] to promote oncogenesis. *Oncogene* **31**, 3733-3740 (2012).

150 Doble, B. W. & Woodgett, J. R. GSK-3: tricks of the trade for a multi-tasking kinase. *Journal of cell science* **116**, 1175-1186 (2003).

151 Pérez-Benavente, B. *et al.* GSK3-SCFFBXW7 targets JunB for degradation in G2 to preserve chromatid cohesion before anaphase. *Oncogene* (2012).

152 Slupianek, A. & Skorski, T. NPM/ALK downregulates p27< sup> Kip1</sup> in a PI-3K-dependent manner. *Experimental hematology* **32**, 1265-1271 (2004).

153 Rassidakis, G. Z. *et al.* Inhibition of Akt increases p27Kip1 levels and induces cell cycle arrest in anaplastic large cell lymphoma. *Blood* **105**, 827-829 (2005).

154 Polyak, K. *et al.* p27Kip1, a cyclin-Cdk inhibitor, links transforming growth factor-beta and contact inhibition to cell cycle arrest. *Genes & development* **8**, 9-22 (1994).

155 Gu, T. L. *et al.* NPM-ALK fusion kinase of anaplastic large-cell lymphoma regulates survival and proliferative signaling through modulation of FOXO3a. *Blood* **103**, 4622-4629 (2004).

156 Singh, R. R. *et al.* Sonic hedgehog signaling pathway is activated in ALK-positive anaplastic large cell lymphoma. *Cancer research* **69**, 2550-2558 (2009).

157 Marzec, M. *et al.* Oncogenic tyrosine kinase NPM/ALK induces activation of the rapamycin-sensitive mTOR signaling pathway. *Oncogene* **26**, 5606-5614 (2007).

158 Gu, L. *et al.* Rapamycin reverses NPM-ALK-induced glucocorticoid resistance in lymphoid tumor cells by inhibiting mTOR signaling pathway, enhancing G1 cell cycle arrest and apoptosis. *Leukemia* **22**, 2091-2096 (2008).

159 Marzec, M. *et al.* Oncogenic tyrosine kinase NPM/ALK induces activation of the MEK/ERK signaling pathway independently of c-Raf. *Oncogene* **26**, 813-821 (2006).

160 Voena, C. *et al.* The tyrosine phosphatase Shp2 interacts with NPM-ALK and regulates anaplastic lymphoma cell growth and migration. *Cancer research* **67**, 4278-4286 (2007).

161 Riera, L. *et al.* Involvement of Grb2 adaptor protein in nucleophosmin-anaplastic lymphoma kinase (NPM-ALK)-mediated signaling and anaplastic large cell lymphoma growth. *Journal of Biological Chemistry* **285**, 26441-26450 (2010).

162 Turner, S. D., Yeung, D., Hadfield, K., Cook, S. J. & Alexander, D. R. The NPM-ALK tyrosine kinase mimics TCR signalling pathways, inducing NFAT and AP-1 by RAS-dependent mechanisms. *Cellular Signalling* **19**, 740-747 (2007).

163 Staber, P. B. *et al.* The oncoprotein NPM-ALK of anaplastic large-cell lymphoma induces JUNB transcription via ERK1/2 and JunB translation via mTOR signaling. *Blood* **110**, 3374-3383 (2007).

164 Fernández, M. *et al.* Involvement of Cot activity in the proliferation of ALCL lymphoma cells. *Biochemical and Biophysical Research Communications* **411**, 655-660 (2011).

165 Vega, F. *et al.* Activation of mammalian target of rapamycin signaling pathway contributes to tumor cell survival in anaplastic lymphoma kinase–positive anaplastic large cell lymphoma. *Cancer research* **66**, 6589-6597 (2006).

166 Leventaki, V. *et al.* NPM-ALK oncogenic kinase promotes cell-cycle progression through activation of JNK/cJun signaling in anaplastic large-cell lymphoma. *Blood* **110**, 1621-1630 (2007).

167 Watanabe, M. *et al.* JunB Induced by Constitutive CD30–Extracellular Signal-Regulated Kinase 1/2 Mitogen-Activated Protein Kinase Signaling Activates the CD30 Promoter in Anaplastic Large Cell Lymphoma and Reed-Sternberg Cells of Hodgkin Lymphoma. *Cancer research* **65**, 7628-7634 (2005).

168 Hsu, F. Y. Y., Johnston, P. B., Burke, K. A. & Zhao, Y. The Expression of CD30 in Anaplastic Large Cell Lymphoma Is Regulated by Nucleophosmin-Anaplastic Lymphoma Kinase–Mediated JunB Level in a Cell Type–Specific Manner. *Cancer research* **66**, 9002-9008 (2006).

169 Wright, C. W., Rumble, J. M. & Duckett, C. S. CD30 activates both the canonical and alternative NF-κB pathways in anaplastic large cell lymphoma cells. *Journal of Biological Chemistry* **282**, 10252-10262 (2007).

170 Lamant, L. *et al.* Gene-expression profiling of systemic anaplastic large-cell lymphoma reveals differences based on ALK status and two distinct morphologic ALK+ subtypes. *Blood* **109**, 2156-2164 (2007).

171 Piva, R. *et al.* Gene expression profiling uncovers molecular classifiers for the recognition of anaplastic large-cell lymphoma within peripheral T-cell neoplasms. *Journal of clinical oncology* **28**, 1583-1590 (2010).

172 Ballester, B. *et al.* Gene expression profiling identifies molecular subgroups among nodal peripheral T-cell lymphomas. *Oncogene* **25**, 1560-1570 (2005).

173 Wu, F., Wang, P., Young, L. C., Lai, R. & Li, L. Proteome-wide identification of novel binding partners to the oncogenic fusion gene protein, NPM-ALK, using tandem affinity purification and mass spectrometry. *Am J Pathol* **174**, 361-370, doi:S0002-9440(10)61296-5 [pii] 10.2353/ajpath.2009.080521 (2009).

174 Crockett, D. K., Lin, Z., Elenitoba-Johnson, K. S. & Lim, M. S. Identification of NPM-ALK interacting proteins by tandem mass spectrometry. *Oncogene* **23**, 2617-2629, doi:10.1038/sj.onc.1207398 1207398 [pii] (2004).

175 Lim, M. S. *et al.* The proteomic signature of NPM/ALK reveals deregulation of multiple cellular pathways. *Blood* **114**, 1585-1595 (2009).

176 Rush, J. *et al.* Immunoaffinity profiling of tyrosine phosphorylation in cancer cells. *Nature biotechnology* **23**, 94-101 (2004).

177 Boccalatte, F. E. *et al.* The enzymatic activity of 5-aminoimidazole-4-carboxamide ribonucleotide formyltransferase/IMP cyclohydrolase is enhanced by NPM-ALK: new insights in ALK-mediated pathogenesis and the treatment of ALCL. *Blood* **113**, 2776-2790, doi:blood-2008-06-161018 [pii] 10.1182/blood-2008-06-161018 (2009).

178 Wu, F. *et al.* Studies of phosphoproteomic changes induced by nucleophosmin-anaplastic lymphoma kinase (ALK) highlight deregulation of tumor necrosis factor (TNF)/Fas/TNF-related apoptosis-induced ligand signaling pathway in ALK-positive anaplastic large cell lymphoma. *Molecular & Cellular Proteomics* **9**, 1616-1632 (2010).

179 Wan, W. *et al.* Anaplastic lymphoma kinase activity is essential for the proliferation and survival of anaplastic large-cell lymphoma cells. *Blood* **107**, 1617-1623 (2006).

180 Cui, J. J. *et al.* Structure Based Drug Design of Crizotinib (PF-02341066), a Potent and Selective Dual Inhibitor of Mesenchymal–Epithelial Transition Factor (c-MET) Kinase and Anaplastic Lymphoma Kinase (ALK). *Journal of medicinal chemistry* **54**, 6342-6363 (2011).

181 Christensen, J. G. *et al.* Cytoreductive antitumor activity of PF-2341066, a novel inhibitor of anaplastic lymphoma kinase and c-Met, in experimental models of anaplastic large-cell lymphoma. *Molecular Cancer Therapeutics* **6**, 3314 (2007).

182 Zou, H. Y. *et al.* An orally available small-molecule inhibitor of c-Met, PF-2341066, exhibits cytoreductive antitumor efficacy through antiproliferative and antiangiogenic mechanisms. *Cancer research* **67**, 4408-4417 (2007).

183 Zillhardt, M., Christensen, J. G. & Lengyel, E. An orally available small-molecule inhibitor of c-Met, PF-2341066, reduces tumor burden and metastasis in a preclinical model of ovarian cancer metastasis. *Neoplasia (New York, NY)* **12**, 1 (2010).

184 Kwak, E. L. *et al.* Anaplastic lymphoma kinase inhibition in non–small-cell lung cancer. *New England Journal of Medicine* **363**, 1693-1703 (2010).

185 Gambacorti-Passerini, C., Messa, C. & Pogliani, E. M. Crizotinib in anaplastic large-cell lymphoma. *New England Journal of Medicine* **364**, 775-776 (2011).

186 Butrynski, J. E. *et al.* Crizotinib in ALK-rearranged inflammatory myofibroblastic tumor. *N Engl J Med* **363**, 1727-1733, doi:10.1056/NEJMoa1007056 (2010).

187 Katayama, R. *et al.* Mechanisms of acquired crizotinib resistance in ALK-rearranged lung cancers. *Science Translational Medicine* **4**, 120ra117 (2012).

188 Katayama, R. *et al.* Therapeutic strategies to overcome crizotinib resistance in non-small cell lung cancers harboring the fusion oncogene EML4-ALK. *Proceedings of the National Academy of Sciences* **108**, 7535-7540 (2011).

189 Sasaki, T. *et al.* The neuroblastoma-associated F1174L ALK mutation causes resistance to an ALK kinase inhibitor in ALK-translocated cancers. *Cancer research* **70**, 10038-10043 (2010).

190 Vander Heiden, M. G., Cantley, L. C. & Thompson, C. B. Understanding the Warburg effect: the metabolic requirements of cell proliferation. *Science* **324**, 1029-1033, doi:324/5930/1029 [pii] 10.1126/science.1160809 (2009).

191 Warburg, O. On the origin of cancer cells. *Science* **123**, 309-314 (1956).

192 Warburg, O., Wind, F. & Negelein, E. The metabolism of tumors in the body. *The Journal of general physiology* **8**, 519-530 (1927).

193 Lunt, S. Y. & Vander Heiden, M. G. Aerobic glycolysis: meeting the metabolic requirements of cell proliferation. *Annu Rev Cell Dev Biol* **27**, 441-464, doi:10.1146/annurev-cellbio-092910-154237 (2011).

194 Vara, J. Á. F. *et al.* PI3K/Akt signalling pathway and cancer. *Cancer treatment reviews* **30**, 193-204 (2004).

195 Elstrom, R. L. *et al.* Akt stimulates aerobic glycolysis in cancer cells. *Cancer research* **64**, 3892-3899 (2004).

196 Kohn, A. D., Summers, S. A., Birnbaum, M. J. & Roth, R. A. Expression of a constitutively active Akt Ser/Thr kinase in 3T3-L1 adipocytes stimulates glucose uptake and glucose transporter 4 translocation. *Journal of Biological Chemistry* **271**, 31372-31378 (1996).

197 Rathmell, J. C. *et al.* Akt-directed glucose metabolism can prevent Bax conformation change and promote growth factor-independent survival. *Molecular and cellular biology* **23**, 7315-7328 (2003).

198 Deprez, J., Vertommen, D., Alessi, D. R., Hue, L. & Rider, M. H. Phosphorylation and activation of heart 6-phosphofructo-2-kinase by protein kinase B and other protein kinases of the insulin signaling cascades. *Journal of Biological Chemistry* **272**, 17269-17275 (1997).

199 Bauer, D. E., Hatzivassiliou, G., Zhao, F., Andreadis, C. & Thompson, C. B. ATP citrate lyase is an important component of cell growth and transformation. *Oncogene* **24**, 6314-6322 (2005).

200 Berwick, D. C., Hers, I., Heesom, K. J., Moule, S. K. & Tavaré, J. M. The identification of ATP-citrate lyase as a protein kinase B (Akt) substrate in primary adipocytes. *Journal of Biological Chemistry* **277**, 33895-33900 (2002).

201 Hatzivassiliou, G. *et al.* ATP citrate lyase inhibition can suppress tumor cell growth. *Cancer cell* **8**, 311-321 (2005).

202 Edinger, A. L. & Thompson, C. B. Akt maintains cell size and survival by increasing mTOR-dependent nutrient uptake. *Science Signalling* **13**, 2276 (2002).

203 Hahn-Windgassen, A. *et al.* Akt activates the mammalian target of rapamycin by regulating cellular ATP level and AMPK activity. *Journal of Biological Chemistry* **280**, 32081-32089 (2005).

204 Gwinn, D. M. *et al.* AMPK phosphorylation of raptor mediates a metabolic checkpoint. *Molecular Cell* **30**, 214-226 (2008).

205 Düvel, K. *et al.* Activation of a metabolic gene regulatory network downstream of mTOR complex 1. *Molecular Cell* **39**, 171-183 (2010).

206 Kim, J., Tchernyshyov, I., Semenza, G. L. & Dang, C. V. HIF-1-mediated expression of pyruvate dehydrogenase kinase: a metabolic switch required for cellular adaptation to hypoxia. *Cell metabolism* **3**, 177-185 (2006).

207 Pelengaris, S., Khan, M. & Evan, G. c-MYC: more than just a matter of life and death. *Nature Reviews Cancer* **2**, 764-776 (2002).

208 Osthus, R. C. *et al.* Deregulation of glucose transporter 1 and glycolytic gene expression by c-Myc. *Journal of Biological Chemistry* **275**, 21797-21800 (2000).

209 Shim, H. *et al.* c-Myc transactivation of LDH-A: implications for tumor metabolism and growth. *Proceedings of the National Academy of Sciences* **94**, 6658-6663 (1997).

210 Fletcher, J. W. *et al.* Recommendations on the use of 18F-FDG PET in oncology. *Journal of Nuclear Medicine* **49**, 480-508 (2008).

211 Palaskas, N. *et al.* 18F-fluorodeoxy-glucose positron emission tomography marks MYC-overexpressing human basal-like breast cancers. *Cancer research* **71**, 5164-5174 (2011).

212 Li, F. *et al.* Myc stimulates nuclearly encoded mitochondrial genes and mitochondrial biogenesis. *Molecular and cellular biology* **25**, 6225-6234 (2005).

213 Gao, P. *et al.* c-Myc suppression of miR-23a/b enhances mitochondrial glutaminase expression and glutamine metabolism. *Nature* **458**, 762-765 (2009).

214 Hitosugi, T. *et al.* Tyrosine phosphorylation inhibits PKM2 to promote the Warburg effect and tumor growth. *Science's STKE* **2**, ra73 (2009).

215 Vander Heiden, M. G. *et al.* Evidence for an alternative glycolytic pathway in rapidly proliferating cells. *Science Signalling* **329**, 1492 (2010).

216 Hitosugi, T. *et al.* Phosphoglycerate Mutase 1 Coordinates Glycolysis and Biosynthesis to Promote Tumor Growth. *Cancer cell* **22**, 585-600 (2012).

217 Semenza, G. L., Roth, P. H., Fang, H. M. & Wang, G. L. Transcriptional regulation of genes encoding glycolytic enzymes by hypoxia-inducible factor 1. *Journal of Biological Chemistry* **269**, 23757-23763 (1994).

218 Fan, J. *et al.* Tyrosine Phosphorylation of Lactate Dehydrogenase A Is Important for NADH/NAD+ Redox Homeostasis in Cancer Cells. *Molecular and cellular biology* **31**, 4938-4950 (2011).

219 Sonveaux, P. *et al.* Targeting lactate-fueled respiration selectively kills hypoxic tumor cells in mice. *The Journal of clinical investigation* **118**, 3930 (2008).

220 Mazurek, S. Pyruvate kinase type M2: A key regulator of the metabolic budget system in tumor cells. *Int J Biochem Cell Biol*, doi:S1357-2725(10)00062-2 [pii] 10.1016/j.biocel.2010.02.005 (2010).

221 Christofk, H. R. *et al.* The M2 splice isoform of pyruvate kinase is important for cancer metabolism and tumour growth. *Nature* **452**, 230-233, doi:nature06734 [pii] 10.1038/nature06734 (2008).

222 Dombrauckas, J. D., Santarsiero, B. D. & Mesecar, A. D. Structural basis for tumor pyruvate kinase M2 allosteric regulation and catalysis. *Biochemistry* **44**, 9417-9429, doi:10.1021/bi0474923 (2005).

223 Christofk, H. R., Vander Heiden, M. G., Wu, N., Asara, J. M. & Cantley, L. C. Pyruvate kinase M2 is a phosphotyrosine-binding protein. *Nature* **452**, 181-186, doi:nature06667 [pii] 10.1038/nature06667 (2008).

224 Hitosugi, T. *et al.* Tyrosine phosphorylation inhibits PKM2 to promote the Warburg effect and tumor growth. *Sci Signal* **2**, ra73, doi:2/97/ra73 [pii] 10.1126/scisignal.2000431 (2009).

225 Anastasiou, D. *et al.* Pyruvate kinase M2 activators promote tetramer formation and suppress tumorigenesis. *Nature Chemical Biology* **8**, 839-847 (2012).

226 Kung, C. *et al.* Small Molecule Activation of PKM2 in Cancer Cells Induces Serine Auxotrophy. *Chemistry & Biology* **19**, 1187-1198 (2012).

227 Chen, J., Jiang, Z., Wang, B., Wang, Y. & Hu, X. Vitamin K< sub> 3</sub> and K< sub> 5</sub> are inhibitors of tumor pyruvate kinase M2. *Cancer letters* (2011).

228 Chen, J. *et al.* Shikonin and its analogs inhibit cancer cell glycolysis by targeting tumor pyruvate kinase-M2. *Oncogene* **30**, 4297-4306 (2011).

229 Vander Heiden, M. G. *et al.* Identification of small molecule inhibitors of pyruvate kinase M2. *Biochemical pharmacology* **79**, 1118-1124 (2010).

230 Lee, J., Kim, H. K., Han, Y. M. & Kim, J. Pyruvate kinase isozyme type M2 (PKM2) interacts and cooperates with Oct-4 in regulating transcription. *The international journal of biochemistry & cell biology* **40**, 1043-1054 (2008).

231 Yang, W. *et al.* Nuclear PKM2 regulates [bgr]-catenin transactivation upon EGFR activation. *Nature* (2011).

232 Luo, W. *et al.* Pyruvate kinase M2 is a PHD3-stimulated coactivator for hypoxia-inducible factor 1. *Cell* **145**, 732-744 (2011).

233 Gao, X., Wang, H., Yang, J. J., Liu, X. & Liu, Z. R. Pyruvate kinase M2 regulates gene transcription by acting as a protein kinase. *Molecular Cell* (2012).

234 Yang, W. *et al.* ERK1/2-dependent phosphorylation and nuclear translocation of PKM2 promotes the Warburg effect. *Nature cell biology* (2012).

235 Bai, R. Y., Dieter, P., Peschel, C., Morris, S. W. & Duyster, J. Nucleophosmin-anaplastic lymphoma kinase of large-cell anaplastic lymphoma is a constitutively active tyrosine kinase that utilizes phospholipase C-γ to mediate its mitogenicity. *Molecular and cellular biology* **18**, 6951-6961 (1998).

236 Hanahan, D. & Weinberg, R. A. Hallmarks of cancer: the next generation. *Cell* **144**, 646-674 (2011).

237 Chen, Y. *et al.* Differential expression of novel tyrosine kinase substrates during breast cancer development. *Molecular & Cellular Proteomics* **6**, 2072-2087 (2007).

238 Daub, H. *et al.* Kinase-selective enrichment enables quantitative phosphoproteomics of the kinome across the cell cycle. *Molecular Cell* **31**, 438 (2008).

239 Sachon, E., Mohammed, S., Bache, N. & Jensen, O. N. Phosphopeptide quantitation using amine-reactive isobaric tagging reagents and tandem mass spectrometry: application to proteins isolated by gel electrophoresis. *Rapid communications in mass spectrometry* **20**, 1127-1134 (2006).

240 Sreekumar, A. *et al.* Metabolomic profiles delineate potential role for sarcosine in prostate cancer progression. *Nature* **457**, 910-914 (2009).

241 Ott, G. R. *et al.* Discovery of a potent Inhibitor of anaplastic lymphoma kinase with in vivo antitumor activity. *ACS Medicinal Chemistry Letters* **1**, 493-498 (2010).

242 Huang da, W., Sherman, B. T. & Lempicki, R. A. Bioinformatics enrichment tools: paths toward the comprehensive functional analysis of large gene lists. *Nucleic Acids Res* **37**, 1-13, doi:gkn923 [pii] 10.1093/nar/gkn923 (2009).

243 Huang da, W., Sherman, B. T. & Lempicki, R. A. Systematic and integrative analysis of large gene lists using DAVID bioinformatics resources. *Nat Protoc* **4**, 44-57, doi:nprot.2008.211 [pii] 10.1038/nprot.2008.211 (2009).

244 Svetnik, V. *et al.* Random forest: a classification and regression tool for compound classification and QSAR modeling. *Journal of chemical information and computer sciences* **43**, 1947-1958 (2003).

245 Xia, J., Mandal, R., Sinelnikov, I. V., Broadhurst, D. & Wishart, D. S. MetaboAnalyst 2.0--a comprehensive server for metabolomic data analysis. *Nucleic Acids Res* **40**, W127-133, doi:gks374 [pii] 10.1093/nar/gks374 (2012).

246 Xia, J., Psychogios, N., Young, N. & Wishart, D. S. MetaboAnalyst: a web server for metabolomic data analysis and interpretation. *Nucleic Acids Res* **37**, W652-660, doi:gkp356 [pii] 10.1093/nar/gkp356 (2009).

247 Kanehisa, M., Goto, S., Sato, Y., Furumichi, M. & Tanabe, M. KEGG for integration and interpretation of large-scale molecular data sets. *Nucleic Acids Res* **40**, D109-114, doi:gkr988 [pii] 10.1093/nar/gkr988 (2012).

248 Ogata, H. *et al.* KEGG: Kyoto Encyclopedia of Genes and Genomes. *Nucleic Acids Res* **27**, 29-34, doi:gkc043 [pii] (1999).

249 Maehara, Y., Anai, H., Tamada, R. & Sugimachi, K. The ATP assay is more sensitive than the succinate dehydrogenase inhibition test for predicting cell viability. *European Journal of Cancer and Clinical Oncology* **23**, 273-276 (1987).

250 Hitosugi, T. *et al.* Tyrosine phosphorylation of mitochondrial pyruvate dehydrogenase kinase 1 is important for cancer metabolism. *Molecular Cell* **44**, 864-877 (2011).

251 Marsin, A., Rider, M., Deprez, J. & Beauloye, C. Phosphorylation and activation of heart PFK-2 by AMPK has a role in the stimulation of glycolysis during ischaemia. *Current Biology* **10**, 1247-1255 (2000).

252 DeBerardinis, R. J. *et al.* Beyond aerobic glycolysis: transformed cells can engage in glutamine metabolism that exceeds the requirement for protein and nucleotide synthesis. *Proceedings of the National Academy of Sciences* **104**, 19345-19350 (2007).

253 Ye, J. *et al.* Pyruvate kinase M2 promotes de novo serine synthesis to sustain mTORC1 activity and cell proliferation. *Proceedings of the National Academy of Sciences* **109**, 6904-6909 (2012).

254 Dang, C. V. Rethinking the Warburg effect with Myc micromanaging glutamine metabolism. *Cancer research* **70**, 859-862 (2010).

255 Mashima, T., Seimiya, H. & Tsuruo, T. De novo fatty-acid synthesis and related pathways as molecular targets for cancer therapy. *British journal of cancer* **100**, 1369-1372 (2009).

256 Christofk, H. R. *et al.* The M2 splice isoform of pyruvate kinase is important for cancer metabolism and tumour growth. *Nature* **452**, 230-233 (2008).

257 David, C. J., Chen, M., Assanah, M., Canoll, P. & Manley, J. L. HnRNP proteins controlled by c-Myc deregulate pyruvate kinase mRNA splicing in cancer. *Nature* **463**, 364-368 (2009).

258 Palacios, R. & Steinmetz, M. Il-3-dependent mouse clones that express B-220 surface antigen, contain Ig genes in germ-line configuration, and generate B lymphocytes in vivo. *Cell* **41**, 727 (1985).

259 Lardy, H. A., Connelly, J. L. & Johnson, D. Antibiotics as Tools for Metabolic Studies. II. Inhibition of Phosphoryl Transfer in Mitochondria by Oligomycin and Aurovertin*. *Biochemistry* **3**, 1961-1968 (1964).

260 Woessmann, W. *et al.* Allogeneic haematopoietic stem cell transplantation in relapsed or refractory anaplastic large cell lymphoma of children and adolescents–a Berlin–Frankfurt–Münster group report. *British journal of haematology* **133**, 176-182 (2006).

261 Marzec, M. *et al.* Oncogenic kinase NPM/ALK induces expression of HIF1α mRNA. *Oncogene* **30**, 1372-1378 (2010).

262 Jope, R. S. & Johnson, G. V. The glamour and gloom of glycogen synthase kinase-3. *Trends Biochem Sci* **29**, 95-102, doi:10.1016/j.tibs.2003.12.004

S0968000403003207 [pii] (2004).

263 Cohen, P. & Frame, S. The renaissance of GSK3. *Nat Rev Mol Cell Biol* **2**, 769-776, doi:10.1038/35096075

35096075 [pii] (2001).

264 Kang, T. *et al.* GSK-3 beta targets Cdc25A for ubiquitin-mediated proteolysis, and GSK-3 beta inactivation correlates with Cdc25A overproduction in human cancers. *Cancer Cell* **13**, 36-47, doi:S1535-6108(07)00371-6 [pii] 10.1016/j.ccr.2007.12.002 (2008).

265 Zhao, Y. *et al.* Glycogen synthase kinase 3alpha and 3beta mediate a glucose-sensitive antiapoptotic signaling pathway to stabilize Mcl-1. *Mol Cell Biol* **27**, 4328-4339, doi:MCB.00153-07 [pii] 10.1128/MCB.00153-07 (2007).

266 Diehl, J. A., Zindy, F. & Sherr, C. J. Inhibition of cyclin D1 phosphorylation on threonine-286 prevents its rapid degradation via the ubiquitin-proteasome pathway. *Genes Dev* **11**, 957-972 (1997).

267 Jinno, S. *et al.* Cdc25A is a novel phosphatase functioning early in the cell cycle. *EMBO J* **13**, 1549-1556 (1994).

268 Summers, S. A. *et al.* The role of glycogen synthase kinase 3β in insulin-stimulated glucose metabolism. *Journal of Biological Chemistry* **274**, 17934-17940 (1999).

269 Ito, M., Zhao, N., Zeng, Z., Chang, C. C. & Zu, Y. Synergistic growth inhibition of anaplastic large cell lymphoma cells by combining cellular ALK gene silencing and a low dose of the kinase inhibitor U0126. *Cancer Gene Ther* **17**, 633-644, doi:cgt201020 [pii] 10.1038/cgt.2010.20 (2010).

270 Ott, G. R., Tripathy, R., Cheng, M., McHugh, R. & Anzalone, A. V. Discovery of a Potent Inhibitor of Anaplastic Lymphoma Kinase with in Vivo Antitumor Activity. *ACS Medicinal Chemistry Letter* **1**, 493-498 (2010).

271 Vermes, I., Haanen, C., Steffens-Nakken, H. & Reutelingsperger, C. A novel assay for apoptosis. Flow cytometric detection of phosphatidylserine expression on early apoptotic cells using fluorescein labelled Annexin V. *J Immunol Methods* **184**, 39-51, doi:002217599500072I [pii] (1995).

272 Keller, A., Nesvizhskii, A. I., Kolker, E. & Aebersold, R. Empirical statistical model to estimate the accuracy of peptide identifications made by MS/MS and database search. *Analytical chemistry* **74**, 5383-5392 (2002).

273 Nesvizhskii, A. I., Keller, A., Kolker, E. & Aebersold, R. A statistical model for identifying proteins by tandem mass spectrometry. *Analytical chemistry* **75**, 4646-4658 (2003).

274 Rush, J. *et al.* Immunoaffinity profiling of tyrosine phosphorylation in cancer cells. *Nat Biotechnol* **23**, 94-101, doi:nbt1046 [pii] 10.1038/nbt1046 (2005).

275 Slupianek, A. *et al.* Role of phosphatidylinositol 3-kinase-Akt pathway in nucleophosmin/anaplastic lymphoma kinase-mediated lymphomagenesis. *Cancer Res* **61**, 2194-2199 (2001).

276 Cross, D. A., Alessi, D. R., Cohen, P., Andjelkovich, M. & Hemmings, B. A. Inhibition of glycogen synthase kinase-3 by insulin mediated by protein kinase B. *Nature* **378**, 785-789, doi:10.1038/378785a0 (1995).

277 Herman, S. E. *et al.* Phosphatidylinositol 3-kinase-delta inhibitor CAL-101 shows promising preclinical activity in chronic lymphocytic leukemia by antagonizing intrinsic and extrinsic cellular survival signals. *Blood* **116**, 2078-2088, doi:blood-2010-02-271171 [pii] 10.1182/blood-2010-02-271171 (2010).

278 van Noort, M., Meeldijk, J., van der Zee, R., Destree, O. & Clevers, H. Wnt signaling controls the phosphorylation status of beta-catenin. *J Biol Chem* **277**, 17901-17905, doi:10.1074/jbc.M111635200 M111635200 [pii] (2002).

279 Bai, R. Y., Dieter, P., Peschel, C., Morris, S. W. & Duyster, J. Nucleophosmin-anaplastic lymphoma kinase of large-cell anaplastic lymphoma is a constitutively active tyrosine kinase that utilizes phospholipase C-gamma to mediate its mitogenicity. *Mol Cell Biol* **18**, 6951-6961 (1998).

280 Frame, S., Cohen, P. & Biondi, R. M. A common phosphate binding site explains the unique substrate specificity of GSK3 and its inactivation by phosphorylation. *Mol Cell* **7**, 1321-1327, doi:S1097-2765(01)00253-2 [pii] (2001).

281 Bostock, C. J., Prescott, D. M. & Kirkpatrick, J. B. An evaluation of the double thymidine block for synchronizing mammalian cells at the G1-S border. *Exp Cell Res* **68**, 163-168, doi:0014-4827(71)90599-4 [pii] (1971).

282 Maurer, U., Charvet, C., Wagman, A. S., Dejardin, E. & Green, D. R. Glycogen synthase kinase-3 regulates mitochondrial outer membrane permeabilization and apoptosis by destabilization of MCL-1. *Mol Cell* **21**, 749-760, doi:S1097-2765(06)00111-0 [pii] 10.1016/j.molcel.2006.02.009 (2006).

283 Boulares, A. H. *et al.* Role of poly(ADP-ribose) polymerase (PARP) cleavage in apoptosis. Caspase 3-resistant PARP mutant increases rates of apoptosis in transfected cells. *J Biol Chem* **274**, 22932-22940 (1999).

284 Meijer, L. *et al.* GSK-3-selective inhibitors derived from Tyrian purple indirubins. *Chem Biol* **10**, 1255-1266, doi:S1074552103002552 [pii] (2003).

285 Fernandez-Vidal, A. *et al.* Upregulation of the CDC25A phosphatase down-stream of the NPM/ALK oncogene participates to anaplastic large cell lymphoma enhanced proliferation. *Cell Cycle* **8**, 1373-1379, doi:8302 [pii] (2009).

286 Cole, A., Frame, S. & Cohen, P. Further evidence that the tyrosine phosphorylation of glycogen synthase kinase-3 (GSK3) in mammalian cells is an autophosphorylation event. *Biochemical Journal* **377**, 249 (2004).

287 Hughes, K., Nikolakaki, E., Plyte, S. E., Totty, N. F. & Woodgett, J. R. Modulation of the glycogen synthase kinase-3 family by tyrosine phosphorylation. *The EMBO journal* **12**, 803 (1993).

288 Wang, Q. M., Fiol, C. J., DePaoli-Roach, A. & Roach, P. J. Glycogen synthase kinase-3 beta is a dual specificity kinase differentially regulated by tyrosine and serine/threonine phosphorylation. *Journal of Biological Chemistry* **269**, 14566-14574 (1994).

289 Angers, S. *et al.* The KLHL12–Cullin-3 ubiquitin ligase negatively regulates the Wnt–β-catenin pathway by targeting Dishevelled for degradation. *Nature cell biology* **8**, 348-357 (2006).

290 Chou, H. Y. *et al.* GSKIP is homologous to the axin GSK3β interaction domain and functions as a negative regulator of GSK3β. *Biochemistry* **45**, 11379-11389 (2006).

291 Muta, T., Kang, D., Kitajima, S., Fujiwara, T. & Hamasaki, N. p32 protein, a splicing factor 2-associated protein, is localized in mitochondrial matrix and is functionally important in maintaining oxidative phosphorylation. *Journal of Biological Chemistry* **272**, 24363-24370 (1997).

292 Fogal, V. *et al.* Mitochondrial p32 protein is a critical regulator of tumor metabolism via maintenance of oxidative phosphorylation. *Molecular and cellular biology* **30**, 1303-1318 (2010).

293 Saltiel, A. R. & Kahn, C. R. Insulin signalling and the regulation of glucose and lipid metabolism. (2001).

294 Ruchatz, H., Coluccia, A. M., Stano, P., Marchesi, E. & Gambacorti-Passerini, C. Constitutive activation of Jak2 contributes to proliferation and resistance to apoptosis in NPM/ALK-transformed cells. *Exp Hematol* **31**, 309-315, doi:S0301472X03000079 [pii] (2003).

295 Marzec, M. *et al.* Oncogenic tyrosine kinase NPM/ALK induces activation of the MEK/ERK signaling pathway independently of c-Raf. *Oncogene* **26**, 813-821, doi:1209843 [pii] 10.1038/sj.onc.1209843 (2006).

296 Lim, M. S. *et al.* The proteomic signature of NPM/ALK reveals deregulation of multiple cellular pathways. *Blood* **114**, 1585-1595, doi:blood-2009-02-204735 [pii] 10.1182/blood-2009-02-204735 (2009).

297 Chen, Y. B., Jiang, C. T., Zhang, G. Q., Wang, J. S. & Pang, D. Increased expression of hyaluronic acid binding protein 1 is correlated with poor prognosis in patients with breast cancer. *Journal of surgical oncology* **100**, 382-386 (2009).

298 Fogal, V., Zhang, L., Krajewski, S. & Ruoslahti, E. Mitochondrial/cell-surface protein p32/gC1qR as a molecular target in tumor cells and tumor stroma. *Cancer research* **68**, 7210-7218 (2008).

299 Ghosh, I., Chowdhury, A. R., Rajeswari, M. R. & Datta, K. Differential expression of hyaluronic acid binding protein 1 (HABP1)/P32/C1QBP during progression of epidermal carcinoma. *Molecular and cellular biochemistry* **267**, 133-139 (2004).

300 Rubinstein, D. B. *et al.* Receptor for the globular heads of C1q (gC1q-R, p33, hyaluronan-binding protein) is preferentially expressed by adenocarcinoma cells. *International journal of cancer* **110**, 741-750 (2004).